Order Number 9013174

Aerodynamics of bodies in shear flow

Guvenen, Haldun, Ph.D.

The University of Arizona, 1989

U·M·I

300 N. Zeeb Rd.
Ann Arbor, MI 48106

AERODYNAMICS OF BODIES IN SHEAR FLOW

by

Haldun Guvenen

A Dissertation Submitted to the Faculty of the

DEPARTMENT OF AEROSPACE AND MECHANICAL ENGINEERING

In Partial Fulfillment of the Requirements
For the Degree of

DOCTOR OF PHILOSOPHY
WITH A MAJOR IN AEROSPACE ENGINEERING

In the Graduate College

THE UNIVERSITY OF ARIZONA

1989

THE UNIVERSITY OF ARIZONA
GRADUATE COLLEGE

As members of the Final Examination Committee, we certify that we have read the dissertation prepared by Haldun Guvenen

entitled Aerodynamics of Bodies in Shear Flow

and recommend that it be accepted as fulfilling the dissertation requirement for the Degree of Doctor of Philosophy.

Edward J. Kerschen	9/26/89 Date
Thomas F. Balsa	8/28/89 Date
K.Y. Fung	Aug 28, 1989 Date
	Date
	Date

Final approval and acceptance of this dissertation is contingent upon the candidate's submission of the final copy of the dissertation to the Graduate College.

I hereby certify that I have read this dissertation prepared under my direction and recommend that it be accepted as fulfilling the dissertation requirement.

Dissertation Director	9/26/89 Date

STATEMENT BY AUTHOR

This dissertation has been submitted in partial fulfillment of requirements for an advanced degree at The University of Arizona and is deposited in the University Library to be made available to borrowers under rules of the Library.

Brief quotations from this dissertation are allowable without special permission, provided that accurate acknowledgment of source is made. Requests for permission for extended quotation from or reproduction of this manuscript in whole or in part may be granted by the head of the major department or the Dean of the Graduate College when in his or her judgment the proposed use of the material is in the interests of scholarship. In all other instances, however, permission must be obtained from the author.

SIGNED: Haldun Guvener

ACKNOWLEDGMENTS

I would like to express my appreciation to my advisor, Professor Edward J. Kerschen, for his careful guidance and support throughout this work. I also would like to thank my committee members, Professors Thomas F. Balsa, K.-Y. Fung, George L. Lamb, and David W. McLaughlin.

I enjoyed collaboration with my colleagues Matthew R. Myers, Edmane Envia, Roland Heinrich, Meelan Choudhari, Chung-Tien Tsai. I thank them all.

This work was performed with the support of NSF Grants MEA-8205002 and MSM-8351929. The author gratefully acknowledges these supports.

TABLE OF CONTENTS

TABLE OF CONTENTS - continued

Page

LIST OF ILLUSTRATIONS

LIST OF ILLUSTRATIONS - continued

LIST OF TABLES

ABSTRACT

This dissertation investigates spanwise periodic shear flow past two-dimensional bodies. The flow is assumed to be inviscid and incompressible. Using singular perturbation techniques, the solution is developed for $\epsilon = L/\ell << 1$, where L represents body cross-sectional size, and ℓ the period of the oncoming flow U(z). The singular perturbation analysis involves three regions: the inner, wake and outer regions. The leading order solutions are developed in all regions, and in the inner region higher order terms are obtained.

In the inner region near the body, the primary flow (U_0, V_0, P_0) corresponds to potential flow past the body with a local free stream value of U(z). The spanwise variation in U(z) produces a weak $O(\epsilon)$ secondary flow W_1 in the spanwise direction. As the vortex lines of the upstream flow are convected downstream, they wrap around the body, producing significant streamwise vorticity in a wake region of thickness O(L) directly behind the body. This streamwise vorticity induces a net volume flux into the wake.

In the outer region far from the body, a nonlifting body appears as a distribution of three-dimensional dipoles, and the wake appears as a sheet of mass sinks. Both singularity structures must be included in describing the leading outer flow. For lifting bodies, the body appears as a lifting line, and the wake appears as a sheet of shed vorticity. The trailing vorticity is found to be equal to the spanwise derivative of the product of the circulation and the oncoming flow. For lifting bodies the first higher order correction to the inner flow is the response of the body to the downwash produced by the trailing vorticity. At large distances from the body, the flow takes on remarkably simple form.

CHAPTER 1

INTRODUCTION

The subject of this study is the interaction of a two dimensional body with a spanwise varying upstream flow. The important feature which distinguishes the present case from that of potential flow is that here the free stream contains vorticity. This vorticity is distorted and stretched as it convects downstream past the body, generating a three-dimensional flow field. Vortical flows of this type have a number of practical applications. For example, they are relevant to the interaction of a boundary layer with a perpendicular strut as illustrated in Fig. 1.1. Secondary flows in turbomachinery are also generated by this type of interaction. Another application is the influence of a propeller slip stream on the flow past aircraft wings.

Although viscous effects are often responsible for producing the shear in the main stream, many features of the interaction of this sheared flow with a body can be predicted by an inviscid analysis. Essentially, the interaction with the strut or the body occurs on such a short scale that the rotational flow responds inviscidly. Of course, an inviscid analysis neglects the thin boundary layers that form on the body surface, and cannot predict the possible separation of this boundary layer.

Compared to the case of irrotational flows, much less is understood about the interaction of bodies with sheared streams. The simplest case of shear flow interactions is that in which the vortex lines are parallel to the generators of the cylindrical body (Tsien 1943). In this two-dimensional flow, vortex lines remain undistorted as they convect downstream past the body. In contrast, the current study involves vortex lines which are

perpendicular to the generator of the body. These vortex lines wrap around the body as they convect downstream, generating a complex three-dimensional flow.

In a review article, Hawtorne (1967) separated inviscid, rotational flows into four categories:

1) Small shear - small disturbance

2) Small shear - large disturbance

3) Large shear - small disturbance

4) Large shear - large disturbance

Here, "shear" refers to the strength of the vorticity in the oncoming flow, and the "disturbance" is that produced by the body. The first category is not very interesting, because to leading order the disturbance produced by the body is an irrotational flow, and the fourth category presents severe difficulties for analysis. Our work involves both the second and third categories.

The earliest work was focused mainly on the small shear - large disturbance category, which is generally called secondary flow. Squire and Winter (1951) developed approximate theories for the secondary flow produced in a cascade of airfoils when the upstream flow has small amplitude of variations along the spanwise direction. Hawtorne (1951) developed a general theory for secondary vorticity, and applied this theory to the case of a uniformly sheared flow passing through a bend and a circular duct. Hawtorne (1954) examined secondary flow past a single airfoil, and showed that the secondary flow was significantly reduced for a wedge or a cusped shape leading edge. Following these initial studies, a number authors have investigated various aspects of the small shear - large disturbance approximation. A fairly complete review of this area is contained in Horlock J.H. and Lakshminarayana B. (1973). The primary feature of the small shear - large disturbance

category is that the flow can be viewed as a weak (or secondary) vortical disturbance to an irrotational primary flow. Since the disturbances are small the vortex line convection and deformation can be calculated using only the irrotational base flow. In recent years this approximation has become known as rapid distortion theory, and has proven useful in the study of turbulence.

In an investigation which originally was not related to secondary flow, Darwin (1953) studied the drift of the fluid particles in irrotational flow fields. The concept of drift is most easily explained by using a coordinate system in which the fluid is at rest far from the body. The drift is then defined as the displacement, in the direction of body motion, of a fluid particle relative to its original position.

Lighthill (1956, 1957a) recognized the utility of Darwin's drift concept for calculation of vortex line deformation in the small shear - large disturbance approximation. He presented elegant results for the flow of a linearly varying free stream past a two-dimensional cylinder and past a sphere. In addition to the secondary flow, Lighthill also calculated certain features of the tertiary flow. Most significantly, it was found that at large distances from the body the tertiary flow decayed more slowly than the secondary flow. This result showed that, viewed as an asymptotic expansion, the small shear - large disturbance approximation was nonuniform at large distances from the body. Lighthill recognized that, far from the body the small shear - large disturbance secondary flow approximation should be replaced by the large shear - small disturbance approximation. In a following paper Lighthill (1957b) analyzed a mass source placed in a parallel shear flow, which is the "fundamental solution" for the large shear - small disturbance category.

Preceding the above work, Von Karman and Tsien (1945) had developed a "lifting line theory" for an airfoil in a parallel shear flow. Their theory also falls into the large shear -

small disturbance category. They represented the airfoil as a line of pressure dipoles, and derived expressions for the downwash produced by the trailing vorticity and for the condition leading to minimum induced drag.

Lighthill's (1957b) analysis has much in common with that of Von Karman and Tsien. However, Lighthill utilized a somewhat different representation for the disturbance flow, and he showed that the small shear - large disturbance and large shear - small disturbance approximations are complementary expansions for this class of problems.

Following Lighthill's (1957b) contribution, Honda (1960, 1961) utilized the large shear - small disturbance approximation to analyze a parallel shear flow past a single airfoil, and passing through a cascade of airfoils. Honda utilized the pressure formulation of Von Karman and Tsien, and ignored the airfoil thickness. The airfoil camber and incidence angle were assumed small in keeping with the small disturbance approximation. Honda concentrated mainly on aerodynamic quantities such as the chordwise pressure distributions, the spanwise distributions of the lift coefficient, and the flow features in the Trefftz plane far downstream of the airfoil(s). Significant deviations from potential flow results were found. Namba (1969) considered subsonic shear flow through a cascade of airfoils, utilizing methods very similar to those of Honda. One very interesting result found by Namba was that, in a shear flow reaching a Mach number of one at a particular spanwise location does not produce dramatic effects found in the corresponding potential flow problem. Rather, the onset of strong compressibility effects is related to the value of an appropriate average Mach number which he calls the "harmonic mean Mach number". Some comparisons of the results of Honda and Namba with experimental measurements, and with predictions of small shear - large disturbance theories, are presented by Horlock J.H. and Lakshminarayana B. (1973).

With the exception of Lighthill's work, most previous investigations have utilized only the small shear - large disturbance approximation or the large shear-small disturbance approximation. We consider a problem in which these two approximations form complementary expansions in a singular perturbation structure. The solution is developed using the method of matched asymptotic expansions. Lighthill's analyses were developed prior to the widespread use of the matched asymptotic expansions, although his work contains the essential ideas. Lighthill's results could be viewed as "fundamental solutions" required to develop our analysis. However, we have found it convenient to utilize a somewhat different solution structure.

The present study examines the interaction of a spanwise periodic, inviscid, incompressible shear flow with a two-dimensional body as illustrated in Fig. 1.2. The spanwise periodicity can be interpreted as flow in a channel or in a turbomachinery duct, for example. The shear is assumed to be "strong" ($U_{max}/U_{min} = O(1)$), but the body cross sectional size L is assumed to be small compared to the period of ℓ of the upstream shear flow. The ratio of length scales $\epsilon = L/\ell$ is assumed small. On the scale ℓ of the shear flow, the large shear - small disturbance approximation is applicable, while on the scale L of the body cross section, a local application of the small shear - large disturbance approximation is valid.

The present problem can be viewed as the extension of lifting line or slender body theory to sheared upstream flows. Prandtl's original development of lifting line theory required the solution of an integral equation for the distribution of the lift force across the span. However, many of Prandtl's assumptions are valid only when the span ℓ of the wing is large compared to the chord L, and Van Dyke (1964) showed that for $\epsilon = L/\ell << 1$ the problem has a singular perturbation structure. Prandtl's integral equation can then be solved

iteratively by quadrature, and furthermore higher order terms in the asymptotic expansion in ϵ can be developed (Van Dyke 1975). Our analysis shows that the application of matched asymptotic expansions also provides significant simplifications for the case of sheared upstream flows.

In Chapter 2, we formulate the problem and develop the inner solution on the scale L of the body cross section. In the analysis of the outer region which scales on the period ℓ of the upstream flow, significant differences are found for nonlifting and lifting bodies. Chapter 3 treats the case of nonlifting bodies, and the lifting bodies are analyzed in Chapter 4. Numerical results are utilized to illustrate various flow features in Chapter 5. Finally, Chapter 6 summarizes the results of this investigation and makes recommendations for the future studies.

CHAPTER 2

THE INNER REGION

In this chapter we first present a mathematical formulation of the problem, and then use perturbation techniques to analyze the flow in the vicinity of the body, i.e. the inner region. Complete solutions are found for the leading terms in the inner region. Certain features of the higher order approximations are also discussed. The perturbation series for the inner region is found to be nonuniform at large distances from the body. The complementary expansions valid far from the body are developed in Chapters 3 and 4.

2.1 Mathematical Formulation

We consider rotational, three-dimensional flow past an infinite length, two-dimensional body. The flow is assumed to be steady, incompressible and inviscid, and hence governed by the continuity and momentum equations in the form

$$\nabla' . \vec{u}' = 0 , \tag{2.1a}$$

$$\vec{u}' . \nabla' \vec{u}' = - \frac{\nabla' p'}{\rho'} . \tag{2.1b}$$

Here $\vec{u}' = (u', v', w')$, p', ρ' are the dimensional velocity, pressure, and density, respectively. Equations (2.1a, b) constitute a system of four equations in the four unknowns u', v', w' and p'.

The body cross sectional shape is specified by the arbitrary function $c(x', y') = 0$. Since

the flow is inviscid, the boundary condition on the body surface is

$$\vec{u}'.\vec{n}' = 0 \text{ on } c(x',y') = 0 \,, \tag{2.2a}$$

where $\vec{n}'$ is the unit vector normal to the body surface. For bodies with a sharp trailing edge, we utilize the Kutta condition while for bodies with a blunt trailing edge, we simply fix the location of the rear stagnation point.

Far upstream of the body, the pressure p_{∞}' is uniform and the velocity is parallel to the x′ direction,

$$\vec{u}' \to u_{\infty}(z')\,\vec{e}_x \,, \quad p' \to p_{\infty}' \text{ as } x' \to -\infty \,, \tag{2.2b}$$

with a magnitude $u_{\infty}(z')$ which is a periodic function of the spanwise coordinate z′.

We now introduce nondimensional dependent variables in the form

$$(U,V,W) = \frac{(u',v',w')}{U_{\infty}} \text{ and } P = \frac{p'-p_{\infty}'}{\rho' U_{\infty}^2} \tag{2.3}$$

where $U_{\infty} = \langle u_{\infty}(z') \rangle$ is the spanwise average of the upstream flow. For nondimensionalization of the independent variables, two length scales must be considered. These are a representative body cross-sectional dimension L and the spatial period ℓ of the upstream flow. We utilize singular perturbation methods to analyze our case

$$\epsilon = L/\ell << 1 \,. \tag{2.4}$$

In the limit $\epsilon \to 0$, the flow near the body becomes almost two-dimensional, with a slow variation in the spanwise direction. Hence, in the inner region near the body, the appropriate nondimensional form of the independent coordinates is

$$(X, Y) = (x', y')/L \quad , \quad z = z'/\ell \, . \tag{2.5}$$

Introducing nondimensionalizations (2.3, 2.5) in (2.1, 2.2) we obtain

$$\frac{\partial U}{\partial X} + \frac{\partial V}{\partial Y} + \epsilon \frac{\partial W}{\partial z} = 0 \tag{2.6a}$$

$$U \frac{\partial U}{\partial X} + V \frac{\partial U}{\partial Y} + \epsilon W \frac{\partial U}{\partial z} = - \frac{\partial P}{\partial X} \tag{2.6b}$$

$$U \frac{\partial V}{\partial X} + V \frac{\partial V}{\partial Y} + \epsilon W \frac{\partial V}{\partial z} = - \frac{\partial P}{\partial Y} \tag{2.6c}$$

$$U \frac{\partial W}{\partial X} + V \frac{\partial W}{\partial Y} + \epsilon W \frac{\partial W}{\partial z} = -\epsilon \frac{\partial P}{\partial z} \tag{2.6d}$$

$$U n_X + V n_Y = 0 \text{ on } C(X, Y) = 0 \tag{2.6e}$$

$$U \to U(z) \, , \; P \to 0 \text{ as } X \to -\infty \, , \tag{2.6f,g}$$

where $\vec{n} = (n_X, n_Y)$ and $U(z) = \dfrac{u_\infty(\ell z)}{U_\infty}$ is the nondimensional upstream flow profile. This completes the mathematical specification of the problem.

2.2 Leading Terms in the Inner Region

As $\epsilon \to 0$, the spanwise velocity W disappears from (2.6a,b,c), and the O(1) leading terms of the X and Y components of velocity and pressure can be obtained from these three equations. Denoting these O(1) terms by U_0, V_0 and P_0 we have

$$\frac{\partial U_0}{\partial X} + \frac{\partial V_0}{\partial Y} = 0 \tag{2.7a}$$

$$U_0 \frac{\partial U_0}{\partial X} + V_0 \frac{\partial U_0}{\partial Y} + \frac{\partial P_0}{\partial X} = 0 \tag{2.7b}$$

$$U_0 \frac{\partial V_0}{\partial X} + V_0 \frac{\partial V_0}{\partial Y} + \frac{\partial P_0}{\partial Y} = 0 \tag{2.7c}$$

$$(U_0, V_0) \cdot (n_X, n_Y) = 0 \text{ on } C(X,Y) = 0 \tag{2.7d}$$

$$U_0 \to U(z) \, , \; P_0 \to 0 \text{ as } X \to -\infty \, . \tag{2.7e,f}$$

We note that (2.7) are identical to those for two dimensional flow past the body, with the spanwise coordinate z entering only parametrically through (2.7e). Equations (2.7) can be solved by introducing a pseudo-potential $\Phi_0(X,Y,z)$ such that

$$U_0 = \frac{\partial \Phi_0}{\partial X} \, , \; V_0 = \frac{\partial \Phi_0}{\partial Y} \, . \tag{2.8}$$

Substitution into (2.7a,d,e) produces the boundary value problem

$$\frac{\partial^2 \Phi_0}{\partial X^2} + \frac{\partial^2 \Phi_0}{\partial Y^2} = 0 \tag{2.9a}$$

$$\nabla \Phi_0 \cdot \vec{n} = 0 \text{ on } C(X,Y)=0 \tag{2.9b}$$

$$\nabla \Phi_0 \rightarrow U(z)\, \vec{e}_X \text{ as } X \rightarrow -\infty \,. \tag{2.9c}$$

Equations (2.9) define a standard boundary value problem of potential theory, whose solution can be expressed as

$$\Phi_0(X,Y,z) = U(z)\, \mathrm{Re}\, [G_0(\zeta)] \,, \tag{2.10}$$

where G_0 is an analytic function of the complex variable $\zeta = X + iY$, and Re denotes the real part. The specific form of G_0 is determined by the body shape $C(X,Y)=0$ and the Kutta condition or specification of the rear stagnation point.

Substituting (2.8) into (2.7b,c), these can be integrated partially with respect to X and Y, leading to

$$\left[\frac{\partial \Phi_0}{\partial X}\right]^2 + \left[\frac{\partial \Phi_0}{\partial Y}\right]^2 + 2P_0 = f(z) \,. \tag{2.11}$$

Utilizing (2.7f) to determine f(z), we obtain

$$P_0 = \frac{1}{2} \left[U^2(z) - q_0^2 \right] \tag{2.12a}$$

where

$$q_0^2 = U_0^2 + V_0^2 \ , \tag{2.12b}$$

or equivalently,

$$P_0 = \frac{1}{2} U^2(z) \left[1 - \frac{dG_0}{d\zeta} \left(\frac{dG_0}{d\zeta} \right)^* \right] , \tag{2.12c}$$

where "*" is the complex conjugate. Equation (2.12) is the Bernoulli equation applied in a plane z = constant.

We now consider (2.6d). It can be seen that the leading term in the spanwise velocity is $O(\epsilon)$, say $W = \epsilon W_1 + O(\epsilon^2)$. We then find

$$U_0 \frac{\partial W_1}{\partial X} + V_0 \frac{\partial W_1}{\partial Y} = q_0 \frac{\partial W_1}{\partial S_0} = - \frac{\partial P_0}{\partial z} , \tag{2.13}$$

where we have introduced a coordinate S_0 along the streamline of the quasi-two-dimensional flow (U_0, V_0). Integration of (2.13) gives

$$W_1(S_0) = - \int_{-\infty}^{S_0} \frac{1}{q_0} \frac{\partial P_0}{\partial z} d\tilde{S}_0 \ , \tag{2.14a}$$

upon noting that $W \to 0$ as $X \to -\infty$. Utilizing $d\Phi_0 = q_0 dS_0$, an equivalent form which is convenient for numerical integration is

$$W_1(\Phi_0) = -\frac{dU(z)}{dz}\int_{-\infty}^{\Phi_0}\left[\frac{1}{\left|\frac{dG_0}{d\zeta}\right|^2} - 1\right] d\tilde{\Phi}_0 \ . \qquad (2.14b)$$

Detailed results for W_1 obtained by numerical integration will be presented in Chapter 5.

The physical mechanism which generates the spanwise flow can be explained in terms of either pressure or vorticity arguments. The explanation in terms of the pressure field is apparent from (2.14a). As the fluid particle moves along a primarily two-dimensional path, the spanwise pressure gradient produces spanwise acceleration. At any position S_0, the integral (2.14a) represents the cumulative effect of the spanwise acceleration from upstream infinity to the position S_0. Alternatively, the generation of spanwise flow can be attributed to distortion of the vorticity field. To a first approximation, the vorticity in the inner region is convected along planes z = constant by the O(1) velocity field (U_0, V_0). As the vortex lines of the upstream flow U(z) are convected downstream, they are rotated and stretched by the gradients of U_0 and V_0, generating additional vorticity which induces spanwise velocities.

Near stagnation points of the quasi-two-dimensional flow (U_0, V_0), we find $q_0 \sim R$, where R is the distance from the stagnation point, while $\partial P_0/\partial z$ is approximately constant. Hence, expressions (2.14a,b) exhibit logarithmic singularities at these points. In reality, viscous effects near the body surface would limit the magnitude of the spanwise velocity.

The solutions we have developed in this section show that, near the body, the leading order terms in U, V and P correspond to two-dimensional potential flow, but with the free-stream velocity appropriate to the particular spanwise location under consideration. The spanwise velocity component is proportional to the local gradient dU(z)/dz of the upstream velocity, and corresponds to a local application of Lighthill's (1956b) solution for uniform

free-stream vorticity U(z) = A + Bz. Locally, the inner region flow can also be considered to fall in Hawtorne's (1967) small shear - large disturbance category.

Higher order corrections to the flow field could be developed by applying an iterative approach to (2.6). Since the leading terms of U, V and P are O(1), while the leading term of W is $O(\epsilon)$, it can be seen from (2.6a,b,c) that an iteration would produce $O(\epsilon^2)$ corrections to U, V and P. Equation (2.6d) would then produce an $O(\epsilon^3)$ correction to W. However, the perturbation series developed by straightforward iteration on (2.6) are found to be nonuniform at large distances from the body. The source of this nonuniformity can be illustrated most simply by considering the large R behavior of the leading terms U_0, V_0, P_0 and W_1.

2.3 Behavior for Large R

The behavior of U_0, V_0 and P_0 for large R ($X = R\cos\theta$, $Y = R\sin\theta$) can be deduced easily from the behavior of $G_0(\zeta)$ for large ζ. From two-dimensional potential flow theory, the complex potential for a closed body behaves as

$$G_0(\zeta) \sim \zeta + \frac{i\Gamma}{2\pi}\log\zeta + \frac{\mu_X + i\mu_Y}{2\pi}\frac{1}{\zeta} + O\left[\frac{1}{\zeta^2}\right] \tag{2.15}$$

as $\zeta \to \infty$. Here Γ, which is related to the circulation around the body, is fixed by the Kutta condition or by specification of the rear stagnation point. The constants μ_X and μ_Y are related to the X and Y dipoles. For nonlifting bodies the circulation is zero.

The corresponding expansions for U_0, V_0 and P_0 are

$$U_0 \sim U(z)\left[1 + \frac{\Gamma}{2\pi}\frac{\sin\theta}{R} - \frac{\mu_X}{2\pi}\frac{\cos 2\theta}{R^2} - \frac{\mu_Y}{2\pi}\frac{\sin 2\theta}{R^2} + O(1/R^3)\right] \tag{2.16a}$$

$$V_0 \sim U(z)\left[-\frac{\Gamma}{2\pi}\frac{\cos\theta}{R} - \frac{\mu_X}{2\pi}\frac{\sin 2\theta}{R^2} + \frac{\mu_Y}{2\pi}\frac{\cos 2\theta}{R^2} + O(1/R^3)\right] \tag{2.16b}$$

$$P_0 \sim \frac{1}{2}U^2(z)\left[-\frac{\Gamma}{2\pi}\frac{2\sin\theta}{R} - \frac{\Gamma^2}{4\pi^2}\frac{1}{R^2} + \frac{\mu_X}{2\pi}\frac{2\cos 2\theta}{R^2} + \frac{\mu_Y}{2\pi}\frac{2\sin 2\theta}{R^2} + O(1/R^3)\right]. \tag{2.16c}$$

We now examine the behavior of the spanwise velocity for large R. Here two separate expansions of the integral (2.14) must be developed. For O(1) values of θ, all points on the streamline are far from the body and the leading behavior of W_1 may be found by setting $q_0 \sim U(z)$ and approximating the streamline by $Y \sim$ constant. We then obtain

$$W_1 \sim \Gamma\frac{1}{\pi}U'(z)(\pi-\theta) + O(1/R) \tag{2.17a}$$

for lifting bodies. For nonlifting bodies of symmetric cross-section, both Γ and μ_Y vanish and we obtain

$$W_1 \sim \frac{dU(z)}{dz}\frac{\mu_X}{2\pi}\frac{2\cos\theta}{R} + O(1/R^2)\,. \tag{2.17b}$$

The asymptotic evaluation of (2.14) is more difficult for small values of θ. Here, some points on the streamline are within O(1) distance from the body, and the variation in q_0 and the streamline distortion must be accounted for in the leading term. It is convenient to separate the integral into two parts

$$\int_{-\infty}^{\Phi_0} (\,)\, d\tilde{\Phi}_0 = \int_{-\infty}^{\infty} (\,)\, d\tilde{\Phi}_0 - \int_{\Phi_0}^{\infty} (\,)\, d\tilde{\Phi}_0 \,.$$

The second integral is $O(R^{-1})$ for lifting bodies or $O(R^{-2})$ for nonlifting bodies and can be neglected, while the first integral is independent of X. We then find

$$W_1 = -\frac{dU(z)}{dz}\, D(\Psi_0), \quad \dot{X} >> 1 \;, \quad \Psi_0 = O(1) \tag{2.17c}$$

where

$$D(\Psi_0) = \int_{-\infty}^{\infty} \left(\frac{1}{\left| \frac{dG_0}{d\zeta} \right|^2} - 1 \right) d\tilde{\Phi} \,. \tag{2.17d}$$

Hence, in a "wake region" of thickness O(L) far downstream of the body, the spanwise velocity is $O(\epsilon)$ and independent of X for both lifting and nonlifting bodies.

A very interesting feature of the above results is that for $R >> 1$ the spanwise velocity component decays more slowly than the X and Y velocity components. This suggests that our perturbation series may be nonuniform for large values of R. To examine this, we compare the orders of magnitude of the terms which have been retained and neglected in the equations.

First consider a lifting body. In the continuity equation (2.6a) we have retained $\partial U/\partial X$ and $\partial U/\partial Y$, which are $O(1/R^2)$ for $R >> 1$. From (2.14), (2.17a), we see that the term $\epsilon\, \partial W/\partial z$, which has been neglected in the continuity equation, is $O(\epsilon^2)$ for all R. When $R = O(1/\epsilon)$, the terms we have neglected are as large as the terms which have been retained.

For the case of a nonlifting body, $\partial U/\partial X$ and $\partial U/\partial Y$ are $O(1/R^3)$ while $\epsilon\, \partial W/\partial z$ is $O(\epsilon^2/R)$ for $R >> 1$. Again we see that our approximation is invalid when $R = O(1/\epsilon)$. Comparisons of the terms which have been retained and neglected in the momentum equations (2.6b, c, d) lead to the same conclusion.

The nonuniformity of the inner region expansion indicates that the problem has a singular perturbation nature. This is not surprising, since the perturbation parameter ϵ is the ratio of two length scales: the body cross sectional scale L and the scale ℓ of the free-stream velocity. The nonuniformity occurs at a distance $r' = O(1)$ from the body. This implies that an outer region, in which all three coordinates scale on ℓ, must be considered. In addition, for $R >> 1$ the spanwise velocity exhibits different behavior for $\theta = O(1)$ and $O(1/\epsilon)$, indicating the presence of a separate "wake region" directly downstream of the body. In this wake region, x' and z' scale on ℓ, while y' scales on L.

The general characteristics of the flow in the outer region can be identified from the $R = O(1/\epsilon)$ behavior of the inner region solution. At this distance from the body, the flow appears as a small perturbation to a parallel shear flow with O(1) vorticity. Hence, here the flow falls into Hawtorne's (1967) large shear - small disturbance category, rather than the large disturbance - small shear category considered in Section 2.2. There are fundamental differences between the cases of nonlifting and lifting bodies. For a nonlifting body, (2.16), (2.17) imply that the outer region corresponds to $O(\epsilon^2)$ perturbation to the base flow U(z). Furthermore, the behavior in (2.16) is that of a two-dimensional dipole, which suggests that the outer solution for the nonlifting case should correspond to a distribution of three-dimensional dipoles of strength $O(\epsilon^2)$. For the case of a lifting body the perturbations are $O(\epsilon)$ and the behavior of (2.16) is that of a point force or vortex. Hence, here the outer solution takes the form of a lifting line of strength $O(\epsilon)$.

In Chapter 3 we proceed to the singular perturbation solution for nonlifting bodies; the case of lifting bodies is considered in Chapter 4.

CHAPTER 3

THEORY FOR NONLIFTING BODIES

In Chapter 2, we analyzed the flow in the inner region, i.e. at O(L) distances from the body. An important conclusion found there is that the inner region perturbation series is nonuniform at large distances from the body. Hence a singular perturbation analysis is required. This analysis involves complementary expansions, in which both r′ and z′ scale on the characteristic dimension ℓ of the upstream flow. Complementary expansions are required in two separate regions: an outer region in which $\theta = O(1)$, and a wake region in which $\theta = O(\epsilon)$. In this chapter, we develop the singular perturbation structure for the case of a nonlifting body. The body shape is assumed to be symmetric about the x-axis.

3.1 General Formulation for the Outer Region

Before addressing the specific case of a nonlifting body, we first develop a general formulation for the equations governing the flow in the outer region. The equations are formulated most conveniently in Cartesian coordinates. Since the appropriate length scale in the outer region is the characteristic dimension ℓ of the upstream flow, we introduce the nondimensional coordinates

$$x = \frac{x'}{\ell} = \epsilon X \, , \; y = \frac{y'}{\ell} = \epsilon Y \, , \; z = \frac{z'}{\ell} \, . \tag{3.1}$$

In Section 2.3, it was shown that in the outer region the flow is a small perturbation to the base flow U(z). Hence we set

$$U = U(z) + u \tag{3.2a}$$

$$V = \quad v \tag{3.2b}$$

$$W = \quad w \tag{3.2c}$$

$$P = \quad p\,, \tag{3.2d}$$

where we anticipate from Section 2.3 that the perturbation quantities are $O(\epsilon^2)$ for a nonlifting body and $O(\epsilon)$ for a lifting body. Substituting (3.1) and (3.2) into the full governing equations (2.6), and neglecting terms that are nonlinear in the perturbation quantities, we obtain the linearized equations

$$\frac{\partial u}{\partial x} + \frac{\partial v}{\partial y} + \frac{\partial w}{\partial z} = 0 \tag{3.3a}$$

$$U(z)\,\frac{\partial u}{\partial x} + w\,\frac{dU(z)}{dz} = -\,\frac{\partial p}{\partial x} \tag{3.3b}$$

$$U(z)\,\frac{\partial v}{\partial x} = -\,\frac{\partial p}{\partial y} \tag{3.3c}$$

$$U(z)\,\frac{\partial w}{\partial x} = -\,\frac{\partial p}{\partial z}\,. \tag{3.3d}$$

The body shrinks to a line singularity as $\epsilon \to 0$ in the outer coordinates, and hence (2.6e) can not be enforced. This boundary condition will be replaced by asymptotic matching with the inner solution. The conditions (2.6f,g) are satisfied by requiring all the perturbations to

vanish as $x \to -\infty$. There are a number of approaches which could be utilized to develop a solution to (3.3).

Lighthill (1957c) considered the spanwise velocity w as the primary variable, and developed the solution for a single three-dimensional mass source in an aperiodic shear flow. The main disadvantage of his approach is that u and v are given in terms of complicated integrals of the primary variable.

Von Karman and Tsien (1945) considered p as the primary variable in their examination of a lifting line in a sheared base flow. Here additional integrations are necessary to determine v and w.

We utilize an approach which is similar to that of Von Karman and Tsien, but has the advantage that all the physical quantities are given by derivatives of a pseudo-potential, $g(x,y,z)$. We set

$$p = U(z) \frac{\partial^2 g}{\partial x^2} . \tag{3.4a}$$

Substituting into (3.3c,d) we can integrate partially with respect to x to obtain

$$v = -\frac{\partial^2 g}{\partial y \partial x} \tag{3.4b}$$

and

$$w = -\frac{1}{U(z)} \frac{\partial^2 (U(z)g)}{\partial z \partial x} , \tag{3.4c}$$

where we have assumed that the right hand sides of (3.4b,c) approach zero as $x \to -\infty$.

Substituting (3.4a,c) into (3.3b), and integrating partially with respect to x, we obtain

$$u = -\frac{\partial^2 g}{\partial x^2} + \frac{U'(z)}{U^2(z)} \frac{\partial (U(z)g)}{\partial z}, \tag{3.4d}$$

where the prime on on U(z) denotes differentiation with respect to z and both terms on the right hand side of (3.4d) are assumed to vanish as $x \to -\infty$. The assumptions on the behavior of g as $x \to -\infty$ which are utilized in deriving (3.4) are verified a posteriori in specific applications.

The mass conservation relationship can be expressed in terms of g in the form

$$\frac{\partial u}{\partial x} + \frac{\partial v}{\partial y} + \frac{\partial w}{\partial z} = -\frac{\partial}{\partial x}[L(g)] \tag{3.5a}$$

where

$$L(g) = \frac{\partial^2 g}{\partial x^2} + \frac{\partial^2 g}{\partial y^2} + \frac{\partial^2 g}{\partial z^2} + h(z)g \tag{3.5b}$$

and

$$h(z) = U(z) \frac{d}{dz}\left[\frac{U'(z)}{U^2(z)}\right]. \tag{3.5c}$$

Our interest is in flow fields that are periodic with respect to the z coordinate, and hence g satisfies the periodic boundary conditions

$$g(0) = g(1) \tag{3.5d}$$

$$g'(0) = g'(1)\ . \tag{3.5e}$$

The solution to (3.5) will be developed utilizing an eigenfunction expansion in z. In the following section, we analyze the eigenvalue problem associated with the operator (3.5b).

3.2 The Eigenvalue Problem

Substituting the separation of variables form

$$g = F(x,y)\ E(z) \tag{3.6a}$$

into the homogeneous equation L(g) = 0, we obtain

$$\frac{\partial^2 F}{\partial x^2} + \frac{\partial^2 F}{\partial y^2} - \lambda^2 F = 0 \tag{3.6b}$$

and

$$\frac{d^2 E}{dz^2} + [h(z) + \lambda^2]E = 0\ , \tag{3.6c}$$

where λ^2 is the separation constant. The boundary conditions (3.5d,e) take the form

$$E(0) = E(1) \tag{3.6d}$$

$$E'(0) = E'(1) . \tag{3.6e}$$

Equations (3.6c, d, e) define an eigenvalue problem of Sturm-Liouville form, which has nontrivial solutions only for certain values of λ^2. By Sturm-Liouville theory there exists a discrete spectrum of real, non-negative eigenvalues

$$\lambda_0^2 < \lambda_1^2 < \lambda_2^2 \ldots \quad \lambda_n^2 \to \infty \text{ as } n \to \infty$$

and the corresponding eigenfunctions $E_n(z)$. The eigenfunctions corresponding to the distinct eigenvalues λ_n^2 and λ_m^2 are orthogonal. With an appropriate choice of the arbitrary constant multiplying $E_n(z)$, the orthogonality relationship can be written as

$$\int_0^1 E_n(z)E_m(z)\, dz = \delta_{mn} \tag{3.7}$$

where δ_{mn} is the Kronecker delta function. Furthermore, the eigenfunctions form a complete set, and hence can be used to represent an arbitrary function f(z) of the form

$$f(z) = \sum_{n=0}^{\infty} f_n\, E_n(z) , \tag{3.8a}$$

$$f_n = \int_0^1 f(z)E_n(z)\, dz . \tag{3.8b}$$

In general the eigenvalues and eigenfunctions must be found by numerical methods. However, by the general methods of Sturm-Liouville theory quoted above, the first eigenvalue is identically zero, and in this special case (3.6b) can be solved exactly. We find

$$\lambda_0 = 0 \tag{3.9a}$$

and

$$E_0(z) = \frac{e_0}{U(z)} \tag{3.9b}$$

where

$$e_0^{-2} = \int_0^1 U^{-2}(z)\, dz\,. \tag{3.9c}$$

3.3 Outer Region Flow Generated by the Dipole Line

We now return to the specific case of a nonlifting body whose shape is symmetric with respect to the x-axis. The analysis of Section 2.3 suggests that for this case the leading term in the outer region is of $O(\epsilon^2)$, and corresponds to the flow field generated by a distribution of three-dimensional mass dipoles. The dipoles are distributed along the line $x = y = 0$, and their axis is oriented in the negative x-direction.

A standard technique to develop the solution for g would be to first determine the fundamental solution $g_f(x,y,z,z_0)$ for a three-dimensional mass source located at the point $(0,0,z_0)$. In the problem specification for g_f, an inhomogeneous term $\delta(x)\delta(y)\delta(z-z_0)$ would

be introduced in the continuity equation (3.3a). Once the fundamental solution g_f has been found, the pseudo-potential $g_d(x,y,z)$ generated by a distribution of three-dimensional dipoles of strength $\mu(z)$ would then be given by the integral

$$g_d(x,y,z) = -\int \mu(z_0) \frac{\partial}{\partial x} [g_f(x,y,z,z_0)]\, dz_0 \ .$$

However, since we are analyzing a flow field which is periodic in the z coordinate, it is natural to utilize an eigenfunction expansion. In this case there seems to be little benefit in developing the fundamental solution, and we proceed directly to the problem for $g_d(x,y,z)$ by introducing a distributed source term $-\epsilon^2 \mu(z) \frac{\partial}{\partial x} (\delta(x)\delta(y))$ in the continuity equation (3.3a). Utilizing (3.5) and integrating partially with respect to x, we find

$$L(g_d) = -\epsilon^2 \mu(z)\delta(x)\delta(y) \ . \tag{3.11}$$

Utilizing the completeness property of the eigenfunctions, we present g_d in the form

$$g_d = \epsilon^2 \sum_{n=0}^{\infty} A_n(x,y)\, E_n(z) \ . \tag{3.12}$$

Multiplying (3.11) by $E_n(z)$, integrating over z from 0 to 1, applying integration by parts twice to the term involving $\partial^2 g/\partial z^2$, and utilizing (3.5d,e) and (3.6c), we find

$$\frac{\partial^2 A_n}{\partial x^2} + \frac{\partial^2 A_n}{\partial y^2} - \lambda_n{}^2 A_n = -\mu_n \delta(x)\delta(y) \tag{3.13a}$$

where

$$\mu_n = \int_0^1 \mu(z) E_n(z)\, dz\,. \tag{3.13b}$$

Now observing that the forcing term of (3.13a) has angular symmetry, i.e. $\delta(x)\delta(y) = \frac{\delta(r)}{2\pi r}$, we introduce cylindrical coordinates to obtain

$$\frac{1}{r}\frac{\partial}{\partial r}\left(r\,\frac{\partial A_n}{\partial r}\right) - \lambda_n{}^2\, A_n = -\mu_n\,\frac{\delta(r)}{2\pi r}\,. \tag{3.14}$$

The solutions of the homogeneous form of (3.14) are $K_0(\lambda_n r)$ and $I_0(\lambda_n r)$, the modified Bessel functions of order zero. The latter solution exhibits exponential growth as $r \to \infty$, and must be rejected since the physical variables (3.4) are required to vanish as $x \to -\infty$.

Integrating (3.14) over a small disk of radius r_0 centered on the origin, and applying the divergence theorem to the left hand side, we find

$$\lim_{r_0 \to 0} r_0\,\frac{dA_n(r_0)}{dr} = -\frac{\mu_n}{2\pi}\,. \tag{3.15}$$

Hence,

$$A_n = \frac{\mu_n}{2\pi}\,K_0(\lambda_n r) \tag{3.16a}$$

and the corresponding result for $n = 0$ is

$$A_0 = -\frac{\mu_0}{2\pi} \log r \,. \tag{3.16b}$$

Equations (3.4), (3.12) and (3.16) represent the outer region velocity and pressure fields (u_d, v_d, w_d) and p_d in terms of the unknown dipole strength distribution $\mu(z)$. It can be verified that as $x \to -\infty$, g_d satisfies the conditions assumed in Section 3.1.

We now determine the dipole strength distribution $\mu(z)$ by matching the leading terms in the inner and outer expansions. We utilize Van Dyke's (1975) rule, which states that the $O(\delta)$ outer expansion, when reexpanded to $O(\Delta)$ in inner variables, matches the $O(\Delta)$ inner expansion, when reexpanded to $O(\delta)$ in outer variables. The comparison of the two expressions can be carried out in either inner or outer variables; the match holds to $O(\delta)$ when carried out in outer variables, or to $O(\Delta)$ when carried out in inner variables.

The function $\mu(z)$ can be determined by matching any physical variable. Here, we utilize the pressure, and match the $O(\epsilon^2)$ outer expansion to the $O(1)$ inner expansion. Utilizing the small argument expansion of the modified Bessel function

$$K_0(\lambda_n \epsilon R) = -\log\left[\frac{1}{2} \lambda_n \epsilon R\right] - E + O(\epsilon^2 \log\epsilon, \epsilon^2) \,,$$

where E is Euler's constant, the expansion of $\dfrac{\partial^2 A_n}{\partial x^2}$ in inner variables takes the form

$$\frac{\partial^2 A_n}{\partial x^2} = \frac{1}{\epsilon^2} \frac{\cos 2\theta}{2\pi R^2} \mu_n + O(1) \,.$$

This expression depends on n only through the coefficient μ_n. Hence, summing over n to determine $\partial^2 g_d / \partial x^2$, and utilizing (3.8), we find from (3.4a) that the $O(\epsilon^2)$ outer expansion

for the pressure when written in inner variables and truncated at O(1), takes the form

$$\frac{\mu(z)}{2\pi}\, U(z)\, \frac{\cos 2\theta}{R^2}\,.$$

From (2.16c), the O(1) inner expansion of the pressure for a nonlifting symmetric body ($\Gamma = \mu_Y = 0$), when expanded to $O(\epsilon^2)$ in outer variables, takes the form

$$\epsilon^2\, \frac{\mu_X}{2\pi}\, U^2(z)\, \frac{\cos 2\theta}{r^2}\,.$$

Comparing these two expressions in either inner or outer variables, we obtain

$$\mu(z) = \mu_X\, U(z)\,. \tag{3.17}$$

Matching of the $O(\epsilon^2)$ outer and O(1) inner expansions for u and v, or matching of the $O(\epsilon^2)$ outer and $O(\epsilon)$ inner expansions for w, also leads to the result (3.17).

Utilizing (3.4, 3.12) with (3.9, 3.16a, 3.16b, 3.17), we obtain the following expressions for the flow field produced by the dipole line

$$\frac{2\pi p_d}{\epsilon^2 \mu_X} = e_0 u_0\, \frac{\cos 2\theta}{r^2} + \sum_{n=1}^{\infty} -u_n \lambda_n U(z) E_n(z) \left\{ \frac{\sin^2\theta}{r} K_1(\lambda_n r) - \frac{1}{2}\lambda_n \cos^2\theta \,[K_0(\lambda_n r) + K_2(\lambda_n r)] \right\} \tag{3.18a}$$

$$\frac{2\pi u_d}{\epsilon^2 \mu_X} = -\frac{1}{U(z)}\, \frac{2\pi p_d}{\epsilon^2 \mu_X} + \sum_{n=1}^{\infty} \frac{U'(z)}{U^2(z)}\, u_n\, K_0(\lambda_n r)\, \frac{d}{dz}[U(z) E_n(z)] \tag{3.18b}$$

$$\frac{2\pi v_d}{\epsilon^2 \mu_X} = \sin 2\theta \left\{ -e_0 u_0 \frac{1}{U(z)} \frac{1}{r^2} + \sum_{n=1}^{\infty} \frac{1}{2} u_n \lambda_n E_n(z) \left[-\frac{1}{r} K_1(\lambda_n r) - \frac{1}{2} \lambda_n (K_0(\lambda_n r) + K_2(\lambda_n r)) \right] \right\} \tag{3.18c}$$

$$\frac{2\pi w_d}{\epsilon^2 \mu_X} = \cos\theta \sum_{n=1}^{\infty} \frac{1}{U(z)} u_n \lambda_n K_1(\lambda_n r) \frac{d}{dz} [U(z) E_n(z)] , \tag{3.18d}$$

where

$$u_n = \int_0^1 U(z) E_n(z) dz , \tag{3.18e}$$

and μ_X is the dipole coefficient of the two-dimensional complex potential (2.15). In Chapter 5, these expressions will be utilized to illustrate important features of the outer region flow field for typical cases.

At distances from the body large compared to the length scale 1 of the upstream flow, we can replace $K_0(\lambda_n r)$ by its large argument expansion $e^{-\lambda_n r}\sqrt{\pi/2\lambda_n r}\,(1 + O(1/r))$. It is seen that contributions from the nonzero values of n are exponentially small compared to the n = 0 term, and the flow field takes the remarkably simple form ($r >> 1$)

$$u_d \sim -\epsilon^2 \frac{\mu_X e_0 u_0}{2\pi U(z)} \frac{\cos 2\theta}{r^2} + O(\text{exp}) \tag{3.19a}$$

$$v_d \sim -\epsilon^2 \frac{\mu_X e_0 u_0}{2\pi U(z)} \frac{\sin 2\theta}{r^2} + O(\text{exp}) \tag{3.19b}$$

$$w_d \sim O(exp) \tag{3.19c}$$

$$p_d \sim \epsilon^2 \frac{\mu_x e_0 u_0}{2\pi} \frac{\cos 2\theta}{r^2} + O(exp)\,, \tag{3.19d}$$

where O(exp) represents exponentially small terms. Despite the fact that the flow is strongly vortical, far from the body the dependence on r and θ is identical to that for two-dimensional potential flow. The velocity perturbations are largest at spanwise positions where the speed of the upstream flow is lowest, and vice versa.

To illustrate the physical processes leading to (3.19), it is useful to examine the governing equations (3.3) in the limit r >> 1. First consider the continuity equation. For r >> 1, the derivatives with respect to x and y become small compared to the derivative with respect to z, and the leading approximation to (3.3a) is $\partial w/\partial z = 0$. The boundary condition on the channel walls then requires that w is zero. Hence, far from the body, a given fluid particle is confined to a plane z = constant, and the r and θ dependence must assume the form appropriate for two-dimensional potential flow. However, the influence of the free stream vorticity enters indirectly through the pressure field. For flow in a plane z = constant, the linearized Bernoulli equation takes the form

$$p(z) + U(z)u(z) = 0\,.$$

Now, from the z momentum equation (3.3d), it can be seen that p must be independent of z. Hence, u (and also v) must be inversely proportional to z. It is significant to note that the above discussion has utilized only the assumption r >> 1 (which implies also that the flow perturbations are small), and hence the results of (3.19) are also valid for O(1) values of ϵ =

L/ℓ.

For O(1) values of r, the velocity component w is of the same order as u and v, and a significant spanwise redistribution of the flow occurs. As the body is approached ($r << 1$), the pressure and x and y components of velocity again assume the form of a two-dimensional potential flow, but here U and V are directly proportional to U(z) (see (2.8) and (2.9)), and the pressure is no longer independent of spanwise position. Finally, since the spanwise velocity component w_d produced by g_d vanishes as $r \rightarrow \infty$ on $\theta = 0$, this solution clearly does not capture the small θ behavior for the spanwise velocity found in (2.17c). In order to resolve this feature, the dipole line solution in the outer region must be supplemented by a separate wake region in which $\theta = O(\epsilon)$. This wake region will be analyzed in the next section. We shall find that the wake region induces additional $O(\epsilon^2)$ flow perturbations in the outer region.

3.4 The Wake Region

In Section 2.3, we examined the large R behavior of the inner solution. It was found that the large R expansion of the spanwise velocity exhibited different behavior for $\theta = O(1)$ and $\theta = O(\epsilon)$. The outer region, which was analyzed in the previous section, matches with the inner solution for O(1) values of θ. However, in order to match with the $R >> 1$, $\theta = O(\epsilon)$ limit of the inner region, an additional "wake region" must be introduced in the asymptotic structure for $\epsilon << 1$. In this section we analyze this wake region.

The analysis of Section 2.3 suggests that, in the wake region, the streamwise and spanwise coordinates scale on the characteristic dimension ℓ of the upstream flow, but y' scales on the body size L. Since the wake region involves distances from the body that are large compared to L, the flow field consists of small perturbations to the base flow U(z).

Hence, the analysis of the wake region can be initiated from (3.3). Transforming from the outer variable y to the wake variable Y, and utilizing the symbol (^) to denote dependent variables in the wake region, we obtain

$$\frac{\partial \hat{u}}{\partial x} + \frac{1}{\epsilon}\frac{\partial \hat{v}}{\partial Y} + \frac{\partial \hat{w}}{\partial z} = 0 \tag{3.20a}$$

$$U(z)\frac{\partial \hat{u}}{\partial x} + \hat{w}\frac{dU(z)}{dz} = -\frac{\partial \hat{p}}{\partial x} \tag{3.20b}$$

$$U(z)\frac{\partial \hat{v}}{\partial x} = -\frac{1}{\epsilon}\frac{\partial \hat{p}}{\partial Y} \tag{3.20c}$$

$$U(z)\frac{\partial \hat{w}}{\partial x} = -\frac{\partial \hat{p}}{\partial z}\,. \tag{3.20d}$$

In (3.20), we have assumed that the perturbation quantities are small, but of equal orders of magnitude. However, the presence of $(1/\epsilon)$ in (3.20a,c) suggests that additional scaling of the variables is required. First, we note that consistency with the $x >> 1$ behavior of the inner expansion requires $\hat{w} = O(\epsilon)$. Secondly, the form of (3.20c) suggests that in the wake region $\hat{p}$ is independent of Y, as is commonly found in "thin layer" analyses of fluid motion. Then, to allow matching with the outer region as $Y \to \mp\infty$, we must have $\hat{p} = O(\epsilon^2)$. The pressure terms in the x and z momentum equations are then negligible, and a nontrivial solution of (3.20b) requires $\hat{u} = O(\epsilon)$. Finally, to avoid an inconsistency between (3.20b) and (3.20a), we must choose $\hat{v} = O(\epsilon^2)$.

Hence, we set

$$\hat{u} = \epsilon\hat{u}_1 + \cdots \tag{3.21a}$$

$$\hat{v} = \epsilon^2 \hat{v}_1 + \cdots \tag{3.21b}$$

$$\hat{w} = \epsilon \hat{w}_1 + \cdots \tag{3.21c}$$

$$\hat{p} = \epsilon^2 \hat{p}_1 + \cdots . \tag{3.21d}$$

Substituting into (3.20), we find

$$\frac{\partial \hat{u}_1}{\partial x} + \frac{\partial \hat{v}_1}{\partial Y} + \frac{\partial \hat{w}_1}{\partial z} = 0 \tag{3.22a}$$

$$U(z) \frac{\partial \hat{u}_1}{\partial x} + \hat{w}_1 \frac{dU(z)}{dz} = 0 \tag{3.22b}$$

$$\hat{p}_1 = \hat{p}_1(x,z) \tag{3.22c}$$

$$\hat{w}_1 = \hat{w}_1(Y,z) \tag{3.22d}$$

where we have integrated (3.20c) partially with respect to Y and (3.20d) partially with respect to x. Since $\hat{w}_1$ does not depend on x, (3.22b) can be integrated partially with respect to x to obtain

$$\hat{u}_1 = -\frac{\hat{w}_1}{U(z)} \frac{dU(z)}{dz} x + \hat{u}_{1_c}(Y,z) . \tag{3.23a}$$

Utilizing (3.23a) to eliminate $\hat{u}_1$, (3.22a) can be integrated to yield

$$\hat{v}_1 = -U(z)\,\frac{\partial}{\partial z}\left[\frac{1}{U(z)}\int_0^Y \hat{w}_1\left(\tilde{Y},z\right)d\tilde{Y}\right], \tag{3.23b}$$

where we have utilized the fact that $\hat{v}_1(x,0,z) = 0$, since the body is symmetric with respect to the x axis.

To complete the leading order solution in the wake region, the unknown functions $\hat{w}_1$, $\hat{u}_{1_c}$ and $\hat{p}_1$ must be determined by matching with the inner and outer regions. First consider the match between the inner and wake regions for the spanwise velocity w. We match the $O(\epsilon)$ inner expansion (2.14) to the $O(\epsilon)$ wake expansion (3.22d). Noting that the expansion of (2.14) in wake variables to $O(\epsilon)$ is given by (2.17c,d), the matching condition requires

$$\hat{w}_1(Y,z) = -\frac{dU(z)}{dz}\,D(Y)\,. \tag{3.24a}$$

Next consider the match between the inner and wake regions for the streamwise velocity U. Matching the O(1) inner expansion to the $O(\epsilon)$ wake expansion provides a consistency check on the solutions, but leaves $\hat{u}_{1_c}(Y,z)$ undetermined. The function $\hat{u}_{1_c}$ can be found only by considering higher order terms in the inner expansion. Later in this chapter, we will show that the next terms in the inner perturbation series for U are $O(\epsilon^2\log\epsilon, \epsilon^2)$. Hence, an $O(\epsilon)$ perturbation to U in the inner region would satisfy homogeneous conditions on the body surface and at $R \to \infty$, and must vanish identically by uniqueness properties of the Laplace equation. Thus, the $O(\epsilon)$ expansion for the inner region is simply given by $U = U_0$, and by (2.16a) the expansion to $O(\epsilon)$ in wake variables is simply U(z). The match of the $O(\epsilon)$ inner and $O(\epsilon)$ wake expansions then requires

$$\hat{u}_{1_c}(Y,z) = 0 \,. \tag{3.24b}$$

Matching of the $O(\epsilon^2)$ wake expansions for $\hat{v}_1$ and $\hat{p}_1$ with the corresponding O(1) inner expansions provides only consistency checks on the analysis.

We now perform the asymptotic matching of the wake and outer regions. First consider the matching of the $O(\epsilon^2)$ wake and outer expansions for the y′ velocity component. Utilizing (3.4b, 3.12, 3.16), we find that the $O(\epsilon^2)$ outer expansion $\epsilon^2 v_d$ vanishes when we substitute $y = \epsilon Y$ and expand to $O(\epsilon^2)$. On the other hand, utilizing (3.24a) in (3.23b), introducing the outer variable y and expanding for small ϵ, we find the result

$$\epsilon^2 \hat{v}_1(x,\pm\infty,z) = \pm\, \epsilon^2\, \frac{1}{2}\, M\, U(z)\, \frac{d}{dz}\left[\frac{U'(z)}{U(z)}\right], \tag{3.25a}$$

where

$$M = \int_{-\infty}^{\infty} D(Y)\, dY \,. \tag{3.25b}$$

Thus, the $O(\epsilon^2)$ expansion in outer variables of the $O(\epsilon^2)$ wake expansion for V is nonzero, and the matching condition is not satisfied. In the following section, this discrepancy is resolved by introducing an additional contribution g_w in the $O(\epsilon^2)$ term of the outer expansion. Essentially, (3.25) is a "wake source" which generates additional flow perturbations in the outer region. However, before analyzing the outer flow g_w induced by (3.25), we first discuss the physical implications of the solution in the wake region.

The spanwise flow in the wake region can be viewed as the residual velocity field resulting from incomplete cancellation of the positive and negative spanwise accelerations which a fluid particle experiences as it moves through the inner region. To leading order, the fluid particle acceleration $\vec{u}'.\nabla\vec{u}'$ vanishes in the wake region, and the spanwise momentum of a fluid particle is independent of x. The streamwise velocity perturbation $\hat{u}_1$ increases linearly with x, but this is not an indication of streamwise flow acceleration. The linear increase in $\hat{u}_1$ simply reflects the spanwise displacement of particles of higher stagnation pressure by the spanwise velocity $\hat{w}_1$. These observations regarding $\hat{u}_1$ are in agreement with those of Von Karman and Tsien (1945).

The integral D(Y) is generally positive for nonlifting bodies, and hence $\hat{w}_1 \alpha$ -dU(z)/dz. This corresponds to spanwise flow from locations of higher stagnation pressure toward locations of lower stagnation pressure. This is consistent with the behavior for the vertical velocity as $Y \rightarrow \pm\infty$, which shows an influx of fluid into the wake at points when U(z) is a maximum, and an outflow of fluid where U(z) is a minimum. However, the streamwise flow perturbation also plays an important role in the mass conservation relationship, as will be seen in the following paragraph.

Substituting (3.24a) into (3.23), we find

$$\hat{u}_1 = \frac{1}{U(z)} \left[\frac{dU(z)}{dz}\right]^2 D(Y)\, x \tag{3.26}$$

This equation illustrates the remarkable feature that, at all locations in the wake except those for which U'(z) = 0, the spanwise flow results in an increase in the streamwise velocity component. Thus, there is a net positive volume flux, and flux of x-momentum, in the

wake region. The momentum flux is discussed in Section 3.5; here we show that the streamwise volume flux in the wake is balanced by a net influx into the wake region. This net influx can be calculated by integrating the vertical velocity (3.25) over one spanwise period. We obtain

$$\text{Influx} = \int_0^1 [\hat{v}_1(x,-\infty,z) - \hat{v}_1(x,+\infty,z)]\, dz = M \int_0^1 \frac{U'^2(z)}{U(z)}\, dz\,, \tag{3.27}$$

which is positive for an arbitrary base flow profile U(z). Hence there is a continuous influx of fluid into the wake region which is seen to balance the increase in streamwise volume flux

$$\int_0^1 \int_{-\infty}^{\infty} \frac{\partial \hat{u}_1}{\partial x}\, dY dz\,.$$

There is clearly a nonuniformity in the expansion at $x = O(1/\epsilon)$, since there the spanwise displacement of the streamline would no longer be small. However, since it does not seem sensible to perform an inviscid analysis on length scales of this order, and our main interest is in the flow behavior on the length scales L and ℓ, this nonuniformity will not be resolved.

An alternative interpretation of the wake region can be presented in terms of the vorticity field. As the vortex lines of the upstream flow convect downstream, they wrap around the body and stretch, eventually forming two long segments of opposite sign parallel to the x axis, as illustrated in Fig. 3.1a. This streamwise vorticity is contained in the wake

region, and to leading order is given by $\partial\hat{w}_1/\partial Y$. The streamwise vorticity in the wake then induces a velocity field in the outer region. For a symmetric, nonlifting body, the wake vorticity field is an antisymmetric function of Y, and the integral of the vorticity with respect to Y vanishes. Hence, the flow in the outer region can be considered to be induced by a distribution of streamwise divortices in the wake, as illustrated in Fig 3.1b.

3.5 Outer Region Flow Generated by Wake

In this section, we calculate the flow field in the outer region induced by the outflow (3.25) from the wake region. Since the flow field in the outer region is a small perturbation to the base flow U(z), the disturbances produced by the dipole line and the wake can be superposed. Hence, we introduce an additional contribution g_w in the pseudo-potential for the outer region. In outer coordinates, the wake region shrinks to the half plane y = 0, x > 0. Noting that the outflow from the wake region is of $O(\epsilon^2)$ and uniform in x, we calculate g_w by introducing a mass source ϵ^2 H(x)δ(y)s(z) in the continuity equation. Here H(x) is the Heaviside step function and s(z) is an unknown source strength. Following the approach of Section 3.3, we find on integrating the continuity equation partially with respect to x that g_w satisfies

$$L(g_w) = -xH(x)\delta(y)s(z) \; . \tag{3.28}$$

To solve (3.28) we set

$$g_w(x,y,z) = \sum_{n=0}^{\infty} B_n(x,y)\, E_n(z) \,. \tag{3.29}$$

Multiplying (3.28) by $E_n(z)$, and integrating over z from 0 to 1, we obtain after integration by parts

$$\frac{\partial^2 B_n}{\partial x^2} + \frac{\partial^2 B_n}{\partial y^2} - \lambda_n{}^2 B_n = -xH(x)\delta(y)s_n \,, \tag{3.30a}$$

where

$$s_n = \int_0^1 s(z)E_n(z)dz \,. \tag{3.30b}$$

We wish to apply a Fourier transform

$$\overline{B}_n(k,y) = \frac{1}{\sqrt{2\pi}} \int_{-\infty}^{\infty} e^{ikx}\, B_n(x,y)\, dx$$

to (3.30a). However, since the source term becomes unbounded as $x \to \infty$, before applying the transform we multiply the source term by $e^{-\beta x}$, $0 < \beta << 1$, where β is an artificial convergence factor which will be set to zero at the end of the analysis.

Upon transformation of (3.30a) we obtain

$$\frac{d^2\overline{B}_n}{dy^2} - (k^2+\lambda_n{}^2)\overline{B}_n = \frac{1}{\sqrt{2\pi}} s_n \frac{\delta(y)}{(k+i\beta)^2} . \tag{3.31a}$$

Equation (3.31a) is easily solved to obtain

$$\overline{B}_n(k,y) = -\frac{1}{\sqrt{2\pi}} s_n \frac{1}{(k+i\beta)^2} \frac{e^{-|y|\sqrt{k^2+\lambda_n{}^2}}}{2\sqrt{k^2+\lambda_n{}^2}} . \tag{3.31b}$$

Applying the inverse transform, we obtain

$$B_n(x,y) = -\frac{1}{4\pi} s_n \int_{-\infty}^{\infty} \frac{e^{-|y|\sqrt{k^2+\lambda_n{}^2}}}{(k+i\beta)^2\sqrt{k^2+\lambda_n{}^2}} e^{-ikx}\, dk . \tag{3.32}$$

Equations (3.29) and (3.32) provide the solution for the pseudo potential $g_w(x,y,z)$ in terms of an unknown wake source distribution s(z).

To determine the source distribution s(z), we match the $O(\epsilon^2)$ y components of velocity in the wake and outer regions. The y component of velocity associated with g_w is given by (3.4b). To carry out the matching, we substitute $y = \epsilon Y$ in $\partial^2\overline{B}_n/\partial y\partial x$ and expand for small ϵ. The leading term simply corresponds to the limit $y \to 0\pm$. We have

$$\lim_{y\to 0\pm} \frac{\partial^2 B_n}{\partial y \partial x} = \mp \frac{s_n}{4\pi} \int_{-\infty}^{\infty} \frac{ik\ e^{-ikx}}{(k+i\beta)^2}\, dk = \mp\, s_n\, \frac{1}{2}\, H(x) , \tag{3.33a}$$

where the last result is obtained by contour integration. Evaluating the sum over n in (3.29)

we obtain

$$v_w(x,0\pm,z) = \pm \frac{1}{2} \epsilon^2 s(z) H(x) . \tag{3.33b}$$

Comparing (3.33b) and (3.25), we see that the $O(\epsilon^2)$ outer and wake expansions for V match if

$$s(z) = M U(z) \frac{d}{dz} \left[\frac{U'(z)}{U(z)} \right] . \tag{3.34}$$

With the wake source strength s(z) determined, we can now complete the asymptotic matching of the wake and outer regions. Matching the $O(\epsilon^2)$ expansions for pressure in the wake and outer regions gives

$$\hat{p}_1(x,z) = U(z) \frac{\partial^2}{\partial x^2} (g_d(x,0,z) + g_w(x,0,z)) . \tag{3.35}$$

Finally, consider the matching of the $O(\epsilon)$ expansions for U and W in the wake region with the $O(\epsilon^2)$ expansions in the outer region. The wake region expressions for U and W contain D(Y), which falls off as $|Y|^{-3}$ as $|Y| \to \infty$. Hence, on substituting $Y = y/\epsilon$ in $\epsilon\hat{u}_1$ and $\epsilon\hat{w}_1$ and expanding for small ϵ, the results vanish to $O(\epsilon^2)$. Similarly, utilizing $g = g_d + g_w$ in (3.4c,d), substituting $y = \epsilon Y$ and expanding for small ϵ, the results vanish to $O(\epsilon)$. Hence, the wake and outer expansions for U and W satisfy the matching condition. This completes the asymptotic matching of the wake and outer regions.

We now examine the physical implications of the outer solution $g_w(x,y,z)$. First observe from (3.30b) and (3.34) that, in the eigenfunction expansion of s(z), the coefficient

s_0 of the lowest order eigenfunction vanishes identically. For the flow field associated with the dipole line, we found in Section 3.3 that the flow field far from the body was dominated by the contribution (3.19) from the lowest order eigenfunction. Hence, we anticipate that, at large distances from the body, the influence of the wake may be less important than that of the dipole line. We shall see that this conclusion is generally valid, except for small angles with respect to the downstream direction.

The singularities of (3.32) are a double pole at $k = -i\beta$ and branch points at $k = \mp i\lambda_n$. As the damping parameter β is allowed to approach zero, the double pole approaches to origin from below the inversion contour which lies along the real k axis. Hence, the residue associated with the double pole contributes for positive values of x. For O(1) values of y and $x >> 1$, the integral (3.32) is dominated by the singularity nearest the real axis, i.e. by the residue contribution. We then find

$$[g_w(x,y,z)]_{\text{residue}} = \frac{1}{2}\, x \sum_{n=1}^{\infty} \frac{s_n}{\lambda_n} e^{-\lambda_n |y|}\, E_n(z) \qquad x >> 1,\ y = O(1)\ , \tag{3.36a}$$

the associated velocity field is

$$u_w(x,y,z) = \frac{1}{2}\, x\, \frac{U'(z)}{U^2(z)} \sum_{n=1}^{\infty} \frac{s_n}{\lambda_n} e^{-\lambda_n |y|}\, \frac{\partial}{\partial z}[U(z)E_n(z)] \tag{3.36b}$$

$$v_w(x,y,z) = \frac{1}{2}\, \mathrm{sgn}(y) \sum_{n=1}^{\infty} s_n\, e^{-\lambda_n |y|}\, E_n(z) \tag{3.36c}$$

$$w_w(x,y,z) = -\frac{1}{2}\frac{1}{U(z)}\sum_{n=1}^{\infty}\frac{s_n}{\lambda_n}e^{-\lambda_n|y|}\frac{\partial}{\partial z}[U(z)E_n(z)] \qquad (3.36d)$$

and the pressure field vanishes. For positions far downstream, (x >> 1) , the fact that the wake sheet is only semi-infinite becomes unimportant, and the flow field (3.36) is identical to that which would be produced by a wake source sheet (or divortex) distribution extending over $(-\infty,\infty)$ in x. Hence, (3.36) is similar to the Trefftz plane of classical lifting line theory for Ppotential flow. The velocity components v_w and w_w are independent of x, while u_w varies linearly with x. As in the case of the wake region, the linear variation of u_w with x simply corresponds to the spanwise displacement of lines of constant pressure by the velocities u_w and v_w.

We next consider the x momentum flux associated with the streamwise velocity perturbation in the Trefftz plane and its relation to to the streamwise velocity in the wake region. The dimensional x-momentum flux perturbation in one spanwise period of the wake region is given by

$$2\rho' U_\infty^2 \int_0^1\int_0^\infty 2\epsilon U(z)\,\hat{u}_1(Y,z)\,L\,dY\,\ell\,dz$$

where we have utilized the fact that the wake is a symmetric function of Y. Utilizing (3.23a) and (3.24a), the momentum flux is given by

$$2\epsilon^2\rho' U_\infty^2 \ell^2 M x \int_0^1 U'^2(z)\,dz$$

Note that the momentum flux perturbation in the wake increases linearly with downstream distance.

The corresponding x-momentum flux in the Trefftz plane is

$$2\,\rho'\,U_\infty^2 \int_0^1\int_0^\infty 2\epsilon^2 U(z)\,u_1(y,z)\,\ell\,dy\,\ell\,dz$$

Utilizing (3.36b) and integrating with respect to y, we obtain

$$2\,\epsilon^2\,\rho'\,U_\infty^2\;\ell^2\;x\int_0^1 \frac{U'(z)}{U(z)}\sum_{n=1}^{\infty}\frac{s_n}{\lambda_n^2}\frac{\partial}{\partial z}[U(z)E_n(z)]\,dz$$

To simplify this integral, it is convenient to consider the function $J_n(z) = U(z)\,E_n(z)$. It is easily shown that J_n satisfies the ordinary differential equation

$$J_n'' - 2\,\frac{U'(z)}{U(z)}\,J_n' + \lambda_n^2\,J_n = 0$$

Hence, the above integral can be expressed as

$$\epsilon^2\,\rho'\,U_\infty^2\;\ell^2\;x\sum_{n=1}^{\infty} s_n\int_0^1\left[\frac{1}{\lambda_n^2}\,J_n''(z) + J_n(z)\right]dz$$

and the first term vanishes by virtue of the periodic boundary conditions (3.6d,e). Utilizing (3.34), and integrating by parts, the streamwise momentum flux in the Trefftz plane is given

by

$$-2\,\epsilon^2\,\rho'\,U_\infty^2\,\ell^2\,M\,x\int_0^1 U'^2(z)\,dz$$

Hence, the positive streamwise momentum flux in the wake is cancelled by exactly by the negative streamwise momentum flux in the Trefftz plane. Thus, there is no drag force on the lifting body, in agreement with the potential flow nature of the body surface pressure field.

For $r >> 1$ and $\theta = O(1)$, the integral (3.32) can be evaluated by the method of steepest descent (See Appendix A). Here, the integration path is shifted to pass through the saddle point $k = -i\lambda_n \cos\theta$ of the exponent, leading to the result

$$B_n \sim \frac{1}{2}\frac{S_n}{\lambda_n}\left[r\cos\theta\, e^{-r\lambda_n \sin\theta}\, H\left(\frac{\pi}{2}-\theta\right) + \frac{1}{\sqrt{2\pi}\,\lambda_n^{3/2}}\,\frac{e^{-r\lambda_n}}{\cos^2\theta\,\sqrt{r}}\,(1+O(1/r))\right] \quad r>>1 \tag{3.37a}$$

where $n \geq 1$, and $y > 0$. (A similar result holds for $y < 0$ by symmetry.) The first term is the residue contribution (3.36a) which arises when the inversion contour is displaced onto the steepest descent path and the second term is the asymptotic ($r >> 1$) value of the integral along the steepest descent path. Note that the first term in (3.37a) exhibits a discontinuity while the second term is infinite at $\theta = \pi/2$. The steepest descent approximation is nonuniformly valid for θ near $\pi/2$, due to the coalescence of the saddle point and the double pole. The treatment of such a case for a simple pole is given

by Van Der Waerden (1950). We follow a similar approach in Appendix A to obtain

$$B_n \sim \frac{1}{2} s_n \left\{ \frac{r\cos\theta e^{-r\lambda_n \sin\theta}}{\lambda_n} \left[H\left(\frac{\pi}{2}-\theta\right) - \frac{1}{2}\mathrm{sgn}\left(\frac{\pi}{2}-\theta\right) \mathrm{erfc}\sqrt{r\lambda_n(1-\sin\theta)} \right] \right.$$

$$\left. + \frac{e^{-r\lambda_n}}{2\lambda_n\sqrt{\pi\lambda_n r}} \left[r\sqrt{1+\sin\theta} + \frac{\sqrt{2} - \frac{1}{2}(1+\sin\theta)^{3/2}}{\lambda_n \cos^2\theta} (1+O(1/r)) \right] \right\}, \qquad (3.37b)$$

where sgn is the signum function.

For $r(1-\sin\theta) >> 1$, the complementary error function can be approximated by

$$\mathrm{erfc}\sqrt{r\lambda_n(1-\sin\theta)} \sim \frac{1}{\sqrt{\pi}} \frac{1}{\sqrt{r\lambda_n(1-\sin\theta)}} e^{-r\lambda_n(1-\sin\theta)}$$

$$\left[1 - \frac{1}{2r\lambda_n(1-\sin\theta)} + \frac{3}{4r^2\lambda_n^2(1-\sin\theta)^2} + O(1/r^3) \right]$$

and (3.37b) can be seen to reduce to (3.37a). However, (3.37b) exhibits a smooth variation in the vicinity of $\theta = \pm \pi/2$.

The pseudo potential g_w is then given by the sum (3.29). However, it should be noted that (3.37b) is an asymptotic expansion for $r >> 1$, with an error term of $O(1/r)$. Thus, since $(B_{n+1})/B_n = O(e^{-(\lambda_{n+1}-\lambda_n)r\sin\theta})$, the higher order terms ($n > 1$) in (3.29) are exponentially small compared to the error in B_1 and should be neglected. Hence, we have

$$g_w \sim \epsilon^2 B_1(r,\theta) E_1(z) \quad , r >> 1 . \qquad (3.38a)$$

The outer region flow field produced by the wake sheet then takes the following form for r >> 1

$$\frac{p_w}{\epsilon^2} = \frac{1}{2}\, U(z)\, s_1\, E_1(z)\, \frac{e^{-r\lambda_1}}{\sqrt{2\pi\lambda_1 r}}(1+O(1/r)) \tag{3.38b}$$

$$\frac{u_w}{\epsilon^2} = -\frac{p_w}{\epsilon^2 U(z)} + \frac{1}{2} s_1 \frac{\frac{dU(z)}{dz}}{U^2(z)} \frac{d}{dz}(U(z)E_1(z)) \left\{ \frac{r\cos\theta e^{-r\lambda_1 \sin\theta}}{\lambda_1} \left[H\left(\frac{\pi}{2}-\theta\right) - \frac{1}{2}\mathrm{sgn}\left(\frac{\pi}{2}-\theta\right)\mathrm{erfc}\sqrt{r\lambda_1(1-\sin\theta)} \right] \right.$$

$$\left. + \frac{e^{-r\lambda_1}}{2\lambda_1\sqrt{\pi\lambda_1 r}} \left[r\sqrt{1+\sin\theta} + \frac{\sqrt{2} - \frac{1}{2}(1+\sin\theta)^{3/2}}{\lambda_1 \cos^2\theta} (1+O(1/r)) \right] \right\} \tag{3.38c}$$

$$\frac{v_w}{\epsilon^2} = \frac{1}{2} s_1 E_1(z) \left\{ e^{-r\lambda_1 \sin\theta} \left[H\left(\frac{\pi}{2}-\theta\right) - \frac{1}{2}\mathrm{sgn}\left(\frac{\pi}{2}-\theta\right)\mathrm{erfc}\sqrt{r\lambda_1(1-\sin\theta)} \right] \right.$$

$$\left. + \frac{e^{-r\lambda_1}}{2\sqrt{\pi\lambda_1 r}} \left[\mathrm{sgn}\left(\frac{\pi}{2}-\theta\right)\sqrt{1-\sin\theta} + \sin\theta \frac{\sqrt{1+\sin\theta}-\sqrt{2}}{\cos\theta} \right] + O(1/r^{3/2}) \right\} \tag{3.38d}$$

$$\frac{w_w}{\epsilon^2} = -\frac{1}{2} \frac{1}{U(z)} s_1 \frac{d}{dz}(U(z)E_1(z)) \left\{ \frac{e^{-r\lambda_1 \sin\theta}}{\lambda_1} \left[H\left(\frac{\pi}{2}-\theta\right) - \frac{1}{2}\mathrm{sgn}\left(\frac{\pi}{2}-\theta\right)\mathrm{erfc}\sqrt{r\lambda_1(1-\sin\theta)} \right] \right.$$

$$\left. + \frac{e^{-r\lambda_1}}{2\lambda_1\sqrt{\pi\lambda_1 r}} \frac{\sqrt{1+\sin\theta} - \sqrt{2}}{\cos\theta} + O(1/r^{3/2}) \right\}. \tag{3.38e}$$

These expressions will be utilized in Chapter 5 to illustrate important features of the outer region flow field. For the present we simply note that the influence of the dipole line and the wake sheet are likely to be equal importance in the spanwise flow readjustment that occurs when $r' = O(1)$.

3.6 Higher Order Approximations

In this section, we consider higher order corrections to the inner region. As shown in Section (2.2), when the inner region is considered in isolation, higher terms first arise at $O(\epsilon^2)$ for U, V and P and $O(\epsilon^3)$ for W. However, these inner region expansions are nonuniform for large R, indicating the singular perturbation nature of the problem. Hence, we anticipate that matching of the inner and outer regions may force lower order terms into the inner expansion.

To investigate this possibility, we examine the expansion of the $O(\epsilon^2)$ outer field in inner coordinates. The $O(\epsilon^2)$ outer field contains contributions from the dipole line and the wake sheet, as developed in Sections 3.3 and 3.5. The expansion of the dipole line flow field in inner coordinates can be obtained from differentiation of the small argument expansion of the Bessel function K_0. We obtain

$$[p_d]_i = \frac{\mu_X}{2\pi}\left\{\frac{\cos 2\theta}{R^2}\,U^2(z) + \epsilon^2 \log\epsilon\; U(z)\sum_{n=1}^{\infty} u_n\, E_n(z)\left[-\frac{\lambda_n{}^2}{2}\right]\right.$$

$$\left. + \epsilon^2 U(z)\sum_{n=1}^{\infty} u_n\, E_n(z)\left[\log\left(\frac{\lambda_n R}{2}\right) - \frac{1}{2}\,E\lambda_n{}^2 - \frac{1}{4}\cos 2\theta\;\lambda_n{}^2\right] + O(\epsilon^4\log\epsilon, \epsilon^4)\right\} \qquad (3.39a)$$

$$[u_d]_i = -\frac{1}{U(z)}[p_d]_i + \frac{\mu_X}{2\pi}\left\{\epsilon^2\log\epsilon\ \frac{U'(z)}{U^2(z)}\sum_{n=1}^{\infty} -u_n\ \frac{d}{dz}[U(z)E_n(z)]\right.$$

$$\left. + \epsilon^2\ \frac{U'(z)}{U^2(z)}\sum_{n=1}^{\infty} u_n\ \frac{d}{dz}[U(z)E_n(z)]\left[-\log\left(\frac{\lambda_n R}{2}\right) - E\right] + O(\epsilon^4\log\epsilon, \epsilon^4)\right\} \qquad (3.39b)$$

$$[v_d]_i = \frac{\mu_X}{2\pi}\sin 2\theta\left\{-\frac{1}{R^2}U(z) + \epsilon^2\sum_{n=1}^{\infty}\frac{1}{4}u_n\lambda_n{}^2 E_n(z) + O(\epsilon^4\log\epsilon, \epsilon^4)\right\} \qquad (3.39c)$$

$$[w_d]_i = \epsilon\frac{\mu_X}{2\pi}\cos\theta\ \frac{2}{R}U'(z) + \frac{\mu_X}{2\pi}\cos\theta\sum_{n=1}^{\infty}\frac{1}{U(z)}u_n\ \frac{d}{dz}[U(z)E_n(z)]$$

$$\left\{\epsilon^3\log\epsilon\ \frac{\lambda_n{}^2 R}{2} + \epsilon^3\left[\frac{\lambda_n{}^2 R}{2}\log\left(\frac{\lambda_n R}{2}\right) - \frac{1}{4}\lambda_n{}^2 R(-2E+1)\right] + O(\epsilon^5\log\epsilon, \epsilon^5)\right\} \qquad (3.39d)$$

The leading terms of (3.39) were previously found to match with the inner region O(1) expansions for P, U and V and the $O(\epsilon)$ expansion for W. The higher order contributions to P, U and V in (3.39) include terms of $O(\epsilon^2)$, with an $O(\epsilon^3)$ contribution in W, as expected from section 2.2. However (3.39) also contains terms of $O(\epsilon^2\log\epsilon)$ and $O(\epsilon^3\log\epsilon)$ which do not arise from an iterative solution of (2.6). The $O(\epsilon^2\log\epsilon)$ terms in (3.39) depend only on the spanwise coordinate, and hence represent a uniform horizontal flow induced by the dipole line. The interpretation of the $O(\epsilon^3\log\epsilon)$ term of the spanwise velocity is less straightforward, but must arise from the action of spanwise pressure gradients.

The expansion of the wake sheet outer field g_w in inner coordinates utilizes (B.7b) of Appendix B in the form

$$B_n = -\frac{1}{4\pi}s_n\left\{-\frac{2}{\lambda_n^2} - \epsilon\frac{\pi}{\lambda_n}R\cos\theta + \epsilon^2\log\epsilon R^2\cos 2\theta + \epsilon^2 R^2\cos 2\theta\left[\log\left(\frac{\lambda_n R}{2}\right) - \frac{3}{2} + E\right]\right.$$

$$\left. + \epsilon^2 R^2[\sin^2\theta + (\pi-\theta)\sin 2\theta] + O(\epsilon^3)\right\} \quad n=1,2,3\ldots . \tag{3.40a}$$

Utilizing (3.29) and (3.4) the flow field for g_w has the inner expansion

$$[p_w]_i = -\frac{1}{2\pi}s(z)U(z)\left\{\epsilon^2\log\epsilon + \epsilon^2\left[E+\log\left(\frac{R}{2}\right)\right]\right\} - \epsilon^2\frac{1}{2\pi}U(z)\sum_{n=1}^{\infty} s_n E_n(z)\log\lambda_n + O(\epsilon^4)$$

(3.40b)

$$[u_w]_i = -\frac{1}{U(z)}[p_w]_i + \epsilon^2\frac{1}{2\pi}\frac{U'(z)}{U^2(z)}\sum_{n=1}^{\infty}\frac{s_n}{\lambda_n^2}\frac{d}{dz}[U(z)E_n(z)] + O(\epsilon^3) \tag{3.40c}$$

$$[v_w]_i = \epsilon^2\frac{1}{2\pi}s(z)(\pi-\theta) + O(\epsilon^3) \tag{3.40d}$$

$$[w_w]_i = -\epsilon^2\frac{1}{4}\frac{1}{U(z)}\sum_{n=1}^{\infty}\frac{s_n}{\lambda_n}\frac{d}{dz}[U(z)E_n(z)] + \epsilon^3\log\epsilon\frac{1}{2\pi}R\cos\theta\frac{1}{U(z)}\sum_{n=1}^{\infty}s_n\frac{d}{dz}[U(z)E_n(z)]$$

$$+\epsilon^3 \frac{1}{2\pi} R \frac{1}{U(z)} \sum_{n=1}^{\infty} s_n \frac{d}{dz}[U(z)E_n(z)]\left\{(\pi-\theta)\sin\theta + \cos\theta\left[-1+E+\log\left[\frac{\lambda_n R}{2}\right]\right]\right\} + O(\epsilon^4) . \tag{3.40e}$$

The $O(\epsilon^2 \log\epsilon)$ terms again correspond to a uniform horizontal flow past the body (with parametric dependence on z). Surprisingly, the inner expansion of the wake sheet outer field leads to a uniform $O(\epsilon^2)$ spanwise flow component in addition to terms of $O(\epsilon^3 \log\epsilon, \epsilon^3)$.

Equations (3.39) and (3.40) suggest that the expansion of the inner flow field takes the form

$$U = U_0 + \epsilon^2 \log\epsilon U_{21} + \epsilon^2 U_2 + \cdots \tag{3.41a}$$

$$V = V_0 + \epsilon^2 \log\epsilon V_{21} + \epsilon^2 V_2 + \cdots \tag{3.41b}$$

$$W = \quad + \epsilon W_1 + \epsilon^2 W_2 + \epsilon^3 \log\epsilon W_{31} + \epsilon^3 W_3 + \cdots \tag{3.41c}$$

$$P = P_0 + \epsilon^2 \log\epsilon P_{21} + \epsilon^2 P_2 + \cdots . \tag{3.41d}$$

Substituting these expansions into the governing equations (2.6), the $O(\epsilon^2 \log\epsilon)$ contributions to U, V and P are found to satisfy

$$\frac{\partial U_{21}}{\partial X} + \frac{\partial V_{21}}{\partial Y} = 0 \tag{3.42a}$$

$$U_0 \frac{\partial U_{2l}}{\partial X} + V_0 \frac{\partial U_{2l}}{\partial Y} + U_{2l} \frac{\partial U_0}{\partial X} + V_{2l} \frac{\partial U_0}{\partial Y} + \frac{\partial P_{2l}}{\partial X} = 0 \tag{3.42b}$$

$$U_0 \frac{\partial V_{2l}}{\partial X} + V_0 \frac{\partial V_{2l}}{\partial Y} + U_{2l} \frac{\partial V_0}{\partial X} + V_{2l} \frac{\partial V_0}{\partial Y} + \frac{\partial P_{2l}}{\partial Y} = 0 \tag{3.42c}$$

$$(U_{2l}, V_{2l}).(n_X, n_Y) = 0 \text{ on } C(X, Y) = 0 \tag{3.42d}$$

and

$$U_{2l} \to U_i(z) \, , \, V_{2l} \to 0 \, , \, P_{2l} \to P_i(z) \text{ as } R \to \infty \tag{3.42e}$$

where

$$U_i(z) = - \frac{P_i(z)}{U(z)} - \frac{\mu_X}{2\pi} \frac{U'(z)}{U^2(z)} \sum_{n=1}^{\infty} u_n \frac{d}{dz}[U(z)E_n(z)]$$

$$P_i(z) = - \frac{1}{2\pi} s(z) \, U(z) - \frac{\mu_X}{2\pi} U(z) \sum_{n=1}^{\infty} \frac{1}{2} u_n \lambda_n^2 E_n(z)$$

where (3.42e) has been introduced in anticipation of the matching with the outer region. It is interesting to note that U_i and P_i do not satisfy the linearized potential flow relation.

Equations (3.42a,d,e) can be solved by introducing a pseudo-potential $\Phi_{2l}(X, Y, z)$ such that

$$U_{2l} = \frac{\partial \Phi_{2l}}{\partial X}, \; V_{2l} = \frac{\partial \Phi_{2l}}{\partial Y} \tag{3.43}$$

substitution into (3.42a, d, e) produces the boundary value problem

$$\frac{\partial^2 \Phi_{2l}}{\partial X^2} + \frac{\partial^2 \Phi_{2l}}{\partial Y^2} = 0 \tag{3.44a}$$

$$\nabla \Phi_{2l} . \vec{n} = 0 \quad \text{on } C(X, Y) = 0 \tag{3.44b}$$

$$\nabla \Phi_{2l} \rightarrow U_i(z) \; \vec{e}_X \text{ as } R \rightarrow \infty \, . \tag{3.44c}$$

This boundary value problem is identical in form to that discussed in Section 2.2, and hence Φ_{2l} is given by

$$\Phi_{2l}(X, Y, z) = U_i(z) \; \mathrm{Re}[G_0(\zeta)] \, . \tag{3.45}$$

Substituting (3.43) into (3.42b, c), integrating these equations partially with respect to X and Y, and using (3.42e) to evaluate the arbitrary function of z, we obtain

$$P_{2l} = - \frac{\partial \Phi_0}{\partial X} \frac{\partial \Phi_{2l}}{\partial X} - \frac{\partial \Phi_0}{\partial Y} \frac{\partial \Phi_{2l}}{\partial Y} - \frac{\mu_X}{2\pi} \frac{U'(z)}{U(z)} \sum_{n=1}^{\infty} u_n \frac{d}{dz}[U(z) E_n(z)] \, . \tag{3.46}$$

The general characteristics of the $O(\epsilon^2 \log \epsilon)$ corrections U_{2l}, V_{2l} and P_{2l} are similar to the leading order terms U_0, V_0 and P_0. Both U_0, V_0, P_0 and U_{2l}, V_{2l}, P_{2l} correspond to two dimensional potential flows.

Now consider the $O(\epsilon^2)$ corrections to the inner flow. Substituting (3.41) into the governing equations (2.6), the $O(\epsilon^2)$ contributions to U, V and P are found to satisfy

$$\frac{\partial U_2}{\partial X} + \frac{\partial V_2}{\partial Y} = -\frac{\partial W_1}{\partial z} \tag{3.47a}$$

$$U_0 \frac{\partial U_2}{\partial X} + V_0 \frac{\partial U_2}{\partial Y} + U_2 \frac{\partial U_0}{\partial X} + V_2 \frac{\partial U_0}{\partial Y} + \frac{\partial P_2}{\partial X} = - W_1 \frac{\partial U_0}{\partial z} \tag{3.47b}$$

$$U_0 \frac{\partial V_2}{\partial X} + V_0 \frac{\partial V_2}{\partial Y} + U_2 \frac{\partial V_0}{\partial X} + V_2 \frac{\partial V_0}{\partial Y} + \frac{\partial P_2}{\partial Y} = - W_1 \frac{\partial V_0}{\partial z} \tag{3.47c}$$

$$(U_2, V_2).(n_X, n_Y) = 0 \quad \text{on} \quad C(X, Y) = 0 \tag{3.47d}$$

and

$$U_2 \rightarrow U_{2i}(z) \, , \; V_2 \rightarrow V_{2i}(z) \, , \; P_2 \rightarrow P_{2i}(z) \text{ as } R \rightarrow \infty \tag{3.47e}$$

where

$$P_{2i}(z) = - \frac{1}{2\pi} s(z) \, U(z) \left[E + \log\left(\frac{R}{2}\right) \right] - \frac{1}{2\pi} U(z) \sum_{n=1}^{\infty} s_n \, E_n(z) \, \log\lambda_n$$

$$+ \frac{\mu_X}{2\pi} U(z) \sum_{n=1}^{\infty} u_n \, E_n(z) \left[\log\left(\frac{\lambda_n R}{2}\right) - \frac{1}{2} E \, \lambda_n{}^2 - \frac{1}{4} \cos 2\theta \, \lambda_n{}^2 \right]$$

$$U_{2i}(z) = -\frac{P_{2i}(z)}{U(z)} + \frac{1}{2\pi}\frac{U'(z)}{U^2(z)}\sum_{n=1}^{\infty}\frac{s_n}{\lambda_n^2}\frac{d}{dz}[U(z)E_n(z)]$$

$$-\frac{\mu_X}{2\pi}\frac{U'(z)}{U^2(z)}\sum_{n=1}^{\infty}u_n(z)\frac{d}{dz}[U(z)E_n(z)]\left[\log\left(\frac{\lambda_n R}{2}\right)+E\right]$$

$$V_{2i}(z) = \frac{1}{2\pi}s(z)(\pi-\theta) + \frac{\mu_X}{2\pi}\sin 2\theta\sum_{n=1}^{\infty}\frac{1}{4}u_n\lambda_n^2 E_n(z)$$

where (3.47e) has been introduced in anticipation of the matching with the outer region.

Equations (3.47a,d,e) can be solved by introducing a pseudo-potential $\Phi_2(X,Y,z)$ such that

$$U_2 = \frac{\partial\Phi_2}{\partial X}, \quad V_2 = \frac{\partial\Phi_2}{\partial Y}. \tag{3.48}$$

Substitution into (3.47a, d, e) produces the boundary value problem

$$\frac{\partial^2\Phi_2}{\partial X^2} + \frac{\partial^2\Phi_2}{\partial Y^2} = -\frac{\partial W_1}{\partial z} \tag{3.49a}$$

$$\nabla\Phi_2.\vec{n} = 0 \quad \text{on } C(X,Y) = 0 \tag{3.49b}$$

$$\nabla\Phi_2 \to U_{2i}(z)\,\vec{e}_X + V_{2i}(z)\,\vec{e}_Y \text{ as } R\to\infty. \tag{3.49c}$$

Since W_1 is given by (2.14) in terms of an integral which can only be evaluated numerically,

the system (3.49) must be solved numerically. We will not develop this solution here.

Substituting (3.48) into (3.47b,c), integrating partially with respect to X and Y, and using (3.47e) to evaluate the arbitrary function of S, we obtain

$$\chi = -\frac{1}{2}\int^{S} \frac{1}{q_0} W_1 \frac{\partial}{\partial z}[U^2(z) - 2P_0]\, d\tilde{S} + \chi_\infty \tag{3.50}$$

where

$$\chi = P_2 + \frac{\partial \Phi_0}{\partial X}\frac{\partial \Phi_2}{\partial X} + \frac{\partial \Phi_0}{\partial Y}\frac{\partial \Phi_2}{\partial Y}$$

and

$$\chi_\infty = P_{2i} + U(z)\, U_{2i}\ .$$

Hence (3.50) relates to the cumulative distortion of the sheets of constant stagnation pressure.

Now consider the $O(\epsilon^2)$ correction to the spanwise velocity. Substituting (3.41) into (2.6d), we find that W_2 satisfies the equation $q_0\, \partial W_2/\partial S = 0$, and hence matching with the outer region leads to the simple result

$$W_2 = -\frac{1}{4}\ \frac{1}{U(z)} \sum_{n=1}^{\infty} \frac{s_n}{\lambda_n} \frac{d}{dz}[U(z)E_n(z)]\ . \tag{3.51}$$

At $O(\epsilon^3 \log\epsilon)$, we obtain the system

$$U_0 \frac{\partial W_{3l}}{\partial X} + V_0 \frac{\partial W_{3l}}{\partial Y} + U_{2l} \frac{\partial W_1}{\partial X} + V_{2l} \frac{\partial W_1}{\partial Y} = -\frac{\partial P_{2l}}{\partial z}, \tag{3.52a}$$

$$W_{3l}\Big|_{X \to -\infty} = \frac{1}{2\pi} R\cos\theta \frac{1}{U(z)} \sum_{n=1}^{\infty} s_n \frac{d}{dz}[U(z)E_n(z)]$$

$$+ \frac{\mu_X}{2\pi}\cos\theta \frac{1}{U(z)} \sum_{n=1}^{\infty} u_n \frac{\lambda_n^2 R}{2} \frac{d}{dz}[U(z)E_n(z)]. \tag{3.52b}$$

Equation (3.52a) can be integrated in the form

$$W_{3l} = \int^{S} \frac{1}{q_0}\left[\frac{q_{2l}}{q_0}\frac{\partial P_0}{\partial z} - \frac{\partial P_{2l}}{\partial z}\right] d\tilde{S}. \tag{3.52c}$$

The indefinite integral (3.52c) contains an arbitrary function of Y and Z which is determined by the asymptotic match (3.52b) with the outer flow as $X \to -\infty$.

To $O(\epsilon^3)$ we obtain

$$U_0 \frac{\partial W_3}{\partial X} + V_0 \frac{\partial W_3}{\partial Y} + U_2 \frac{\partial W_1}{\partial X} + V_2 \frac{\partial W_1}{\partial Y} + W_1 \frac{\partial W_1}{\partial z} = -\frac{\partial P_2}{\partial z}, \tag{3.53a}$$

$$W_3\Big|_{X \to -\infty} = \frac{1}{2\pi} R \frac{1}{U(z)} \sum_{n=1}^{\infty} s_n \frac{d}{dz}[U(z)E_n(z)]\left\{(\pi-\theta)\sin\theta + \cos\theta\left[-1+E+\log\left(\frac{\lambda_n R}{2}\right)\right]\right\}$$

$$+ \frac{\mu_X}{2\pi} \cos\theta \sum_{n=1}^{\infty} \frac{1}{U(z)} u_n \frac{d}{dz}[U(z)E_n(z)]\left[\frac{\lambda_n{}^2 R}{2} \log\left(\frac{\lambda_n R}{2}\right) - \frac{1}{4} \lambda_n{}^2 R(-2E+1)\right] . \tag{3.53b}$$

Equation (3.53 a) can again be integrated in the form

$$W_3 = \int^S \frac{1}{q_0}\left[\frac{q_2}{q_0} \frac{\partial P_0}{\partial z} - W_1 \frac{\partial W_1}{\partial z} - \frac{\partial P_2}{\partial z}\right] d\tilde{S} , \tag{3.53c}$$

with (3.53 b) determining the arbitrary function of Y and Z.

We now briefly discuss higher order approximations for the outer region. Expanding (2.15) to higher order, we have for a symmetric nonlifting body

$$G_0(\zeta) = \zeta + \frac{\mu_X}{2\pi} \frac{1}{\zeta} + \frac{\mu_{XX}}{2\pi} \frac{1}{\zeta^2} + \frac{\mu_{XXX}}{2\pi} \frac{1}{\zeta^3} + O\left(\frac{1}{\zeta^4}\right) , \tag{3.54}$$

where μ_{XX} is zero if the body has fore-and-aft symmetry. For the case of nonzero μ_{XX} (a Joukowski airfoil, for example), the asymptotic matching condition shows that an $O(\epsilon^3)$ quadrupole line must be present in the outer region. The case of zero μ_{XX} but nonzero μ_{XXX} leads to a $O(\epsilon^4)$ octupole line in the outer region. The above discussion of higher order approximations to the inner region has shown that an $O(\epsilon^2 \log\epsilon)$ term arises in the inner region. The asymptotic matching conditions then require that a $O(\epsilon^4 \log\epsilon)$ dipole line be present in the outer region.

Hence, the solutions in the outer regions have expansions of the form

$$U = U(z) + \epsilon^2 u_2 + \epsilon^3 u_3 + \epsilon^4 \log\epsilon u_{41} + \epsilon_4 u_4 + \cdots \tag{3.55a}$$

$$V = \epsilon^2 v_2 + \epsilon^3 v_3 + \epsilon^4 \log\epsilon v_{41} + \epsilon_4 v_4 + \cdots \tag{3.55b}$$

$$W = \epsilon^2 w_2 + \epsilon^3 w_3 + \epsilon^4 \log\epsilon w_{41} + \epsilon_4 w_4 + \cdots \tag{3.55c}$$

$$P = \epsilon^2 p_2 + \epsilon^3 p_3 + \epsilon^4 \log\epsilon p_{41} + \epsilon_4 p_4 + \cdots . \tag{3.55d}$$

The solutions for the $O(\epsilon^3)$ and $O(\epsilon^4 \log\epsilon)$ terms, which correspond to singularity lines, can be determined by straightforward applications of the same procedures used earlier in this chapter. However, a serious difficulty arises in calculation of the $O(\epsilon^4)$ solution. Substituting the above expansion into (2.6) expressed in outer coordinates, we find that the $O(\epsilon^4)$ terms satisfy the equations

$$\frac{\partial u_4}{\partial x} + \frac{\partial v_4}{\partial y} + \frac{\partial w_4}{\partial z} = 0 \tag{3.56a}$$

$$U(z)\,\frac{\partial u_4}{\partial x} + w_4\,\frac{\partial U(z)}{\partial z} + \frac{\partial p_4}{\partial x} = -\,u_2\,\frac{\partial u_2}{\partial x} - v_2\,\frac{\partial u_2}{\partial y} - w_2\,\frac{\partial u_2}{\partial z} \tag{3.56b}$$

$$U(z)\,\frac{\partial v_4}{\partial x} + \frac{\partial p_4}{\partial y} = -\,u_2\,\frac{\partial v_2}{\partial x} - v_2\,\frac{\partial v_2}{\partial y} - w_2\,\frac{\partial v_2}{\partial z} \tag{3.56c}$$

$$U(z)\,\frac{\partial w_4}{\partial x} + \frac{\partial p_4}{\partial z} = -\,u_2\,\frac{\partial w_2}{\partial x} - v_2\,\frac{\partial w_2}{\partial y} - w_2\,\frac{\partial w_2}{\partial z} . \tag{3.56d}$$

As expected, the equations governing the $O(\epsilon^4)$ terms in the outer region contain the same linear operators as those governing the $O(\epsilon^2)$ terms. However, at $O(\epsilon^4)$ the equations

are inhomogeneous, with source terms involving products of the $O(\epsilon^2)$ terms. Unfortunately, the $O(\epsilon^2)$ terms are only known in the form of Fourier integrals, and the nonlinear character of the right hand sides of (3.56) introduces difficulties in obtaining a particular solution. Hence, we do not pursue the analysis of the $O(\epsilon^4)$ terms in the outer region further.

3.7 Summary for Nonlifting Bodies

In summary, we have used singular perturbation techniques to analyze rotational, spanwise periodic flow past a nonlifting, two-dimensional body. The body cross-sectional size L is assumed to be small compared to the period ℓ of the oncoming flow U(z). The singular perturbation analysis involves three regions: the inner, wake and outer regions.

In the inner region, the primary flow (U_0, V_0, P_0) corresponds to potential flow past the body with a local free stream value of U(z). The spanwise variation in U(z) produces a weak $O(\epsilon)$ secondary flow W_1 in the spanwise direction. This spanwise flow distorts the vortex lines of the upstream flow. In particular, these vortex lines wrap around the body as they convect downstream, producing significant streamwise vorticity in a wake region directly behind the body. In the outer region, the body appears as a distribution of three-dimensional dipoles, and the wake appears as a sheet of mass sources (or equivalently, as a divortex sheet).

At large distances from the body, the flow takes on the remarkably simple form (3.19). In the vicinity of the downstream direction, this must be supplemented by the Trefftz plane flow field (3.36).

Higher order approximations to the inner region were considered. Terms of $O(\epsilon^2 \log\epsilon)$ in (U, V, P) and $O(\epsilon^2, \epsilon^3 \log\epsilon, \epsilon^3)$ in W arise in the analysis and have been calculated in closed

form. The equations governing the $O(\epsilon^2)$ terms in (U, V, P) have been found. However, the latter equations involve source terms which must be evaluated numerically, and hence the solution of these equations would require a substantial numerical effort, which have not been attempted. Similarly, in the outer region the $O(\epsilon^3, \epsilon^4 \log\epsilon)$ terms can be calculated analytically, whereas the equations governing the $O(\epsilon^4)$ contributions have nonlinear source terms which must be evaluated numerically.

CHAPTER 4

THEORY FOR LIFTING BODIES

In this chapter, we utilize singular perturbation techniques to analyze the flow field produced by a lifting body interacting with a periodic, parallel shear flow. The flow in the inner region near the the body was analyzed in Chapter 2. There it was found that the inner region perturbation series was nonuniform at distances $R = O(1/\epsilon)$ from the body. In this chapter, we develop the complementary outer expansion which holds at distances $r = \epsilon R = O(1)$. In addition, for streamlines that have passed within an O(1) distance of the body, a separate wake region far downstream of the body must be considered. After developing the leading order expansions in the outer and wake regions, we calculate the next term in the inner region expansion. Finally, the difficulties in extending the outer region analysis to higher order are discussed.

4.1 Outer Region Flow Generated by the Lifting Line

The analysis of Section 2.3 suggests that the leading term in the outer region is of $O(\epsilon)$, and corresponds to the flow generated by a spanwise distribution of three-dimensional lift forces. Hence, introducing the lift force distribution $\epsilon f(z)\delta(x)\delta(y)$ in the y momentum equation, the linearized equations (3.4) in the outer region take the form

$$\frac{\partial u_1}{\partial x} + \frac{\partial v_1}{\partial y} + \frac{\partial w_1}{\partial z} = 0 \tag{4.1a}$$

$$U(z)\frac{\partial u_1}{\partial x} + w_1 \frac{dU(z)}{dz} = -\frac{\partial p_1}{\partial x} \tag{4.1b}$$

$$U(z)\frac{\partial v_1}{\partial x} = -\frac{\partial p_1}{\partial y} + \epsilon f(z)\delta(x)\delta(y) \tag{4.1c}$$

$$U(z)\frac{\partial w_1}{\partial x} = -\frac{\partial p_1}{\partial z}, \tag{4.1d}$$

where $f(z) = \dfrac{f'}{\rho' U_\infty{}^2 \ell}$ is the unknown distribution of the nondimensional lift force.

Equations (4.1b,d) can be integrated in the form (3.4d,c), while substituting (3.4a) in (4.1c) and integrating partially with respect to x leads to

$$v_1 = -\frac{\partial^2 g_1}{\partial y \partial x} + \frac{\epsilon f(z)}{U(z)} H(x)\delta(y), \tag{4.2}$$

where we have assumed that $(g_1)_{yx}$ vanishes as $x \to -\infty$. Substituting these expressions for the velocity field into the continuity equation (4.1a), and integrating partially with respect to x, we obtain

$$L(g_1) = \epsilon x H(x) \frac{d\delta(y)}{dy} \frac{f(z)}{U(z)}. \tag{4.3}$$

Equation (4.3) is solved by Fourier transform techniques. The details are similar to those in Section 3.5, and hence we simply quote the final result

$$g_1 = \epsilon \sum_{n=0}^{\infty} C_n(x,y) E_n(z) \tag{4.4a}$$

$$C_n(x,y) = -\frac{1}{4\pi} f_n \ \mathrm{sgn}(y) \int_{-\infty}^{\infty} \frac{e^{-|y|\sqrt{k^2+\lambda_n^2}}}{(k+i\beta)^2} e^{-ikx}\, dk\,, \tag{4.4b}$$

where

$$f_n = \int_0^1 \frac{f(z)}{U(z)} E_n(z)\, dz\,. \tag{4.4c}$$

The pressure field produced by (4.4) is particularly simple, since differentiating (4.4b) twice with respect to x and taking the limit $\beta \to 0$ gives

$$\frac{\partial^2 C_n}{\partial x^2} = \frac{1}{4\pi} f_n \ \mathrm{sgn}(y) \int_{-\infty}^{\infty} e^{-|y|\sqrt{k^2+\lambda_n^2}} e^{-ikx}\, dk = \frac{1}{2\pi} \lambda_n f_n \sin\theta K_1(\lambda_n r)\,. \tag{4.5}$$

Utilizing (4.4a) and (3.4a) the pressure field is then given by

$$p_l = \epsilon \frac{1}{2\pi} \sin\theta\ U(z) \sum_{n=0}^{\infty} f_n\, \lambda_n\, K_1(\lambda_n r)\, E_n(z) \tag{4.6}$$

where, as $r \to 0$

$$\lambda_n\, K_1(\lambda_n r) = \frac{1}{r}\,.$$

To determine the lift force spanwise distribution f(z), we match the inner and outer

regions. Consider the matching of the O(1) inner pressure field (2.12c) and the O(ϵ) outer pressure field (4.6). The expansion to O(ϵ) in outer variables of (2.12c) is given by (2.16c)

$$- \epsilon \frac{1}{2\pi} U^2(z)\, \Gamma \frac{\sin\theta}{r} .$$

Substituting $r = \epsilon R$ in (4.6), expanding for small ϵ and truncating at O(1), we find

$$\frac{1}{2\pi} f(z) \frac{\sin\theta}{R} .$$

Comparing these expressions in either inner or outer variables, the matching condition gives

$$f(z) = - \Gamma U^2(z) . \tag{4.7}$$

Hence, the matching at leading order corresponds to the familiar potential flow Kutta Joukowski Theorem relating circulation and lift. Matching of the remaining variables is most conveniently done by expanding $C_n(r,\theta)$ for small r. The small r expansion of (4.4b) is obtained utilizing composite expansion techniques in Appendix B. We find that matching of the O(ϵ) outer expansions and O(1) inner expansions for U or V, or matching the O(ϵ) outer and O(ϵ) inner expansions for W, also leads to the result (4.7).

Returning to (4.4), we now examine the physical flow features associated with g_l. The singularities of (4.4b) are a double pole at $k = -i\beta$ ($\beta \to 0$) and branch points at $\mp i\lambda_n$. For $x > 0$, the double pole of C_n produces the residue contribution

$$\frac{1}{2} f_n \times \mathrm{sgn}(y)\, e^{-\lambda_n |y|} .$$

The velocity field corresponding to this residue contribution is the Trefftz plane. Utilizing (3.4c,d) and (4.2), the Trefftz plane velocity field is

$$u_1(x,y,z) = \epsilon \frac{U'(z)}{U^2(z)} \sum_{n=1}^{\infty} \frac{1}{2} f_n \times \mathrm{sgn}(y)\, e^{-\lambda_n |y|} \frac{\partial}{\partial z}[U(z)E_n(z)] \tag{4.8a}$$

$$v_1(x,y,z) = \epsilon \sum_{n=1}^{\infty} \frac{1}{2} f_n \lambda_n H(x)\, e^{-\lambda_n |y|} E_n(z) \tag{4.8b}$$

$$w_1(x,y,z) = -\epsilon \frac{1}{U(z)} \sum_{n=1}^{\infty} \frac{1}{2} f_n H(x)\, \mathrm{sgn}(y)\, e^{-\lambda_n |y|} \frac{\partial}{\partial z} [U(z)E_n(z)] , \tag{4.8c}$$

while the pressure field vanishes. Note that the second term of (4.2) has cancelled with the result produced by differentiating sgn(y). The y component of velocity is an even function of y, while u_1 and w_1 are odd in y and discontinuous across y = 0. As in Section 3.5 the streamwise velocity grows linearly with x, due to the spanwise convection of surfaces of constant stagnation pressure by w_1.

The discontinuity in w_1 across wake is associated with streamwise vorticity which, on the outer scale, is concentrated in a sheet of zero thickness. The streamwise vorticity per unit length, $\gamma(z)$ is given by

$$\gamma(z) = w_1(0+,z) - w_1(0-,z) = \epsilon 2\Gamma \frac{dU(z)}{dz} . \tag{4.9}$$

In the lifting line theory for uniform upstream flow, the trailing vorticity is equal to the spanwise derivative of the circulation about the body. Here, we find that the trailing vorticity is equal to the spanwise derivative of the product of the circulation $\Gamma U(z)$ and the oncoming flow $U(z)$, or from (4.7) to the spanwise derivative of the lift force on the body. The velocity $v_1(0,z)$ is the downwash in the Trefftz plane induced by the trailing vorticity $\gamma(z)$.

Next consider the behavior of the velocity field for $r >> 1$. Utilizing the method of steepest descent, we find that the integral is dominated by the vicinity of the saddle point $k = -i\lambda_n \cos\theta$, leading to the result

$$C_n = \frac{1}{2} f_n \left\{ e^{-\lambda_n r \sin\theta} \cos\theta \; r \; H\left(\frac{\pi}{2} - \theta\right) + \frac{e^{-r\lambda_n}}{\sqrt{2\pi\lambda_n}\lambda_n} \frac{\sin\theta}{\cos^2\theta} \frac{1}{\sqrt{r}} (1+O(1/r)) \right\} \qquad (4.10a)$$

for $y > 0$. (A similar result holds for $y < 0$ by symmetry.) However, as in Section 3.5 this result is not valid for $\theta \to \pi/2$, due to the coalescence of the double pole and the saddle point. In Appendix A we utilize a method similar to that of Van Der Waerden (1950) to derive the uniformly valid expansion

$$C_n = \frac{1}{2} f_n \left\{ r\cos\theta e^{-r\lambda_n \sin\theta} \left[H\left(\frac{\pi}{2}-\theta\right) - \frac{1}{2}\mathrm{sgn}\left(\frac{\pi}{2}-\theta\right) \mathrm{erfc}\sqrt{r\lambda_n(1-\sin\theta)} \right] \right.$$

$$\left. + \frac{e^{-r\lambda_n}}{2\sqrt{\pi\lambda_n r}} \left[r\sqrt{1+\sin\theta} + \frac{\sqrt{2}\sin\theta - \frac{1}{2}(1+\sin\theta)^{3/2}}{\lambda_n \cos^2\theta} (1+O(1/r)) \right] \right\} \qquad (4.10b)$$

Despite the fact that unbounded terms arise in the r >> 1 expansion of C_0, these disappear when we utilize (3.4) and (4.2) to calculate the velocity field. We find

$$\frac{u_1}{\epsilon} = \frac{\Gamma}{2\pi U(z)} e_0 u_0 \frac{\sin\theta}{r} + \frac{\Gamma}{2\pi} \sin\theta u_1 E_1(z) \sqrt{\frac{\pi\lambda_1}{2r}} e^{-\lambda_1 r}[1+O(1/r)]$$

$$- \frac{1}{2}\Gamma u_1 \frac{\frac{dU(z)}{dz}}{U^2(z)} \frac{d}{dz}(U(z)E_1(z)) \left\{ r\cos\theta e^{-r\lambda_1 \sin\theta} \left[H\left(\frac{\pi}{2}-\theta\right) - \frac{1}{2}\mathrm{sgn}\left(\frac{\pi}{2}-\theta\right) \mathrm{erfc}\sqrt{r\lambda_1(1-\sin\theta)} \right] \right.$$

$$\left. + \frac{e^{-r\lambda_1}}{2\sqrt{\pi\lambda_1 r}} \left[r\sqrt{1+\sin\theta} + \frac{\sqrt{2}\sin\theta - \frac{1}{2}(1+\sin\theta)^{3/2}}{\lambda_1 \cos^2\theta} (1+O(1/r)) \right] \right\} \qquad (4.11a)$$

$$\frac{v_1}{\epsilon} = - \frac{\Gamma}{2\pi U(z)} e_0 u_0 \frac{\cos\theta}{r} - \frac{1}{2}\Gamma u_1 E_1(z) \left\{ \lambda_1 e^{-r\lambda_1 \sin\theta} \left[H\left(\frac{\pi}{2}-\theta\right) - \frac{1}{2}\mathrm{sgn}\left(\frac{\pi}{2}-\theta\right) \mathrm{erfc}\sqrt{r\lambda_1(1-\sin\theta)} \right] \right.$$

$$\left. + \sqrt{\frac{\lambda_1}{\pi}} \frac{e^{-r\lambda_1}}{2\sqrt{r}} \left[\mathrm{sgn}\left(\frac{\pi}{2}-\theta\right) \sqrt{1-\sin\theta} + \sin\theta \frac{\sqrt{1+\sin\theta} - \sqrt{2}\sin\theta}{\cos\theta} \right] + O(1/r^{3/2}) \right\} \qquad (4.11b)$$

$$\frac{w_1}{\epsilon} = \frac{1}{2}\Gamma \frac{1}{U(z)} u_1 \frac{d}{dz}(U(z)E_1(z)) \left\{ e^{-r\lambda_1 \sin\theta} \left[H\left(\frac{\pi}{2}-\theta\right) - \frac{1}{2}\mathrm{sgn}\left(\frac{\pi}{2}-\theta\right) \mathrm{erfc}\sqrt{r\lambda_1(1-\sin\theta)} \right] \right.$$

$$\left. + \frac{e^{-r\lambda_1}}{2\sqrt{\pi\lambda_1 r}} \frac{\sqrt{1+\sin\theta} - \sqrt{2}\sin\theta}{\cos\theta} + O(1/r^{3/2}) \right\} \qquad (4.11c)$$

and from (4.6) the corresponding expansion for the pressure is

$$\frac{p_1}{\epsilon} = -\frac{\Gamma}{2\pi}e_0 u_0 \frac{\sin\theta}{r} - \frac{\Gamma}{2\pi}\sin\theta u_1 U(z)E_1(z)\sqrt{\frac{\pi\lambda_1}{2r}}e^{-\lambda_1 r}[1+O(1/r)]\,. \qquad (4.11d)$$

For large r, the terms $n > 1$ in the sum (4.4a) are exponentially small relative to the error in C_1, and hence have been neglected.

Equations (4.11) show that, far from the body, the flow field exhibits an exponential decay to a simple asymptotic state. In this asymptotic state the fluid particles move in planes z = constant, and the dependence on r and θ is identical to that for a two-dimensional, potential flow with circulation. The asymptotic flow disturbances exhibit an amplitude dependence on spanwise position proportional to 1/U(z). The physical mechanisms leading to the results are similar to those discussed in Section 3.3 for the far field (3.20) of the dipole line.

4.2 The Wake Region

In this section, we analyze the wake region for the case of a lifting body. This wake region matches with the $X >> 1$, $\Psi = O(1)$ asymptotic behavior (2.17c) of the inner region spanwise velocity. We shall find that the wake region also resolves the discontinuity across y = 0 for the spanwise velocity in the outer region.

The wake region for a lifting body has many features in common with the case of a nonlifting body, which was analyzed in Section 3.4. The main difference for the case of a lifting body is that the circulation about the body and the associated trailing vorticity deflects the wake region downwards so that it is no longer centered on the line Y = 0. The

vertical position $y'_0(x',z')$ of the streamline which passes through the rear stagnation point of the body is given in dimensional form by

$$y_0'(x',z') = y_s' + \int_{x_s'}^{x'} \frac{v'}{u'} d\tilde{x}' , \tag{4.12a}$$

where the integration path is along the line Ψ = constant. Utilizing separate approximations for the integrand in the regions $x' = O(L)$ and $x' = O(l)$, we have

$$Y_0(x,z) = Y_s + \int_{X_s}^{\frac{\alpha}{\epsilon}} \frac{V_0}{U_0} dX + \frac{1}{\epsilon} \int_{\alpha}^{x} \frac{v_1(\tilde{x}',y,z)}{U(z)} d\tilde{x}' , \tag{4.12b}$$

where $Y_0 = y_0'/L$ and $\epsilon << \alpha(\epsilon) << 1$. The first integral can be evaluated indirectly by noting that, in the inner region,the streamline $\Psi = 0$ is given by $Im(G) = 0$. For $X = \alpha/\epsilon >> 1$, we find from (2.15) that $Im(G) = 0$ on the line

$$Y = - \frac{\Gamma}{2\pi} \log\left[\frac{\alpha}{\epsilon}\right] + O\left[\frac{\epsilon}{\alpha}\right] . \tag{4.12c}$$

The leading order term of the second integral (in 4.12b) can be found by setting $y = 0$ in the integrand. From (4.2) and (4.4) we have

$$v_1(x,0,z) = \epsilon\left\{\frac{f_0E_0(z)}{2\pi x} + \sum_{n=1}^{\infty} f_nE_n(z)\left[\frac{1}{2}\lambda_n + \frac{e^{-\lambda_n x}}{2\pi}\int_0^{\infty}\frac{\sqrt{t^2+2\lambda_n t}}{t+\lambda_n}e^{-tx}\,dt\right]\right\}. \quad (4.12d)$$

Integrating with respect to x, and expanding the result for small α, we have

$$\frac{1}{\epsilon}\int_{\alpha}^{x} v_1\frac{x,0,z}{U(z)}\,dx = \Gamma\,\frac{\log\alpha}{2\pi} - \sum_{n=1}^{\infty}\frac{f_nE_n(z)}{U(z)}(1+E+\log\lambda_n) + \frac{i}{U(z)}\frac{f_0E_0(z)}{2\pi}\log x$$

$$+\sum_{n=1}^{\infty}\frac{f_nE_n(z)}{U(z)}\left\{\frac{1}{2}\lambda_n x + \frac{1}{2\pi}\left[e^{-\lambda_n x}\int_0^{\infty}\frac{\sqrt{t^2+2\lambda_n t}}{(t+\lambda_n)^2}e^{-tx}\,dt\right]\right\} + O(\alpha)\,. \quad (4.12e)$$

Combining (4.12c,e), we find that the dependence on $\alpha(\epsilon)$ cancels out to the order of our approximation, giving

$$Y_0 = \frac{\Gamma}{2\pi}\log\epsilon - \sum_{n=1}^{\infty}\frac{f_nE_n(z)}{U(z)}(1+E+\log\lambda_n) + \frac{1}{U(z)}\frac{f_0E_0(z)}{2\pi}\log x$$

$$+\sum_{n=1}^{\infty}\frac{f_nE_n(z)}{U(z)}\left\{\frac{1}{2}\lambda_n x + \frac{1}{2\pi}\left[e^{-\lambda_n x}\int_0^{\infty}\frac{\sqrt{t^2+2\lambda_n t}}{(t+\lambda_n)^2}e^{-tx}\,dt\right]\right\} + O(\alpha) + O\left[\frac{\epsilon}{\alpha}\right]. \quad (4.12f)$$

Hence,the downward deflection of the wake is large compared to L, but small compared to ℓ.

The wake region has an O(L) thickness centered on the surface $y_0(x,z)$, hence we introduce the dependent variables

$$\tilde{x} = x \tag{4.13a}$$

$$\tilde{Y} = \frac{y-y_0(x,z)}{\epsilon} \tag{4.13b}$$

$$\tilde{z} = z\,. \tag{4.13c}$$

The wake region analysis of Section 3.4 for the case of a nonlifting body provides guidance for the scaling of the dependent variables. There we found $O(\epsilon)$ perturbations for the x and z components of velocity, and $O(\epsilon^2)$ perturbations for the pressure and Y component of velocity. The physical balances that led to these scalings are also appropriate for the case of a lifting body, except that the $O(\epsilon^2)$ term in V is preceded by an $O(\epsilon)$ term representing the downwash produced by the bound and trailing vorticity. Hence we have the expansions

$$U = U(\tilde{z}) + \epsilon\tilde{u}_1(\tilde{x},\tilde{Y},\tilde{z}) + \cdots \tag{4.14a}$$

$$V = \epsilon\tilde{v}_0(\tilde{x},\tilde{Y},\tilde{z}) + \epsilon^2\tilde{v}_1(\tilde{x},\tilde{Y},\tilde{z}) + \cdots \tag{4.14b}$$

$$W = \epsilon\tilde{w}_1(\tilde{x},\tilde{Y},\tilde{z}) + \cdots \tag{4.14c}$$

$$P = \epsilon^2\tilde{p}_1(\tilde{x},\tilde{Y},\tilde{z}) + \cdots\,. \tag{4.14d}$$

Substituting (4.14) in the full governing equations (2.6) and applying the chain rule to (4.13) to obtain

$$\frac{\partial}{\partial x} = \frac{\partial}{\partial \tilde{x}} - \frac{\partial Y_0}{\partial x} \frac{\partial}{\partial \tilde{Y}} \tag{4.15a}$$

$$\frac{\partial}{\partial y} = \frac{1}{\epsilon} \frac{\partial}{\partial \tilde{Y}} \tag{4.15b}$$

$$\frac{\partial}{\partial z} = \frac{\partial}{\partial \tilde{z}} - \frac{\partial Y_0}{\partial z} \frac{\partial}{\partial \tilde{Y}} . \tag{4.15c}$$

We find upon separating orders of ϵ that of leading order the continuity equation reduces to

$$\frac{\partial \tilde{v}_0}{\partial \tilde{Y}} = 0 , \tag{4.16a}$$

while leading order terms of the momentum equations are

$$U(\tilde{z}) \frac{\partial \tilde{u}_1}{\partial \tilde{x}} + \tilde{w}_1 \frac{dU(\tilde{z})}{d\tilde{z}} = 0 \tag{4.16b}$$

$$U(\tilde{z}) \frac{\partial \tilde{v}_0}{\partial \tilde{x}} = - \frac{\partial \tilde{p}_1}{\partial \tilde{Y}} \tag{4.16c}$$

$$\frac{\partial \tilde{w}_1}{\partial \tilde{x}} = 0 . \qquad (4.16d)$$

It should be noted that $V/U = O(L/\ell)$ in the wake region, and hence convection by $\tilde{v}_0$ enters at leading order in the operator $\vec{u}'.\nabla$. However, since $\partial Y_0/\partial x = \tilde{v}_0/U(z)$, the appearance of this convection term is suppressed by the coordinate transformation (4.13).

Equation (4.16a) immediately integrates to $\tilde{v}_0 = \tilde{v}_0(\tilde{x},\tilde{z})$, and matching with the $O(\epsilon)$ expansion in the outer region gives

$$\tilde{v}_0(\tilde{x},\tilde{z}) = \frac{f_0 E_0(z)}{2\pi x} + \sum_{n=1}^{\infty} f_n E_n(z) \left\{ \frac{1}{2}\lambda_n + \frac{e^{-\lambda_n \tilde{x}}}{2\pi} \int_0^{\infty} \frac{\sqrt{t^2+2\lambda_n t}}{t+\lambda_n} e^{-t\tilde{x}} \, dt \right\} . \qquad (4.17a)$$

Equation (4.16c) can be integrated partially with respect to $\tilde{Y}$ to obtain

$$\tilde{p}_1 = -U(\tilde{z}) \frac{\partial \tilde{v}_0}{\partial \tilde{x}} \tilde{Y} + \tilde{p}_c(\tilde{x},\tilde{z}) . \qquad (4.17b)$$

The function $\tilde{p}_c(\tilde{x},\tilde{z})$ is determined by matching of the expansions for pressure in the wake and outer regions. The leading order matching condition involves the $O(\epsilon)$ outer expansion and the $O(\epsilon^2)$ wake expansion. The expressions (4.6) and (4.17b) are found to satisfy the leading order matching condition. (Upon applying the operator $\partial/\partial\tilde{x}$ to (4.17a),the integral can be evaluated in terms of $K_1(\lambda_n\tilde{x})$). However, the leading order matching leaves $\tilde{p}_c(\tilde{x},\tilde{z})$ undetermined, since this function disappears when (4.17b) is expanded to $O(\epsilon)$ in outer variables. A match with the $O(\epsilon^2)$ outer expansion is required to determine $\tilde{p}_c(\tilde{x},\tilde{z})$. Hence, we have found that the leading order terms for V and P in the wake region are

essentially contained in the outer expansions. This result is not surprising, since neither the inner nor outer expansions for those variables showed any signs of nonuniformity with respect to variations in θ.

Now consider (4.16b,d) governing $\tilde{w}_1$ and $\tilde{u}_1$. These equations are identical in form to (3.22b,d) for the case of a nonlifting body. The integrations and matching of the wake and inner regions proceed exactly as in Section 3.4, leading to the results

$$\tilde{u}_1 = \frac{1}{U(\tilde{z})} \left[\frac{dU(\tilde{z})}{d\tilde{z}} \right]^2 D(\tilde{Y})\, \tilde{x} \tag{4.18a}$$

and

$$\tilde{w}_1 = -\frac{dU(\tilde{z})}{d\tilde{z}} D(\tilde{Y}) . \tag{4.18b}$$

The $O(\epsilon)$ expansions for U and W in the wake and outer regions are found to satisfy the matching condition, providing a partial check on the analysis. The only new feature arising in the matching is that here $D(\tilde{Y}) \to \pm \Gamma$ for $\tilde{Y} \to \mp \infty$, as compared to $|Y|^{-3}$ decay found for nonlifting bodies in Section 3.4. The behavior found here arises due to the presence of net streamwise vorticity in the wake region.

Finally, we consider the next higher approximation to the continuity equation

$$\frac{\partial \tilde{u}_1}{\partial \tilde{x}} - \frac{\partial Y_0}{\partial \tilde{x}} \frac{\partial \tilde{u}_1}{\partial \tilde{Y}} + \frac{\partial \tilde{v}_1}{\partial \tilde{Y}} + \frac{\partial \tilde{w}_1}{\partial \tilde{z}} - \frac{\partial Y_0}{\partial \tilde{z}} \frac{\partial \tilde{w}_1}{\partial \tilde{Y}} = 0 . \tag{4.19a}$$

This can be integrated partially with respect to $\tilde{Y}$ to give

$$\tilde{v}_1 = -\int_0^{\tilde{Y}} \left[\frac{\partial \tilde{u}_1}{\partial \tilde{x}} + \frac{\partial \tilde{w}_1}{\partial \tilde{z}} \right] d\tilde{Y}' + \frac{\partial Y_0}{\partial \tilde{x}} \tilde{u}_1 + \frac{\partial Y_0}{\partial \tilde{z}} \tilde{w}_1 + \tilde{v}_c(\tilde{x},\tilde{z}) . \qquad (4.19b)$$

The first term of (4.19b) is identical to the result (3.23b) for the case of a nonlifting body. The two additional terms involving derivatives of Y_0 represent vertical velocities produced by deformation of the wake sheet out of the plane y = 0. Asymptotic matching of the $O(\epsilon^2)$ wake expansion and $O(\epsilon)$ outer expansion for V provides a consistency check, but leaves $\tilde{v}_c(\tilde{x},\tilde{z})$ undetermined. A match with the $O(\epsilon^2)$ outer expansion is required to determine $\tilde{v}_c(\tilde{x},\tilde{z})$.

The physical interpretation of the wake region flow field is very similar to that for the case of a nonlifting body. Streamwise vorticity is generated by the wrapping of vortex lines around the body. The most significant difference compared to the case of a nonlifting body is that here the wake region contains net vorticity, i.e.

$$\int_{-\infty}^{\infty} \tilde{\omega}_x \, d\tilde{Y} = \tilde{w}_1(\tilde{x},\infty,\tilde{z}) - \tilde{w}_1(\tilde{x},-\infty,\tilde{z}) = 2\Gamma \frac{dU(z)}{dz} .$$

This net streamwise vorticity appears as a sheet of trailing vorticity when viewed in outer coordinates, see (4.9). Since the influence of this trailing vorticity arises directly in the solution for the outer region, the leading terms in the inner and outer regions can be found without explicitly considering the wake region. In contrast, the wake region made an essential contribution to the leading term in the outer region for the case of a nonlifting

body. Numerical results and further discussion of the wake region will be presented in Chapter 5.

4.3 Higher Order Approximation for the Inner Region

In this section, we develop the first higher order correction to the flow in the inner region. As discussed in Section 3.6, when the inner region is considered in isolation, higher order terms first arise at $O(\epsilon^2)$ for U, V and P and $O(\epsilon^3)$ for W. However, since these inner region expansions are nonuniform for large R, we anticipate that matching of the inner and outer regions may force lower order terms into the inner expansion.

To examine this, we expand the $O(\epsilon)$ outer field in inner coordinates. From (B.10) of Appendix B, the expansion in inner coordinates of the coefficient C_n in the pseudo potential g_1 takes the form

$$C_n(\epsilon,R,\theta) = -\frac{1}{2\pi} f_n \left\{ \epsilon \log\epsilon R\sin\theta + \epsilon \left[R\log R\sin\theta - R\cos\theta(\pi-\theta) + R\sin\theta \left(\log\frac{\lambda_n}{2} + E \right) \right] \right.$$

$$\left. + \epsilon^2 R^2 \frac{\pi}{2}\lambda_n \sin\theta\cos\theta \right\} + O(\epsilon^3) . \qquad (4.20a)$$

The case n = 0 must be treated separately; the relevant results are given in (B.11). Utilizing (3.4) and (4.2), the physical flow variables take the form

$$[U(z) + \epsilon u_1]_i = U(z) + \frac{1}{2\pi}\frac{\sin\theta}{R}\Gamma\, U(z) + O(\epsilon^2\log\epsilon, \epsilon^2) \qquad (4.20b)$$

$$[\epsilon v_1]_i = -\frac{\Gamma}{2\pi} U(z) \frac{\cos\theta}{R} + \epsilon V_i(z) + O(\epsilon^2) \tag{4.20c}$$

$$[\epsilon p_1]_i = -\frac{1}{2\pi} \frac{\sin\theta}{R} \Gamma U^2(z) + O(\epsilon^2 \log\epsilon, \epsilon^2) \tag{4.20d}$$

$$[\epsilon w_1]_i = \epsilon \frac{1}{\pi} \Gamma U'(z) (\pi-\theta) + O(\epsilon^2) , \tag{4.20e}$$

where

$$V_i(z) = \frac{1}{4} \sum_{n=0}^{\infty} f_n \lambda_n E_n(z) .$$

The leading terms of (4.20) were previously found to match with the inner region O(1) expansions for U, V and P and the O(ϵ) expansion for W. However, our expansion of the outer solution g_1 in inner coordinates to higher order shows the existence of an O(ϵ) contribution to the vertical velocity. This contribution is the downwash produced by the trailing vorticity in the wake region, and is exactly half the value (4.8b) at y = 0 far downstream in the Trefftz plane. This result is due to the semi-infinite nature of the trailing vortex sheet and is entirely consistent with classical lifting line theory for potential flow.

We now develop the inner region flow field corresponding to this downwash velocity. Substituting the expansions

$$U = U_0 + \epsilon U_1 + \cdots \tag{4.21a}$$

$$V = V_0 + \epsilon V_1 + \cdots \tag{4.21b}$$

$$W = \epsilon W_1 + \epsilon^2 W_2 + \cdots \tag{4.21c}$$

$$P = P_0 + \epsilon P_1 + \cdots . \tag{4.21d}$$

into the governing equations (2.6), the $O(\epsilon)$ contributions to U, V and P are found to satisfy

$$\frac{\partial U_1}{\partial X} + \frac{\partial V_1}{\partial Y} = 0 \tag{4.22a}$$

$$U_0 \frac{\partial U_1}{\partial X} + V_0 \frac{\partial U_1}{\partial Y} + U_1 \frac{\partial U_0}{\partial X} + V_1 \frac{\partial U_0}{\partial Y} + \frac{\partial P_1}{\partial X} = 0 \tag{4.22b}$$

$$U_0 \frac{\partial V_1}{\partial X} + V_0 \frac{\partial V_1}{\partial Y} + U_1 \frac{\partial V_0}{\partial X} + V_1 \frac{\partial V_0}{\partial Y} + \frac{\partial P_1}{\partial Y} = 0 \tag{4.22c}$$

$$(U_1, V_1).(n_X, n_Y) = 0 \quad \text{on} \quad C(X, Y) = 0 \tag{4.22d}$$

and

$$V_1 \rightarrow V_i(z) \, , \, U_1, P_1 \rightarrow 0 \text{ as } R \rightarrow \infty \, , \tag{4.22e}$$

where (4.22e) has been introduced in anticipation of the matching with the outer region.

Equations (4.22a,d,e) can be solved by introducing a pseudo-potential $\Phi_1(X, Y, z)$ such that

$$U_1 = \frac{\partial \Phi_1}{\partial X}\,,\; V_1 = \frac{\partial \Phi_1}{\partial Y}\,. \tag{4.23}$$

Substitution into (4.22a,d,e) produces the boundary value problem

$$\frac{\partial^2 \Phi_1}{\partial X^2} + \frac{\partial^2 \Phi_1}{\partial Y^2} = 0 \tag{4.24a}$$

$$\nabla \Phi_1 . \vec{n} = 0 \quad \text{on } C(X,Y) = 0 \tag{4.24b}$$

$$\nabla \Phi_1 \rightarrow V_i(z)\ \vec{e}_Y \text{ as } R \rightarrow \infty\,. \tag{4.24c}$$

Equations (4.24) define a standard boundary value problem of potential theory, whose solution can be expressed as

$$\Phi_1(X,Y,z) = V_i(z)\ \ \mathrm{Re}[G_1(\zeta)]\,, \tag{4.25}$$

where G_1 is an analytic of the complex variable $\zeta = X + iY$, and Re denotes the real part. The specific form of G_1 is determined by the body shape $C(X,Y) = 0$. Substituting (4.23) into (4.22b,c), integrating these equations partially with respect to X and Y, and using (4.22e) to evaluate the arbitrary function of z, we obtain

$$P_1 = -\frac{\partial \Phi_0}{\partial X}\frac{\partial \Phi_1}{\partial X} - \frac{\partial \Phi_0}{\partial Y}\frac{\partial \Phi_1}{\partial Y}\,. \tag{4.26}$$

The general characteristics of the $O(\epsilon)$ corrections U_1, V_1 and P_1 are the same as the leading order terms U_0, V_0 and P_0. Both U_0, V_0, P_0 and U_1, V_1, P_1 correspond to two-

dimensional potential flow. In fact, the calculation of the O(1) and O(ϵ) terms can easily be combined by simply solving the following potential flow problem for $\hat{\Phi} = \Phi_0 + \epsilon\Phi_1$.

$$\frac{\partial^2\hat{\Phi}}{\partial X^2} + \frac{\partial^2\hat{\Phi}}{\partial Y^2} = 0 \tag{4.27a}$$

$$\nabla\hat{\Phi}.\vec{n} = 0 \quad \text{on } C(X,Y) = 0 \tag{4.27b}$$

$$\nabla\hat{\Phi} \rightarrow U(z)\,\vec{e}_X + \epsilon V_i(z)\,\vec{e}_Y \text{ as } R\rightarrow\infty\,, \tag{4.27c}$$

where the X and Y components of velocity are given by

$$\hat{U} = \frac{\partial\hat{\Phi}}{\partial X}\,, \tag{4.27d}$$

$$\hat{V} = \frac{\partial\hat{\Phi}}{\partial Y} \tag{4.27e}$$

and the pressure is given by

$$\hat{P} = \frac{1}{2}\left[U^2(z) + \epsilon^2 V_i^2(z) - \left(\frac{\partial\hat{\Phi}}{\partial X}\right)^2 - \left(\frac{\partial\hat{\Phi}}{\partial Y}\right)^2\right]. \tag{4.27f}$$

Equation (4.26) is the O(ϵ) component of (4.27f).

Now consider the O(ϵ^2) correction to the spanwise velocity. Substituting (4.21) into (2.6d), we obtain a second order equation for W_2

$$U_0 \frac{\partial W_2}{\partial X} + V_0 \frac{\partial W_2}{\partial Y} = -\left[U_1 \frac{\partial W_1}{\partial X} + V_1 \frac{\partial W_1}{\partial Y} + \frac{\partial P_1}{\partial z}\right]. \tag{4.28a}$$

This equation can be integrated to yield

$$W_2 = -\int^{S} \frac{1}{q_0} \left[U_1 \frac{\partial W_1}{\partial X} + V_1 \frac{\partial W_1}{\partial Y} + \frac{\partial P_1}{\partial z}\right] d\tilde{S} . \tag{4.28b}$$

The indefinite integral (4.28b) contains an arbitrary function of Y and Z which is determined by asymptotic matching with the outer flow as $X \rightarrow -\infty$. The large R behavior of U_1, V_1 and P_1 are given by

$$U_1 = - V_i(z) \frac{\Gamma_1}{2\pi} \frac{Y}{X^2+Y^2} + O\left(\frac{1}{R^2}\right) \tag{4.29a}$$

$$V_1 = V_i(z)\left[1 + \frac{\Gamma_1}{2\pi} \frac{X}{X^2+Y^2}\right] + O\left(\frac{1}{R^2}\right) \tag{4.29b}$$

$$P_1 = U(z)V_i(z) \left[\frac{\Gamma X+\Gamma_1 Y}{2\pi(X^2+Y^2)} + O\left(\frac{1}{R^2}\right)\right]. \tag{4.29c}$$

Utilizing the results of (2.17a), we then find

$$W_2 = \frac{\Gamma}{2\pi}\left[\frac{1}{2} V_i'(z) + \frac{3}{2} V_i(z) \frac{U'(z)}{U(z)}\right] \log R + O(1) . \tag{4.29d}$$

Hence, the second order expansion $W = \epsilon W_1 + \epsilon^2 W_2 + O(\epsilon^3)$ exhibits a nonuniformity for large R. This nonuniformity can be traced to the fact that the expansion in the inner region assumes that fluid particles are convected along the streamlines of the leading order velocity field (U_0, V_0). Though the magnitude of the perturbation velocity (U_1, V_1) remains bounded relative to that of (U_0, V_0), the actual streamlines diverge from those of (U_0, V_0) at large distances from the body.

We shall now show that the nonuniformity in W for large R can be removed by utilizing the potential flow (4.27) which incorporates both the O(1) and $O(\epsilon)$ components. Writing $\hat{W} = \epsilon W_1 + \epsilon^2 W_2$, (2.13) and (4.28a) can be combined in the form

$$\hat{U} \frac{\partial \hat{W}}{\partial X} + \hat{V} \frac{\partial \hat{W}}{\partial Y} = - \frac{\partial \hat{P}}{\partial z} . \tag{4.30a}$$

Integrating we find

$$\hat{W} = - \int_{-\infty}^{S} \frac{1}{\hat{q}} \frac{\partial \hat{P}}{\partial z} \, d\tilde{S} . \tag{4.30b}$$

This expression exhibits no nonuniformities for large R.

4.4 Higher Order Approximation For The Outer Region

In this section, we briefly comment on the $O(\epsilon^2)$ correction to the flow in the outer region. Introducing outer coordinates into the $O(\epsilon)$ expansions for U, V and P in the inner region, and expanding to $O(\epsilon^2)$, we find

$$[U_0+\epsilon U_1]_0 = U(z)\left[1 + \epsilon\,\frac{\Gamma}{2\pi}\,\frac{\sin\theta}{r}\right] + \epsilon^2\left\{U(z)\left[-\frac{\mu_X}{2\pi}\,\frac{\cos 2\theta}{r^2} - \frac{\mu_Y}{2\pi}\,\frac{\sin 2\theta}{r^2}\right]\right.$$

$$\left. -V_i(z)\,\frac{\Gamma_1}{2\pi}\,\frac{\sin\theta}{r}\right\} + O(\epsilon^3) \tag{4.31a}$$

$$[V_0+\epsilon V_1]_0 = \epsilon\left[-U(z)\,\frac{\Gamma}{2\pi}\,\frac{\cos\theta}{r} + V_i(z)\right] + \epsilon^2\left\{U(z)\left[-\frac{\mu_X}{2\pi}\,\frac{\sin 2\theta}{r^2} + \frac{\mu_Y}{2\pi}\,\frac{\cos 2\theta}{r^2}\right]\right.$$

$$\left. +V_i(z)\,\frac{\Gamma_1}{2\pi}\,\frac{\cos\theta}{r}\right\} + O(\epsilon^3) \tag{4.31b}$$

$$[P_0+\epsilon P_1]_0 = -\epsilon\,\frac{1}{2}\,U^2(z)\,\frac{\Gamma}{2\pi}\,\frac{2\sin\theta}{r} + \epsilon^2\left\{\frac{1}{2}\,U^2(z)\left[-\frac{\Gamma^2}{4\pi^2}\,\frac{1}{r^2} + \frac{\mu_X}{2\pi}\,\frac{2\cos 2\theta}{r^2} + \frac{\mu_Y}{2\pi}\,\frac{2\sin 2\theta}{r^2}\right]\right.$$

$$\left. + U(z)V_i(z)\,\frac{\Gamma\cos\theta+\Gamma_1\sin\theta}{2\pi r}\right\} + O(\epsilon^3)\,. \tag{4.31c}$$

Applying the same operation to the $O(\epsilon^2)$ inner expansion for the spanwise velocity, we find

$$[\epsilon W_1+\epsilon^2 W_2]_0 = \epsilon\,\frac{\Gamma}{\pi}\,U'(z)\,(\pi-\theta) + \epsilon^2\left\{-\frac{\Gamma^2}{2\pi^2}\,U'(z)\,(\pi-\theta)\,\frac{1}{y} - \frac{\Gamma}{\pi}\,\frac{V_i(z)U'(z)}{U(z)}\right.$$

$$+\frac{\Gamma_1}{2\pi}\frac{1}{U(z)}\frac{d}{dz}[U(z)V_i(z)]\,(\pi-\theta)+\frac{dU(z)}{dz}\left[\frac{\mu_X}{2\pi}\frac{2x}{x^2+y^2}+\frac{\mu_Y}{2\pi}\frac{2y}{x^2+y^2}\right]$$

$$+\frac{y}{4U(z)}\sum_{n=0}^{\infty} f_n\,\lambda_n\,\frac{d}{dz}[U(z)E_n(z)]\Bigg\}+O(\epsilon^3)\,. \tag{4.31d}$$

The $O(\epsilon)$ terms in (4.31) match to the $O(\epsilon)$ component g_1 of the outer region. From the $O(\epsilon^2)$ components of U, V and P, we anticipate that the $O(\epsilon^2)$ outer flow should contain a correction to the lifting line strength and dipole lines with axes oriented in the x and y directions. These components of the $O(\epsilon^2)$ term in the outer expansion can be derived utilizing the same methods as in Secs. 3.2 and 4.1.

Returning to the full equations (2.6), we introduce outer coordinates and substitute the expansions

$$U = U(z) + \epsilon u_1 + \epsilon^2 u_2 + \cdots \tag{4.32a}$$

$$V = \epsilon v_1 + \epsilon^2 v_2 + \cdots \tag{4.32b}$$

$$W = \epsilon w_1 + \epsilon^2 w_2 + \cdots \tag{4.32c}$$

$$P = \epsilon p_1 + \epsilon^2 p_2 + \cdots\,. \tag{4.32d}$$

Collecting the $O(\epsilon^2)$ terms, we find

$$U(z)\frac{\partial u_2}{\partial x} + w_2\frac{dU(z)}{dz} + \frac{\partial p_2}{\partial x} = -u_1\frac{\partial u_1}{\partial x} - v_1\frac{\partial u_1}{\partial y} - w_1\frac{\partial u_1}{\partial z} \tag{4.33a}$$

$$U(z)\frac{\partial v_2}{\partial x} + \frac{\partial p_2}{\partial y} = -u_1\frac{\partial v_1}{\partial x} - v_1\frac{\partial v_1}{\partial y} - w_1\frac{\partial v_1}{\partial z} \tag{4.33b}$$

$$U(z)\frac{\partial w_2}{\partial x} + \frac{\partial p_2}{\partial z} = -u_1\frac{\partial w_1}{\partial x} - v_1\frac{\partial w_1}{\partial y} - w_1\frac{\partial w_1}{\partial z} \tag{4.33c}$$

$$\frac{\partial u_2}{\partial x} + \frac{\partial v_2}{\partial y} + \frac{\partial w_2}{\partial z} = 0\,. \tag{4.33d}$$

As expected, the equations governing the $O(\epsilon^2)$ terms in the outer region contain the same linear operators as those governing the $O(\epsilon)$ terms. However, at $O(\epsilon^2)$ the equations are inhomogeneous, with source terms involving products of the $O(\epsilon)$ terms. Unfortunately, the $O(\epsilon)$ terms are known only in the form of Fourier integrals, and the nonlinear character of the right hand sides of (4.33) introduces difficulties in obtaining a particular solution. Hence, we do not pursue the analysis of the $O(\epsilon^2)$ terms in the outer region further.

4.5 Summary for Lifting Bodies

In summary, we have used singular perturbation techniques to analyze rotational, spanwise periodic flow past a lifting, two-dimensional body. The body cross-sectional size L is assumed to be small compared to the period ℓ of the oncoming flow U(z). The singular perturbation analysis involves three regions: the inner, wake and outer regions.

As in the case of nonlifting bodies, the primary flow (U_0, V_0, P_0) in the inner region corresponds to potential flow past the body with the local free stream value of U(z). The spanwise variation in U(z) produces a weak $O(\epsilon)$ secondary flow W_1 in the spanwise direction. The vortex lines of the upstream flow wrap around the body as they convect

downstream, producing significant streamwise vorticity in a wake region directly behind the body. In the outer region, the body appears as an $O(\epsilon)$ lifting line, and the wake appears as a sheet of shed vorticity. In contrast to the case of nonlifting bodies, here a separate analysis of the wake region is not required in order to capture the influence of the wake on the outer region. The trailing vorticity is found to be equal to the spanwise derivative of the product of the circulation $\Gamma U(z)$ and the oncoming flow $U(z)$, in contrast to classical lifting line theory where the trailing vorticity is equal to the spanwise derivative of the circulation about the body.

Similar to the case of nonlifting bodies, the flow takes on the remarkably simple form (4.11) at large distances from the body. In the vicinity of the downstream direction, this must of course be supplemented by the Trefftz plane flow field (4.8).

Higher order approximations to the inner region have been considered. The first correction to the inner flow is the response to a spanwise varying downwash of $O(\epsilon)$. The strength of this downwash is half the magnitude of the vertical velocity in the Trefftz plane, a fact consistent with classical lifting line theory for potential flow.

Further analysis of the outer region shows that nonlinear source terms in the governing equations appear at $O(\epsilon^2)$. Since numerical methods would be required to obtain a particular solution, the calculation of these terms was not pursued.

CHAPTER 5

NUMERICAL RESULTS

In this chapter we present numerical results which illustrate features of the flow fields analyzed in the preceding chapters. In Section 5.1, the inner region spanwise velocity field is examined for nonlifting and lifting circular cylinders. Section 5.2 examines the spanwise velocity (or equivalently, the drift function) for streamlines that pass close to the body surface. Certain features of the outer flow fields produced by the wake region and the singularity lines which represent the body are discussed in Section 5.3.

5.1 The Inner Region Spanwise Velocity Component

In this section we present results for W_1 for the cases of lifting and nonlifting circular cylinders. As shown in Chapter 2, the leading term W_1 of the spanwise velocity component is given in terms of the integral (2.14b)

$$W_1(\Phi) = -\frac{dU(z)}{dz}\int_{-\infty}^{\Phi}\left(\left|\frac{dG}{d\zeta}\right|^{-2} - 1\right)d\tilde{\Phi} \tag{5.1a}$$

which must be evaluated numerically. (The subscript 0 which appears on G, Φ and Ψ in Chapter 2 is omitted in this chapter.)

We first discuss the numerical scheme used to calculate W_1. As can be seen from (5.1a), the integration is carried out along streamlines. For the case of a lifting circular cylinder, we have

$$G = \zeta + \frac{i\Gamma}{2\pi}\log\zeta + \frac{1}{\zeta} \tag{5.1b}$$

where

$$G = \Phi + i\Psi, \quad \zeta = X + iY\,. \tag{5.1c}$$

The integrand of (5.1a) is calculated by differentiating (5.1b). However, the resulting expression is a function of (X,Y) rather than (Φ,Ψ). Since (5.1b) cannot be inverted in closed form, the inversion was accomplished numerically using the Muller root finding algorithm for complex functions.

To begin the calculation, we choose a point Φ_0 sufficiently far upstream of the body. The coordinate transformation $\beta = 1/\Phi$ was utilized to map the domain $(-\infty,\Phi_0)$ into a finite region $(1/\Phi_0,0)$. The behavior of the integrand for $\beta \to 0^-$ is found by examining behavior of the integrand as $\Phi \to -\infty$. Expanding the integrand of (5.1a) for large Φ (or ζ), we obtain

$$\left|\frac{dG}{d\zeta}\right|^{-2} - 1 = -\frac{i}{2\pi}\Gamma\,\frac{\zeta^*-\zeta}{\zeta\zeta^*} - \frac{1}{4\pi^2}\Gamma^2\,\frac{1}{\zeta\zeta^*} + \frac{\zeta^2+\zeta^{*2}}{\zeta^2\zeta^{*2}} - \frac{\Gamma^2}{4\pi^2}\,\frac{(\zeta^*-\zeta)^2}{\zeta^2\zeta^{*2}} - \frac{i}{2\pi}\Gamma\,\frac{\zeta^*-\zeta}{\zeta^2\zeta^{*2}}$$

$$+ \frac{i}{4\pi^3}\Gamma^3\,\frac{\zeta^*-\zeta}{\zeta^2\zeta^{*2}} - \frac{i}{\pi}\Gamma\,\frac{(\zeta^*-\zeta)(\zeta^2+\zeta^{*2})}{\zeta^3\zeta^{*3}} + \frac{i}{8\pi^3}\Gamma^3\,\frac{(\zeta^*-\zeta)^3}{\zeta^3\zeta^{*3}} + O\left[\frac{1}{\zeta^4}\right]. \tag{5.2}$$

To express (5.2) in terms of Φ, we invert (5.1b) for large G and ζ to obtain

$$\zeta = G - \frac{i}{2\pi}\Gamma\log G - \frac{\Gamma^2}{4\pi^2}\,\frac{\log G}{G} - \frac{1}{G} + O\left[\frac{(\log G)^2}{G^2}, \frac{\log G}{G^2}, \frac{1}{G^2}\right]. \tag{5.3}$$

Utilizing (5.3) in (5.2), for large Φ and O(1) Ψ the integrand takes the form

$$\left|\frac{dG}{d\zeta}\right|^{-2} - 1 = \frac{\Gamma^2}{2\pi^2}\frac{\log|\Phi|}{\Phi^2} + \left[-\frac{\Gamma}{\pi}\Psi - \frac{\Gamma^2}{4\pi^2} + 2\right]\frac{1}{\Phi^2} + \frac{\Gamma^3}{2\pi^2}\frac{\log|\Phi|}{\Phi^3}$$

$$+ \left[\frac{\Gamma^2}{\pi}\Psi + \frac{\Gamma^3}{2\pi^2} - 2\Gamma\right]\frac{1}{\Phi^3} + O\left(\frac{(\log|\Phi|)^2}{\Phi^4}, \frac{\log|\Phi|}{\Phi^4}, \frac{1}{\Phi^4}\right). \qquad (5.4)$$

We then find for $\beta << 1$

$$\left(\left|\frac{dG}{d\zeta}\right|^{-2} - 1\right)\frac{d\Phi}{d\beta} = \frac{\Gamma}{2\pi^2}\log|\beta| + \left[-\frac{\Gamma}{\pi}\Psi - \frac{\Gamma^2}{4\pi^2} + 2\right] + O(\beta\log|\beta|, \beta)\,. \qquad (5.5)$$

The first term is an integrable singularity arising from the $O(\Phi^{-2}\log|\Phi|)$ term in (5.4). This integrable singularity was subtracted from the integrand and evaluated analytically. The remaining integral was evaluated numerically utilizing Romberg integration (Ferziger 1981). Typically a value of Φ_0 five diameters upstream of the body was used. The numerical integration typically converged typically in five iterations with a relative error of less than 10^{-7}.

For $\Phi > \Phi_0$ we utilized the $O(h^4)$ Simpson's rule. For O(1) values of Ψ, a step size $\Delta\Phi = 0.05$ produced satisfactory results. However, for small values of Ψ the integrand becomes large and varies rapidly in the vicinity of the stagnation point where $q \rightarrow 0$. To maintain accuracy for streamlines passing near the stagnation point, the mesh size was decreased by a factor of 8 in regions where $q < 0.5$. Values of $|\Psi| < 0.01$ ($q < 0.2$) were not considered in the numerical integration. Asymptotic expansions for $\Psi << 1$ are developed in Appendix C. Since we considered only body shapes which are symmetric about the y axis, the integrand

was also symmetric and values for $x > 0$ were found by symmetry. Two-dimensional contour plots were obtained using the SURFACEII plotting routine, which does not require the data on a uniform x-y grid.

We now present contour plots of the spanwise velocity W_1. Fig. 5.1a shows the contours of W_1 for a nonlifting circular cylinder in a region encompassing ten cylinder radii. The local features in a two cylinder radii region are shown in Fig. 5.1b. The results are in agreement with Lighthill's (1956) sketch of secondary flow contours for this case. The asymptotic expression (2.17b), which represent circles with a common tangent perpendicular to the flow direction at the origin, is plotted as a dashed line in Fig. 5.1a and is seen to be reasonably accurate for $R > 4$, except in the wake region downstream of the cylinder. For all points upstream of the symmetry line $x = 0$, W_1 is seen to be positive. This corresponds to from spanwise positions of high stagnation pressure toward spanwise positions of low stagnation pressure. Near the forward stagnation point, values of W_1 tend to infinity as expected from (5.1a). The asymptotic expression (2.17b) is antisymmetric about the y-axis, with $W_1 = 0$ on $x = 0$. The numerically computed contour $W_1 = 0$ lies remarkably close to the y axis except very near the body. Substantial asymmetries in the spanwise velocity occur for smaller values of R, with pockets of negative W_1 just downstream of the body. The origin of the asymmetry can be seen by returning to (2.14a). The spanwise pressure gradient $\partial P_0/\partial z$ exhibits symmetry about the y axis, with equal regions of positive and negative values. Hence the asymmetry in W_1 arises solely from the presence of $1/q_0$ in the integral of (2.14a). Essentially, for streamlines near the body, the fluid particles spend more time in low speed regions than in high speed regions. The cumulative result is a spanwise flow from regions of high stagnation pressure to regions of low stagnation pressure for points near the body surface and in the downstream wake. The wake structure behind the

body is evident in Fig. 5.1a. More details of the wake region are presented in the following section.

Contours of the spanwise velocity W_1 for a lifting cylinder with the stagnation point 1^0 below the forward nose of the cylinder (Γ = 0.2193134) are shown in Figs. 5.2a,b. The behavior of W_1 near the body is very similar to the nonlifting case. High positive values of W_1 are again found in front of the body; the contours $W_1 > 0.5$ are almost the same as for the nonlifting case. The wake structures for $\theta = 1^0$ and for the nonlifting case are also quite similar. However, at further distances from the body significant differences between the two cases are evident (Fig. 5.2a). Essentially, the circulation has produced a counterclockwise rotation of the W_1 contours. The contours exhibit more asymmetry with respect to the x axis as the distance from the body increases. In fact, the asymptotic expression (2.17a) far upstream of the body shows that the $W_1 = 0$ contour eventually reaches the position $\theta = \pi$. Note also that the largest negative value found in the downstream pocket above the body is approximately -0.5, which is significantly higher than the value of -0.2 below the body. In view of (2.14a), this is explained by the circulation producing higher flow speeds above the body and lower flow speeds below.

Spanwise velocity contours corresponding to $\theta_s = 5^0$ (Γ = 1.0952314) are presented in Figures 5.3a,b. Very near the body (Fig. 5.3b) the features are fairly similar to the previous cases. However, the contours farther from the body are dramatically different than for the nonlifting body case. The differences are evident even at distances as small as R = 2. As the distance from the body increases, the curves fairly rapidly approach straight lines, in agreement with the asymptotic formula (2.17a). Compared to Fig. 5.2b, there is more asymmetry of the pockets behind the body. The largest negative value above the body is -1.1, and there are no negative values in the region below the body.

The spanwise velocity contours for $\theta_s = 30^0$ are shown in Figs. 5.4a,b. Much larger values of W_1 are found near the body (Fig. 5.4b). This is related to global changes in the inner region flow field, rather than to changes in the local stagnation point region flow field. The W_1 contours again approach straight lines at moderate distances from the body in agreement with (2.17a), but the "virtual origin" for each line appears to lie roughly on the cylinder surface. We also note that, in contrast to the previous figures, the closed contours behind the body have essentially disappeared.

5.2 The Spanwise velocity in the Wake Region

In this section we present results for the spanwise velocity W_1 in the wake region, which is given by (2.17). The behavior of W_1 as $|\Psi| \to \infty$ and $|\Psi| \to 0$ will be discussed before presenting numerical results for all values of Ψ.

As noted in Chapter 2, W_1 has a logarithmic singularity at $\Psi = 0$ which is produced by the stagnation points on the body. The strength of the logarithmic singularity can be determined from a local analysis of the stagnation regions as shown in Appendix C. For the case of a nonlifting circular cylinder Darwin (1953) found that $W_1 \sim -\log|\Psi|$ as $|\Psi| \to 0$. Our analysis in Appendix C shows that the leading term is

$$W_1 \sim -\frac{1}{\sqrt{1-\Gamma^2/16\pi^2}} \log|\Psi|$$

for the case of a circular cylinder with circulation. Hence, circulation increases the strength of the singularity essentially by increasing the "size" of the stagnation point region.

For large $|\Psi|$, W_1 decays as $O(|\Psi|^{-3})$ for nonlifting bodies, whereas for lifting bodies

$W_1 \rightarrow \mp\Gamma + O(|\Psi|^{-3})$ as $\Psi \rightarrow \pm\infty$, as discussed in Chapters 3 and 4. It is interesting to compare the latter result with that found for potential flow lifting line theory. For three-dimensional potential flow past a lifting body, there is a sheet of trailing vorticity behind the body which produces a jump in spanwise velocity, ΔW_1, which equals the spanwise derivative of the circulation about the body. In the present rotational flow problem, the outer solution contains a similar jump in spanwise velocity (4.9), but the jump is equal to the spanwise derivative of the lift force (or equivalently the product of the circulation and the oncoming flow). We have considered body shapes (or stagnation point locations) which are independent of z, and hence the local circulation is proportional to the local oncoming flow speed, producing the factor of 2 in (4.9).

There is a second important distinction between the "jumps" in spanwise velocity which occur for the potential flow problem and for the case of a rotational upstream flow. For the rotational flow problem, the apparent discontinuity in the outer solution for W is resolved by a smooth variation in W on the scale L of the body thickness. This "inviscid wake" remains at thickness L even at infinite Reynolds numbers. In contrast, the trailing vortex sheet for the potential flow problem shrinks to zero thickness as the Reynolds number approaches infinity. For uniform upstream flows, our analysis must reduce to the potential flow lifting line solution, and hence it must contain a trailing vortex sheet of zero thickness in this limit. An important question then arises as to the presence or absence of a finite jump in the spanwise velocity component across $\Psi = 0$ for the case of rotational flow.

In Appendix C, we address this issue by developing asymptotic expansions of the wake region spanwise velocity component for $|\Psi| << 1$. We find

$$W_{1_{u,l}} = - \frac{dU(z)}{dz} D(\Psi) = - \frac{dU(z)}{dz} [C_0 \log|\Psi| + C_{u,l} + O(\log|\Psi|, \Psi)] \qquad (5.6a)$$

where the subscripts u,l refer to Ψ greater than and less than zero, and

$$C_0 = - \frac{1}{\sqrt{1-\Gamma^2/16\pi^2}} \qquad (5.6b)$$

$$C_{u,l} = 2 (I_{1,1} + I_{1,3} + \frac{1}{2\sqrt{1-\Gamma^2/16\pi^2}} [\log 16(1-\Gamma^2/16\pi^2)^{3/2} + \log(\alpha+\Phi_s)] - 2(\Phi_{u,l}-\Phi_s) . \qquad (5.6c)$$

In (5.6c), $I_{1,1}$ and $I_{1,3}$ are integrals given by (C.6b) which must be evaluated numerically for the case of a cylinder with circulation, and α appears in the limits of these integrals. Φ_s is the value of the potential of the forward stagnation point, and Φ_u and Φ_l are the values of the potential on the cylinder surface at $\theta = \pi/2$ and $\theta = - \pi/2$ respectively.

We note that the coefficient C_0 of the leading term is the same for positive and negative Ψ. This term arises from the local region in the vicinity of the stagnation point(s). The constant term $C_{u,l}$ is in general different for positive and negative Ψ. For the case of a circular cylinder without circulation, $\Phi_u = \Phi_l$ and the potential $G(\zeta)$ simplifies so that $I_{1,1}$ and $I_{1,3}$ can be evaluated in closed form, leading to $C_u = C_l = \log 8 - 2$. This result was first found by Darwin (1953). Results for C_u for nonzero circulation are presented in Table C.1.

It is interesting to note that $I_{1,1}$ and $I_{1,3}$ disappear when the difference $C_u - C_l$ is considered, leading to the remarkably simple result

$$C_u - C_l = -\Gamma \, . \tag{5.7a}$$

Physically, the jump in spanwise velocity represents a concentrated sheet of trailing vorticity along the line $\Psi = 0$, downstream of the rear stagnation point,

$$W_1 \Big|_{\Psi=0-}^{\Psi=0+} = \Gamma \, \frac{dU(z)}{dz} \tag{5.7b}$$

Note that this jump is independent of streamwise location. The origin of this concentrated vortex sheet is essentially the same as the vortex sheet which occurs in potential flow past three-dimensional lifting bodies. Namely, the concentrated vortex sheet arises from streamwise vorticity generated in the three-dimensional boundary layer in the body surface, which has zero thickness in our infinite Reynolds number limit.

It is curious that the strength of the concentrated trailing vortex sheet is exactly equal to the spanwise derivative of the circulation about the cylinder. This is identical to the result found for three-dimensional potential flows. In the potential flow case, the strength of the trailing vortex sheet is easily determined by an argument based on the solenoidal property of vorticity. In the rotational flow case such arguments are not simple, because the entire flow contains vorticity. Direct calculations for the other body shapes have shown that in general the strength of the concentrated trailing vortex sheet is not equal to the spanwise derivative of the circulation.

We now present numerical results for the total drift. The numerical method utilized was identical to that used for obtaining the W_1 contours. However, here we used a step size $\Delta\Phi = 0.025$ for the points outside the stagnation point region ($q > 0.5$), and the step size within

the stagnation point region ($q < 0.5$) was reduced by a factor of 8. The total drift for a nonlifting circular cylinder is shown on Fig. 5.5a. The logarithmic singularity at $\Psi = 0$ is clearly evident and the majority of the drift volume, defined as

$$M = \int_{-\infty}^{\infty} D(\Psi)\, d\Psi$$

is seen to be confined in a width of approximately two cylinder diameters. Utilizing our numerical results, we evaluated the drift volume using Romberg integration, with a coordinate transformation to reduce the integration domain to a finite region and analytical removal of the logarithmic singularity at $\Psi = 0$. Darwin's result $M = \pi$ was recovered to 5 digit accuracy. In Fig. 5.5b, the two term small Ψ asymptotic expansion (5.8) is compared to the numerical results. The agreement is quite good even out to $|\Psi| = 0.5$.

The total drift curves for lifting circular cylinders with $\theta_s = 1^0$, 5^0 and 30^0, respectively, are shown in Figs. 5.6a,b,c. As the circulation increases, the large $|\Psi|$ asymptotes are approached more slowly. The step change across $\Psi = 0$ is easily seen even in the presence of the logarithmic singularity. In Fig. 5.6d, the two term small $|\Psi|$ expansion (5.8) is compared to the numerical result for $\theta_s = 30^0$. Here the differences between the asymptotic and numerical results at the larger values of $|\Psi|$ are more noticeable.

5.3 Outer Flow Fields Produced by the Wake Region And The Body Singularity Lines

In this section we examine certain features of the outer flow field produced by the wake region and by the singularity line(s) representing the body. We first consider the flow

fields produced by the wake region. The influence of the wake region on the outer region is particularly simple in the Trefftz plane far downstream from the body. We consider this region first.

Calculations of the outer region flow fields requires the solution of the eigenvalue problem (3.6). This was obtained numerically, using second order central differences. The resulting tridiagonal matrix eigenvalue problem was solved using the IMSL banded symmetric matrix eigenvalue solver EIGBS. For the oncoming flow profile we chose

$$U(z) = 1 + A \cos z \tag{5.8}$$

where A = 1/2. The values of first ten eigenvalues are shown in Table 5.1. We note they are very close to integer values.

We first examine the case of a nonlifting circular cylinder. The outer flow in the Trefftz plane is induced by the vertical component of the velocity in the wake region. As shown in Section 3.5, this vertical velocity approaches a constant as $Y \to \pm\infty$. This provides the inner boundary condition for the Trefftz plane flow field. In Fig. 5.7, the source strength s(z) of (3.34) with is plotted as a function of the spanwise coordinate. We have used the value $M = \pi$ corresponding to a circular cylinder. As discussed in Section 5.1, the spanwise velocity in the wake region is predominantly from regions of high stagnation pressure towards regions of low stagnation pressure. Hence it is not surprising that the spanwise movement leads to an accumulation of fluid in regions of low stagnation pressure resulting in an outflux from the wake region corresponding to a positive s(z). For the particular profile chosen s(z) is positive for $2\pi/3 < z < 4\pi/3$. There is a corresponding influx into the wake region in regions of high stagnation pressure, as shown in Fig. 5.7. The

average value of s(z) is negative, indicating a net influx of fluid into the wake, and this influx is balanced by an increase in the streamwise velocity component within the wake as discussed in Section 3.4. The increase du/dx is also plotted as a function of z in Fig. 5.7, and is seen to be positive for all z. It was shown in Section 3.4 that the integrated value of du/dx across the Y-z plane in the wake region exactly cancels the integral of s(z) with respect to z. This was verified numerically to an accuracy of seven digits. It is important, however, to note that the cancellation occurs only in the aggregate. At any given position z, the inflow s(z) and the streamwise outflow $\frac{du}{dx}(z)$ are not equal, and the difference is balanced by the spanwise velocity w.

As noted in Section 3.5, at large distances from the body the influence of the wake is generally less important than the dipole line. The only exception is in the Trefftz plane, which is the region far downstream of the body and relatively close to the wake. The pressure field vanishes in the Trefftz plane, and the streamwise velocity (3.36b), varies linearly with x, corresponding to the spanwise shift of streamlines of constant stagnation pressure by the spanwise velocity w_w. This behavior is very similar to that observed in the wake region. As (3.36) shows, v_w and w_w are independent of x, hence we can define a stream function $\Psi(y,z)$ such that

$$v_w = U(z)\ \frac{\partial \Psi}{\partial z} \tag{5.9a}$$

and

$$w_w = -U(z)\ \frac{\partial \Psi}{\partial y} \tag{5.9b}$$

where

$$\Psi(y,z) = \mathrm{sgn}(y) \sum_{n=1}^{\infty} -\frac{1}{2} s_n \frac{1}{\lambda_n^2} e^{-\lambda_n |y|} \frac{1}{U^2(z)} \frac{\partial}{\partial z} [U(z)\, E_n(z)] \,. \tag{5.9c}$$

The resulting contours of $\Psi(y,z)$ for $y > 0$ are shown in Fig. 5.8. Note that Ψ is an odd function of y and discontinuous across $y = 0$, corresponding to a discontinuous vertical velocity and continuous spanwise velocity. Ten eigenvectors were used in the computations, and the corresponding values of s_n are shown in Table 5.1. The direction of the flow in the Trefftz plane is shown by arrows on the contours; the spanwise position for $v_w = 0$, $z = 2\pi/3$, corresponds to the zero crossing in Fig. 5.7. The spanwise velocity w_w is zero at $z = 0,\pi$ as is evident in the graph. The amplitude of the velocity decays exponentially for large y.

We now examine the wake region for a lifting body. For lifting bodies, there is a nonzero net vorticity in the wake region and this induces a downwash that varies across the span. The downwash (4.8b) in the Trefftz plane, which is twice the value $V_i(z)$ in (4.20), is plotted in Fig. 5.9. The downwash is positive in regions of low stagnation pressure and negative in regions of high stagnation pressure. This is easily explained by examining the spanwise variations in lift force and the associated trailing vorticity. The curve for the downwash is remarkably similar to the wake outflow (or source strength) curve shown in Fig. 5.7. However the detailed expressions are not identical. For example, $V_i(z)$ is positive for $z > 0.641\pi$ whereas s(z) is positive for $z > 2\pi/3$.

Next, consider the cross-stream flow field in the Trefftz plane associated with lifting bodies. Utilizing (5.9) with the velocity field (4.8), we obtain

$$\Psi(y,z) = \sum_{n=1}^{\infty} \frac{1}{2} f_n \frac{1}{\lambda_n} e^{-\lambda_n |y|} \frac{1}{U^2(z)} \frac{\partial}{\partial z} [U(z)\, E_n(z)] . \qquad (5.10)$$

where $f_n = -\Gamma u_n$. In Fig. 5.10 we present Trefftz plane contours for the case $\theta_s = 5^0$ corresponding to $\Gamma = 1.0952314$. Again ten eigenvectors were used in the computations, and the values of u_n are shown in Table 5.1. Note that Ψ is an even function of y and discontinuous across y = 0, corresponding to a continuous vertical velocity and discontinuous spanwise velocity. The direction of the flow in the Trefftz plane is shown by arrows on the contours. We note that the velocity perturbations decay exponentially for large y.

Finally, for the case of nonlifting bodies we compare the contributions to the outer flow by the dipole line and the wake. Comparisons of the streamwise velocity perturbation directly upstream of the body ($\theta = \pi$) are made for r = 4 and r = 6. The large r asymptotic form (3.38) was used for calculation of the wake contribution, and for consistency the large r expansion of (3.18) was utilized for calculating the dipole line contribution. The contributions from the higher order eigenfunctions are exponentially small for r >> 1, and hence we have kept only two terms (n = 0 and 1) in the eigenfunction series.

In Fig. 5.11a for r = 6, the contribution u_0 which arises from the dipole line is seen to be nearly identical to the total flow perturbation u_t. The dipole line and wake contributions u_{1d} and u_{1w} from the n = 1 eigenfunctions are seen to be quite small by comparison. The contribution u_{1w} is of opposite sign to u_{1d} with a ratio $u_{1w}/u_{1d} = -0.2499879$. Hence, at this distance from the body, the wake exerts only a minor influence on the flow field.

Corresponding results for r = 4 are shown in Fig. 5.11b. The contribution u_0 from the dipole line is again the dominant term, but here the contributions from the n = 1 eigenfunctions are not negligible. The influence of the wake increases (or decreases) the

flow speed in regions of high (or low) stagnation pressure. Some error has probably been introduced by utilizing asymptotic representations and ignoring the higher order eigenfunctions at this location. At O(1) values of r, the full eigenfunction series should be included in the calculations.

n	λ_n	u_n	s_n
-	--------	---------	---------
0	0.	1.428462	0.
1	1.022210	1.220916	-2.003956
2	2.038405	0.055937	-0.365092
3	3.026351	-0.004779	0.068754
4	4.019296	-0.000538	0.013667
5	5.014873	0.000072	-0.002865
6	6.011646	0.000011	-0.000625
7	7.008968	-0.000002	0.000140
8	8.006505	0.	-0.000032
9	9.004056	0.	-0.000007

Table 5.1 Eigenvalues and the coefficients in the eigenfunction expansion of U(z), and s(z).

CHAPTER 6

CONCLUSIONS

In this dissertation we have examined periodic shear flow past two-dimensional bodies. The flow was assumed to be inviscid and incompressible, and the shapes of the oncoming flow velocity profile and the body were arbitrary. The governing equations were solved using singular perturbation techniques for $\epsilon = L/\ell << 1$, where L is the body cross-sectional size and ℓ is the period of the oncoming flow. Our analysis involved three regions: the inner, wake and outer regions. In the inner region, the flow corresponds to the small shear - large disturbance category of Hawtorne (1967), while in the outer and wake regions the flow corresponds to Hawtorne's large shear - small disturbance category.

In the inner region, the leading order variables (U_0, V_0, P_0) correspond to potential flow past the body with a local free stream value of U(z). The spanwise variation in U(z) produces a weak $O(\epsilon)$ secondary flow W_1 in the spanwise direction. This spanwise flow distorts the vortex lines of the upstream flow. In particular, these vortex lines wrap around the body as they convect downstream, producing significant streamwise vorticity in a wake region directly behind the body. The inner flow solutions are found to be nonuniform far away from the body, indicating the presence of an outer region. In addition, for large R the spanwise velocity has different behavior for O(1) values of θ and for small angles behind the body, indicating the presence of a wake region. The analysis of the outer and wake regions are quite different for nonlifting and lifting bodies.

For nonlifting bodies, in the outer region, the body appears as a distribution of three-dimensional dipoles of strength $O(\epsilon^2)$, and the wake appears as a sheet of $O(\epsilon^2)$ mass sinks

(or equivalently, as a divortex sheet). Physically, the vortex lines of the upstream flow wrap around the body, leading to two counter rotating lines of vortices which produce a steady suction of volume flux into the wake. This was seen to be balanced by the increase of the streamwise velocity in the wake region which originated from spanwise shifts of the lines of constant stagnation pressure. The positive momentum flux produced by the wake streamwise velocity is cancelled by a negative contribution in the outer region Trefftz plane, and hence even in the presence of the wake there is no drag force on the body.

For lifting bodies, the body appears as a lifting line of strength $O(\epsilon)$, and the wake appears as a sheet of shed vorticity. Physically the bound vorticity in the body varies along the span, resulting in vorticity shed behind the body on the scale of the body thickness. In contrast to the case of nonlifting bodies, here a separate analysis of the wake region is not required in order to capture the first order influence of the wake on the outer region. The trailing vorticity is found to be equal to the spanwise derivative of the product of the circulation $\Gamma U(z)$ and the oncoming flow $U(z)$, in contrast to classical lifting line theory where the trailing vorticity is equal to the spanwise derivative of the circulation about the body.

For both nonlifting and lifting bodies, at large distances from the body, the flow takes on simple forms. In the vicinity of the downstream direction, these must be supplemented by the Trefftz plane flow field.

Higher order approximations to the inner region were considered. For nonlifting bodies, terms of $O(\epsilon^2 \log\epsilon)$ in (U, V, P) were calculated corresponding to an induced uniform flow approaching the body. Similarly, $O(\epsilon^2, \epsilon^3 \log\epsilon, \epsilon^3)$ terms in W were calculated in closed form. The equations governing the $O(\epsilon^2)$ terms in (U, V, P) were found. However, since these equations involve source terms which must be evaluated numerically, we did not

attempt to solve them. Similarly, in the outer region terms of $O(\epsilon^3, \epsilon^4 \log\epsilon)$ can be calculated analytically, whereas the equations governing the $O(\epsilon^4)$ contributions have nonlinear source terms which must be evaluated numerically.

For lifting bodies, higher order approximations to the inner region show that the first correction to the inner flow is the response to a spanwise varying downwash of $O(\epsilon)$. This is induced by the vorticity shed from the body, whose variation along the span results in downwash in regions of high stagnation pressure and upwash in regions of low stagnation pressure. The strength of this downwash is one half the magnitude of the vertical velocity in the Trefftz plane, a fact consistent with classical lifting line theory for potential flow. Further analysis of the outer region for a lifting body shows that nonlinear source terms in the governing equations appear at $O(\epsilon^2)$. Since numerical methods would be required to obtain a particular solution, the calculation of these terms was not attempted.

Further details of the flow fields were illustrated using numerical methods. The numerical work utilized an oncoming velocity profile $U = (1 + \frac{1}{2}\cos z)$, and a circular cylinder as the body shape. Spanwise velocity contours in the inner region were obtained for lifting and nonlifting circular cylinders. Even very small amounts of circulation dramatically changed the form of these contours. For $R > 4$, the numerical results were quite close to the inner region asymptotic expressions for the spanwise velocity. Curves of total drift were obtained for lifting and nonlifting circular cylinders and logarithmic singularities as $\Psi \to 0$ were observed for both cases. The small Ψ behavior was examined using asymptotic methods and we found that, for a circular cylinder, there is a concentrated sheet of shed vorticity at $\Psi = 0$ of strength half that observed on the outer scale. The coefficient of the logarithmic term in the asymptotic expansion was found to depend only on the flow gradient at the stagnation point. The global wake characteristics in the outer

region were illustrated by plotting the spanwise variations of the wake source strength for nonlifting bodies, and the downwash for lifting bodies. For nonlifting bodies, there is a net mass flux into the wake, but some local outflow is observed in the region of low stagnation pressure.

For lifting bodies, the trailing vorticity produces upwash in regions of low stagnation pressure, and downwash in regions of high stagnation pressure. Trefftz plane flow contours were obtained for nonlifting and lifting bodies, and discontinuities in the vertical and spanwise velocities, respectively, were found at $\Psi = 0$. Finally, numerical results for the flow perturbation upstream of a nonlifting cylinder showed that the disturbance approached its simple large r form rather quickly.

In summary, in the present work the wake region has been shown to exert an important influence on vortical flow past nonlifting bodies. The case of a lifting body essentially extends Prandtl's lifting line theory to vortical flows. An interesting observation for this case is the presence of a concentrated vortex sheet, embedded within a larger scale region of spanwise vorticity, in the wake behind the body.

Extensions of the present investigation in a number of directions can be suggested. Further numerical work on other body shapes would clearly be of interest. Within the framework of incompressible flow, two main extensions can be identified. The first is the case of semi-infinite chord bodies. Here, the asymptotic expansion may have a significantly different structure, since the integral (2.14) for W_1 exhibits convergence problems as $\Phi \rightarrow -\infty$. Secondly, analyses of finite span bodies and nonperiodic upstream flow could be carried out. In this situation, it is possible for the vortex loops formed by wrapping of free-stream vorticity around the body to slip off the ends of the finite span body.

Appendix A

LARGE ARGUMENT ASYMPTOTIC EXPANSION OF SINGULAR FOURIER INTEGRALS

First we consider the large r behavior of (3.32) which arises in the case of nonlifting bodies. The function $B_n(x,y)$ defined by (3.32) is a symmetric function of y; we shall restrict attention to $y > 0$ ($0<\theta<\pi$). We then have

$$I = \int_{-\infty}^{\infty} B_d \, e^{-rb(k)} \, dk \tag{A.1a}$$

where

$$x = r\cos\theta \ , \ y = r\sin\theta \ , \tag{A.1b}$$

$$B_d = \frac{1}{(k+i\beta)^2} \frac{1}{\sqrt{k^2+\lambda_n{}^2}} \tag{A.1c}$$

and

$$b(k) = \sqrt{k^2+\lambda_n{}^2}\,\sin\theta + ik\cos\theta \ . \tag{A.1d}$$

We first apply the method of steepest descent. The method of steepest descent consists

of determining the integration contour onto a path which passes through a saddle point at which db/dk = 0. The steepest descent contour is chosen such that Im(b(k)) is constant and Re(b(k)) decreases monotonically in both directions away from the saddle point. By a Laplace type argument the integral is then dominated by the vicinity of the saddle point. Of course, any poles crossed in the deformation from the original contour onto the steepest descent path must be incorporated appropriately. From (A.1d) it can be shown that the saddle point is

$$k_0 = -i\lambda_n \cos\theta \,, \tag{A.2}$$

and in the vicinity of the saddle point the steepest descent path is parallel to the real k axis. For large k, the steepest descent path approaches the asymptotes

$$k_{Im} \sim - \frac{k_{Re} \cos\theta}{|\sin\theta|} \quad \text{as} \quad k_{Re} \to \infty \tag{A.3a}$$

$$k_{Im} \sim \frac{k_{Re} \cos\theta}{|\sin\theta|} \quad \text{as} \quad k_{Re} \to -\infty \,. \tag{A.3b}$$

Closed contours including both the steepest descent path and the original integration path are shown in Figs. (A.1a, b). The residue theorem will be applied to these closed contours.

It can be shown that the arcs at infinity, namely I_R, make no contribution. For $0 < \theta < \pi/2$ the double pole at $k = -i\beta$ is inside the contour, while for $\pi/2 < \theta < \pi$ it is outside. Following the Laplace type argument, the integral along the steepest descent contour is evaluated by expanding b(k) to second order around the saddle point, and taking only the leading term in the expansion of $B_d(k)$. Combining these results, we obtain the asymptotic

expansion

$$I = -2\pi\left[\frac{e^{-\lambda_n r\sin\theta}\cos\theta}{\lambda_n} r + \frac{e^{-r\lambda_n}}{\sqrt{2\pi\lambda_n}\lambda_n{}^2\cos^2\theta}\frac{1}{\sqrt{r}}(1+O(1/r))\right] \qquad 0 < \theta < \frac{\pi}{2}, \qquad \text{(A.4a)}$$

$$I = -2\pi\left[\frac{e^{-r\lambda_n}}{\sqrt{2\pi\lambda_n}\lambda_n{}^2\cos^2\theta}\frac{1}{\sqrt{r}}(1+O(1/r))\right] \qquad \frac{\pi}{2} < \theta < \pi \qquad \text{(A.4b)}$$

where the additional term in (A.4a) is the residue term contribution. The error term of relative order 1/r arises from the approximations in the vicinity of the saddle point. A similar set of expressions hold for $y < 0$ by symmetry.

The asymptotic expansion (A.4) is nonuniform in the vicinity of $\theta = \pi/2$. This nonuniformity arises due to the coalescence of the double pole and the saddle point. To develop an expansion which is uniformly valid in the vicinity of $\theta = \pi/2$ we apply the method of Van Der Waerden (1950). We start by reexpressing the integral (A.1a) in terms of an independent variable s where

$$b(k) = b(k_0) + s^2 \ . \qquad \text{(A.5a)}$$

Hence we have

$$I = e^{-r\lambda_n}\int_{C'} P(s)e^{-rs^2}\, ds \qquad \text{(A.5b)}$$

where

$$P(s) = B_d(k(s)) \frac{dk}{ds} \tag{A.5c}$$

and the steepest descent contour now corresponds to the real s axis with the saddle point at the origin. In order to write down an explicit expression for P(s) the inverse map

$$k = -i(s^2+\lambda_n)\cos\theta + \sin\theta\, s\sqrt{s^2+2\lambda_n} \tag{A.5d}$$

is required. Here the branch cuts are taken as shown in Fig. A.2, and we take the branch of $\sqrt{s^2+2\lambda_n}$ which is positive for real values of s. Substituting (A.5d) in (A.1c), and evaluating dk/ds, we find

$$P(s) = 2 \frac{1}{\left[s\sqrt{s^2+2\lambda_n}\sin\theta - i(s^2+\lambda_n)\cos\theta\right]^2} \frac{1}{\sqrt{s^2+2\lambda_n}}. \tag{A.5e}$$

It can be shown that the double pole at $k = -i\beta$ maps to a double pole at $s_0 = \pm i\sqrt{\lambda_n - \lambda_n\sin\theta - \beta\cos\theta}$ where the plus or minus sign is taken for θ less than or greater than $\pi/2$ respectively. The original integration contour along the real axis in the k plane maps to the curve C′ passing just above the double pole in the s plane.

We now deform the original contour of integration to the real axis in the s plane. For angles not close to $\pi/2$ our result (A.4) is recovered by approximating P(s) by P(0). To derive a result which is uniformly valid in θ, we proceed as follows. Noting that the difficulty arises from the presence of the pole we represent P(s) in the form

$$P(s) = \frac{A}{(s-s_0)^2} + \frac{B}{s-s_0} + T(s) , \tag{A.6a}$$

where T(s) is analytic for all values of θ, and s_0 is the location of the double pole. It turns out that B = 0. Substituting (A.6a) into (A.5b) we can write the integral in the form

$$I = A\, e^{-r\lambda_n} \int_{-\infty}^{\infty} \frac{e^{-rs^2}}{(s-s_0)^2}\, ds + e^{-r\lambda_n} \int_{-\infty}^{\infty} T(s) e^{-rs^2}\, ds - 2\pi\, \frac{e^{-\lambda_n r\sin\theta} r\cos\theta}{\lambda_n} H\left[\frac{\pi}{2} - \theta\right] \tag{A.6b}$$

where the last term in (A.6b) is the residue contribution. After an integration by parts the first integral in (A.6b) can be written in a form involving only a simple pole which is evaluated in Van Der Waerden (1950). Then we have

$$\int_{-\infty}^{\infty} \frac{e^{-rs^2}}{(s-s_0)^2}\, ds = -2\sqrt{\pi r} + 2\pi r \sqrt{-s_0^2}\, e^{-rs_0^2}\, \mathrm{erfc}\sqrt{-rs_0^2} . \tag{A.6c}$$

The leading term in the second integral can be obtained by setting s = 0 in T. By (A.6a) we have

$$T(0) = P(0) - \frac{A}{s_0^2} \tag{A.6d}$$

and

$$\int_{-\infty}^{\infty} T(0)e^{-rs^2}\,ds = T(0)\sqrt{\frac{\pi}{r}}\,. \tag{A.6e}$$

The final result is

$$I = -2\pi\left\{\frac{r\cos\theta e^{-r\lambda_n\sin\theta}}{\lambda_n}\left[H\left(\frac{\pi}{2}-\theta\right)-\frac{1}{2}\mathrm{sgn}\left(\frac{\pi}{2}-\theta\right)\right]\mathrm{erfc}\sqrt{r\lambda_n(1-\sin\theta)}\right]$$

$$+\frac{e^{-r\lambda_n}}{2\lambda_n\sqrt{\pi\lambda_n r}}\left[r\sqrt{1+\sin\theta}+\frac{\sqrt{2}-\frac{1}{2}(1+\sin\theta)^{3/2}}{\lambda_n\cos^2\theta}(1+O(1/r))\right]\right\}. \tag{A.7}$$

The result for values of $y < 0$ can be obtained by symmetry. This completes the analysis for the case of nonlifting bodies.

For the case of lifting bodies, we consider the large r asymptotic behavior of (4.4b). Again the function defined by (4.4b) is an even function of y. We shall restrict attention to $y > 0$ ($0<\theta<\pi$). We then have

$$I = \int_{-\infty}^{\infty} B_f\, e^{-rb(k)}\, dk\,, \tag{A.8a}$$

where

$$B_f = \frac{1}{(k+i\beta)^2}\,, \tag{A.8b}$$

and b(k) is given by (A.1d). Following the above procedure we obtain the steepest descent approximation

$$I = -2\pi\left\{e^{-\lambda_n r\sin\theta}\cos\theta\ r\ H\left[\frac{\pi}{2} - \theta\right] + \frac{e^{-r\lambda_n}}{\sqrt{2\pi\lambda_n}\,\lambda_n}\,\frac{\sin\theta}{\cos^2\theta}\,\frac{1}{\sqrt{r}}\,(1+O(1/r))\right\}. \qquad (A.9)$$

In comparison to (A.4), the only differences are a factor of λ_n in residue contribution and $\lambda_n\sin\theta$ in the saddle point contribution. As in the case of (A.4), (A.9) is nonuniform in the vicinity of $\theta = \pi/2$.

To develop a uniformly valid expression, we again follow Van Der Waerden (1950). We have

$$I = e^{-r\lambda_n}\int_{C'} P_f(s)e^{-rs^2}\,ds\,, \qquad (A.10a)$$

where

$$P_f(s) = 2\,\frac{1}{\left[s\sqrt{s^2+2\lambda_n}\sin\theta - i(s^2+\lambda_n)\cos\theta\right]^2}\,\frac{\left[(s^2+\lambda_n)\sin\theta - i\cos\theta s\sqrt{s^2+2\lambda_n}\right]}{\sqrt{s^2+2\lambda_n}}\,. \qquad (A.10b)$$

$P_f(s)$ also contains a double pole at $s = s_0$. Isolating the double pole as in (A.6a), and evaluating the resulting integrals, we obtain

$$I = -2\pi\left\{r\cos\theta e^{-r\lambda_n \sin\theta}\left[H\left(\frac{\pi}{2}-\theta\right)-\frac{1}{2}\operatorname{sgn}\left(\frac{\pi}{2}-\theta\right)\right]\operatorname{erfc}\sqrt{r\lambda_n(1-\sin\theta)}\right]$$

$$+\frac{e^{-r\lambda_n}}{2\sqrt{\pi\lambda_n r}}\left[r\sqrt{1+\sin\theta}+\frac{\sqrt{2}\sin\theta-\frac{1}{2}(1+\sin\theta)^{3/2}}{\lambda_n\cos^2\theta}(1+O(1/r))\right]\Bigg\} \qquad \text{(A.11)}$$

The result for values of $y < 0$ can be obtained by symmetry.

Appendix B

SMALL ARGUMENT ASYMPTOTIC EXPANSION OF FOURIER INTEGRALS

In this appendix, we examine the small r behavior of integrals arising in the analysis of nonlifting and lifting bodies.

First consider the integral (3.32) arising for the case of a nonlifting body. We have

$$I_n = \int_{-\infty}^{\infty} \frac{e^{-\sqrt{k^2+\lambda_n^2}\,|y| - ikx}}{(k+i\beta)^2\sqrt{k^2+\lambda_n^2}}\,dk \qquad n = 1,2,\ldots . \tag{B.1}$$

Taking $y > 0$, $x > 0$ and closing the contour (see Fig. B.1) in the lower half plane we obtain

$$I_n = -\frac{2\pi}{\lambda_n} r\cos\theta e^{-\lambda_n r\sin\theta} - 2e^{-\lambda_n r\cos\theta}\int_0^{\infty} \frac{e^{-tr\cos\theta}\cos\left(\sqrt{t^2+2\lambda_n}\,tr\sin\theta\right)}{(t+\lambda_n)^2\sqrt{t^2+2\lambda_n t}}\,dt \tag{B.2a}$$

where

$$x = r\cos\theta \quad , \quad y = r\sin\theta \, . \tag{B.2b}$$

Here the first term is the residue contribution and the second term arises from the wrap around the branch cut.

Since t and r appear as a product in (B.2a), it is natural to expect that the small r behavior of the integral can be obtained from the large t behavior of the integrand. Hence we introduce the transformation

$$u = r\sqrt{t^2+2\lambda_n t} \tag{B.3}$$

where the choice of the square root has been chosen to simplify the argument of the cosine function. We then have

$$I_n = -\frac{2\pi}{\lambda_n} r\cos\theta e^{-\lambda_n r\sin\theta} - 2r^2\int_0^\infty f(u)du \tag{B.4a}$$

where

$$f(u) = \frac{e^{-\sqrt{u^2+r^2\lambda_n^2}\cos\theta}\cos(u\sin\theta)}{(u^2+r^2\lambda_n^2)^{3/2}} . \tag{B.4b}$$

Since r<<1, it is tempting to simply expand f(u) for small r,

$$f(u)_{global} = \frac{e^{-u\cos\theta}\cos(u\sin\theta)}{u^3} + O(r^2) . \tag{B.5a}$$

However (B.5a) behaves as u^{-3} for small u and hence is not integrable. This result shows that we must introduce a local region where u = O(r) in addition to the global region u = O(1). Introducing u = rU in (B.4b) and expanding for small r, we obtain

$$f(u)_{local} = \frac{1}{r^3}\frac{1}{(U^2+\lambda_n^2)^{3/2}} - \frac{1}{r^2}\frac{\cos\theta}{U^2+\lambda_n^2} - \frac{1}{r}\frac{U^2\sin^2\theta}{2(U^2+\lambda_n^2)^{3/2}}$$

$$+\frac{1}{r}\frac{\cos^2\theta}{2(U^2+\lambda_n^2)^{1/2}} + \frac{U^2\sin^2\theta\cos\theta}{2(U^2+\lambda_n^2)} - \frac{\cos^3\theta}{6} + O(r) . \qquad \text{(B.5b)}$$

It can be seen that the local expansion of f is not integrable as $U \to \infty$. To determine a uniformly valid expansion for the integrand, we utilize the additive composite expansion (Van Dyke 1975)

$$f \sim f_{global} + f_{local} - f_{common} , \qquad \text{(B.5c)}$$

where the common term can be obtained by expressing the global (or local) expansion in the local (or global) variable and reexpanding to appropriate order. We find

$$f(u)_{common} = \frac{1}{r^3U^3} - \frac{\cos\theta}{r^2U^2} - \frac{\sin^2\theta}{2rU} + \frac{\cos^2\theta}{2rU} + \frac{\sin^2\theta\cos\theta}{2} - \frac{\cos^3\theta}{6} + O(r) . \qquad \text{(B.5d)}$$

It can be seen that the composite expansion (B.5c) is uniformly valid for all values of u, with an error of $O(r^2)$ in the global region and an error of O(r) in the local region. The larger error term in the local region is permissible since the extent of this region is O(r) in terms of the variable u.

We now calculate the integral of f(u). This is done considering the terms f_{local}, f_{global} and f_{common} separately. Since the individual terms are not integrable over $(0,\infty)$, we introduce finite limits (A,B). After combining the integrals of the three terms, the limits $A \to 0$ and $B \to \infty$ will be evaluated. First consider the integral of the local expansion. We have

$$\int_A^B f(u)_{local}\,du = r\int_{\frac{A}{r}}^{\frac{B}{r}} f(u)_{local}\,dU = \frac{1}{r^2}\,\frac{1}{\lambda_n{}^2} - \frac{1}{r}\,\frac{\cos\theta}{\lambda_n}\,\frac{\pi}{2} - \frac{\cos 2\theta}{2}\log r$$

$$+ \frac{\cos 2\theta}{2}\log 2 - \frac{\cos 2\theta}{2}\log\lambda_n - \frac{\sin^2\theta}{2} + \frac{\sin^2\theta\cos\theta}{2}\lim_{B\to\infty} B - \frac{\cos^3\theta}{6}\lim_{B\to\infty} B$$

$$+ \frac{\cos 2\theta}{2}\lim_{B\to\infty}\log B + O(r)\,. \qquad \text{(B.6a)}$$

Note that the integral diverges as $B \to \infty$. Next consider the integral of the global expansion. We have

$$\int_A^B f(u)_{global}\,du = \int_A^B \frac{\cos(u\sin\theta)}{u^3}\; e^{-u\cos\theta}\,du = \frac{3}{4}\cos 2\theta - \frac{1}{2}\,E\cos 2\theta$$

$$+ \theta\sin\theta\cos\theta + \frac{1}{2}\lim_{A\to 0}\frac{1}{A^2} - \cos\theta\lim_{A\to 0}\frac{1}{A} - \frac{\cos 2\theta}{2}\lim_{A\to 0}\log A + O(r)\,. \qquad \text{(B.6b)}$$

Note that this integral diverges as $A \to 0$. The integral of the common term is

$$\int_A^B f(u)_{common}\,du = \frac{\sin^2\theta\cos\theta}{2}\lim_{B\to\infty} B - \frac{\cos^3\theta}{6}\lim_{B\to\infty} B + \frac{\cos 2\theta}{2}\lim_{B\to\infty}\log B$$

$$+ \frac{1}{2}\lim_{A\to 0}\frac{1}{A^2} - \cos\theta\lim_{A\to 0}\frac{1}{A} - \frac{\cos 2\theta}{2}\lim_{A\to 0}\log A + O(r)\,. \qquad \text{(B.6c)}$$

This integral diverges both as $B \to \infty$ and as $A \to 0$. This is necessary for the common term

to remove the nonuniformities in the local and global expansions.

Combining the local, global and common terms, (B.5c) leads to

$$f = \frac{1}{r^2}\frac{1}{\lambda_n{}^2} - \frac{1}{r}\frac{\cos\theta}{\lambda_n}\frac{\pi}{2} - \log r\,\frac{\cos 2\theta}{2} - \frac{\cos 2\theta}{2}\left[\log\frac{\lambda_n}{2} + E - \frac{3}{2}\right]$$

$$-\frac{\sin^2\theta}{2} + \theta\sin\theta\cos\theta + O(r)\,. \tag{B.7a}$$

Utilizing (B.4a) we find

$$I_n = -\frac{2}{\lambda_n{}^2} - r\,\frac{\pi\cos\theta}{\lambda_n} + r^2\log r\cos 2\theta + r^2\cos 2\theta\left[\log\frac{\lambda_n}{2} + E - \frac{3}{2}\right]$$

$$+r^2\sin^2\theta + r^2(\pi-\theta)\sin 2\theta + O(r^3)\,. \tag{B.7b}$$

This completes the evaluation of the integral for $x > 0$ and $y > 0$. The case for $x < 0$ is similar except that we close the contour in the upper half plane. The same expression (B.7b) is found. The case $y < 0$ follows from the symmetry properties of the original integral (B.1), which shows that the expressions (B.7b) is valid for negative as well as positive values of y.

We now consider the integral (4.4b) arising for the case of lifting bodies. We have

$$I_n = \mathrm{sgn}(y)\int_{-\infty}^{\infty} \frac{e^{-\sqrt{k^2+\lambda_n^2}\,|y| - ikx}}{(k+i\beta)^2}\,dk\,. \tag{B.8}$$

Taking $y > 0$, $x > 0$ and closing the contour (see Fig. B.1) in the lower half plane, and using

the transformation (B.3) we obtain

$$I_n = -2\pi r\cos\theta e^{-\lambda_n r\sin\theta} - 2r\int_0^\infty f_1(u)du \tag{B.9a}$$

where

$$f_1(u) = \frac{e^{-\sqrt{u^2+r^2\lambda_n^2}\cos\theta}}{(u^2+r^2\lambda_n^2)^{3/2}}\sin(u\sin\theta)\,u\,. \tag{B.9b}$$

We form a composite expansion for $f_1(u)$ of (B.9b) following a similar procedure we used for f(u) of (B.4b) and integrate the result to obtain

$$I_n = 2\left[r\sin\theta\log r - r\cos\theta(\pi-\theta) + r\sin\theta\left(\log\frac{\lambda_n}{2}+E\right) + r^2\frac{\pi}{2}\lambda_n\sin\theta\cos\theta\right] + O(r^3)\,. \tag{B.10}$$

The case n = 0 must be treated separately, because $\lambda_n = 0$ and the integral of f(u) in (B.9) does not converge at its lower limit. However, it can be seen from (4.4), (4.2) and (3.4) that for n = 0 the physical variables only contain $\partial^2 I_0/\partial x^2$ and $\partial^2 I_0/\partial x\partial y$. It is most convenient to return to the original integral (B.8), and evaluate the derivatives under the integral sign. The resulting integrals can be evaluated directly by deforming the contour around the branch cut in the lower half plane. We find

$$\frac{\partial^2 I_0}{\partial x^2} = -2\,\frac{\sin\theta}{r} + O(r)\,, \tag{B.11a}$$

$$\frac{\partial^2 I_0}{\partial x \partial y} = 2\ \frac{\cos\theta}{r} + O(r)\ . \qquad \text{(B.11b)}$$

The case of $x < 0$ is again handled by closing the contour in the upper half plane, and the result for values of $y < 0$ is obtained by symmetry, to show that expressions (B.10) and (B.11) are still valid.

APPENDIX C

SMALL Ψ ASYMPTOTIC EXPANSIONS FOR THE DRIFT OF A CIRCULAR CYLINDER

In this appendix, we calculate the small Ψ expansion of the drift function for the case of a lifting circular cylinder. This choice of body shape allows us to study the influence of body lift forces in the simplest analytical framework. The special case of a nonlifting circular cylinder has already been analyzed by Darwin (1953) and will be used as a check. From (2.17d), we have the total drift expression as

$$D(\Psi) = \int_{-\infty}^{\infty} \left[\frac{1}{q^2} - 1 \right] d\Phi \,, \tag{C.1a}$$

where

$$q^2 = \left(\frac{dG}{d\zeta} \right) \left(\frac{dG}{d\zeta} \right)^* \tag{C.1b}$$

and the integral is evaluated along a streamline Ψ = constant. (The subscript 0 which appears on G, Φ and Ψ in Chapter 2 is omitted in this appendix.) For the case of a circular cylinder, the integrand is symmetric about the y axis (see Fig. C.1), and D(Ψ) can be evaluated by integrating from x = -∞ to x = 0 and doubling the result.

As mentioned in Section 5.2, the drift function D(Ψ) has a logarithmic singularity at Ψ

= 0, the streamline which passes through the downstream stagnation point. This singularity arises because $q^2 \to 0$ at the upstream and downstream stagnation points. Hence the integral (C.1) does not exist for $\Psi = 0$. For small values of Ψ, say $\Psi = \Psi_1$ or $\Psi = \Psi_2$ as illustrated on Fig. C.1, the stagnation point regions require special treatment in the evaluation of $D(\Psi)$. In this appendix, we apply singular perturbation techniques to determine the asymptotic expansion for $D(\Psi)$.

Denoting the value of Φ at $x = 0$ by Φ_u or Φ_l for $\Psi > 0$ and $\Psi < 0$ respectively, we have

$$D_{u,l}(\Psi) = 2 \int_{-\infty}^{\Phi_{u,l}} \left[\frac{1}{q^2} - 1 \right] d\tilde{\Phi} . \tag{C.2}$$

For small Ψ, the integrand has different expansions in regions A, B, and $C_{u,l}$ (see Fig C.1). In regions A and $C_{u,l}$, the integrand can be expanded in a Taylor series about $\Psi = 0$. In contrast, in region B the integrand does not exist for $\Psi = 0$ at the stagnation point $\Phi = \Phi_s$, and hence we must include the nonzero value of Ψ even in the leading term. However, we have the simplification that the leading behavior in this region is plane stagnation flow,

$$G - \Phi_s = \frac{1}{2} G_s''(\zeta - \zeta_s)^2 + O(\zeta - \zeta_s)^3 \tag{C.3a}$$

where

$$G_s'' = \left. \frac{d^2 G}{d\zeta^2} \right|_{\zeta = \zeta_s} . \tag{C.3b}$$

In order for the nonzero value of Ψ to enter at leading order in the stagnation point region as $\Psi \to 0$, it is then clear that we must choose the stagnation point variable as $\hat{\Phi} = (\Phi - \Phi_s)/\Psi$.

To evaluate the integral (C.2), we separate the integration range into $(-\infty, \Phi_s)$ and $(\Phi_s, \Phi_{u,l})$. First consider

$$I_1 = \int_{-\infty}^{\Phi_s} \left[\frac{1}{q^2} - 1 \right] d\Phi \,. \tag{C.4}$$

We develop a uniformly valid expansion for the integral by utilizing the additive composite of Van Dyke (1975). In the global region A upstream of the cylinder, we utilize the regular perturbation

$$\frac{1}{q^2} - 1 = \left| \frac{dG}{d\zeta} \right|^{-2}_{\Psi=0} - 1 + O(\Psi) \,. \tag{C.5a}$$

For the local region near the stagnation point, we utilize (C.3a) to obtain

$$\frac{1}{q^2} = \frac{1}{|G_s''|^2 (\zeta - \zeta_s)^2} + O\left(\frac{1}{\zeta - \zeta_s} \right) . \tag{C.5b}$$

On inverting (C.3) to express $\zeta - \zeta_s$ in terms of $(\hat{\Phi}, \Psi)$, we obtain the local expansion

$$\frac{1}{q^2} = \frac{1}{2\,|G_s''|\,|\Psi|\,\sqrt{\hat{\Phi}^2 + 1}} + O\left(\frac{1}{\sqrt{|\Psi|}} \right) . \tag{C.5c}$$

The common term is obtained by expressing (C.5a) in terms of $\hat{\Phi}$, or (C.5c) in terms of Φ,

and expanding to appropriate order. We find the common term

$$\frac{1}{q^2} = \frac{1}{2\,|G_s''|\,(\Phi_s - \Phi)} + O\left[\frac{1}{\sqrt{\Phi_s - \Phi}}\right]. \tag{C.5d}$$

Expressing all terms in the global coordinate for convenience, the asymptotic expansion of (C.4) is given by

$$I_1 \sim \int_{-\infty}^{\Phi_s} \left\{ \left[\left| \frac{dG}{d\zeta} \right|^{-2}_{\Psi=0} - 1 \right] + \frac{1}{2\,|G_s''|\,\sqrt{(\Phi-\Phi_s)^2 + \Psi^2}} - \frac{1}{2\,|G_s''|\,(\Phi_s - \Phi)} \right\} d\Phi \,. \tag{C.6a}$$

The first term of (C.6a) requires numerical integration, while the second and third terms can be evaluated analytically. Note that the global term is not integrable as $\Phi \rightarrow \Phi_s$, the local term is not integrable as $\Phi \rightarrow -\infty$, and the common term is not integrable at either of the limits. Thus, for convergence as $\Phi \rightarrow -\infty$, the local and common terms must be grouped together, and for convergence as $\Phi \rightarrow \Phi_s$ the global and common terms must be grouped together. This is achieved by breaking the integration domain $(-\infty, \Phi_s)$ into two regions, and grouping terms as follows:

$$I_1 = I_{1,1} + I_{1,2} + I_{1,3} + I_{1,4} \tag{C.6b}$$

where

$$I_{1,1} = \int_{-\infty}^{-\alpha} \left[\left| \frac{dG}{d\zeta} \right|^{-2}_{\Psi=0} - 1 \right] d\Phi$$

$$I_{1,2} = \int_{-\infty}^{-\alpha} \left[\frac{1}{2\,|G_s''|\,\sqrt{(\Phi-\Phi_s)^2 + \Psi^2}} - \frac{1}{2\,|G_s''|\,(\Phi_s - \Phi)} \right] d\Phi$$

$$I_{1,3} = \int_{-\alpha}^{\Phi_s} \left[\left| \frac{dG}{d\zeta} \right|^{-2}_{\Psi=0} - 1 - \frac{1}{2\,|G_s''|\,(\Phi_s - \Phi)} \right] d\Phi$$

$$I_{1,4} = \int_{-\alpha}^{\Phi_s} \frac{1}{2\,|G_s''|\,\sqrt{(\Phi-\Phi_s)^2 + \Psi^2}}\, d\Phi \,.$$

Here α has an arbitrary value in the range $-\Phi_s < \alpha < \infty$.

The first and third integrals in (C.6b), $I_{1,1}$ and $I_{1,3}$, are evaluated numerically, while the second and fourth integrals have the analytical expressions

$$I_{1,2} = \frac{1}{4\sqrt{1-16\Gamma^2/\pi^2}} \left\{ \ln 2 - \ln\left[(\Phi_s+\alpha) + \sqrt{(\Phi_s+\alpha)^2 + \Psi^2} \right] + \ln(\alpha+\Phi_s) \right\} \qquad \text{(C.7a)}$$

$$I_{1,4} = \frac{1}{4\sqrt{1-16\Gamma^2/\pi^2}} \left\{ \ln\left[(\Phi_s+\alpha) + \sqrt{(\Phi_s+\alpha)^2 + \Psi^2} \right] - \ln|\Psi| \right\}. \qquad \text{(C.7b)}$$

Note that some cancellation occurs between $I_{1,2}$ and $I_{1,4}$.

Now consider the second part of the drift integral

$$I_2 = \int_{\Phi_s}^{\Phi_u} \left[\frac{1}{q^2} - 1 \right] d\Phi \,. \tag{C.8a}$$

We again utilize the additive composite of Van Dyke (1975) to obtain

$$I_2 \sim \int_{\Phi_s}^{\Phi_u} \left\{ \left[\left| \frac{dG}{d\zeta} \right|_{\Psi=0}^{-2} - 1 \right] - \frac{1}{2\,|G_s''|\,\sqrt{(\Phi-\Phi_s)^2 + \Psi^2}} - \frac{1}{2\,|G_s''|\,(\Phi - \Phi_s)} \right\} d\Phi \tag{C.8b}$$

where the three terms correspond to the global, local and common expressions, respectively.

It turns out that all terms in (C.8b) can be evaluated in closed form. However, when considered individually, the first and last terms are not integrable at $\Phi = \Phi_s$. Hence, in treating these terms we temporarily replace the lower limit by $\Phi_s + \sqrt{1-16\Gamma^2/\pi^2}\;\theta'$, where θ' is a small parameter which will be allowed to approach zero after combining the individual integrals. Integration of the first term, $I_{2,1}$, can be simplified by using the variable θ, since $\Psi = 0$ corresponds to $r = 1$.

$$I_{2,1} = \int_{\Phi_s+\sqrt{1-16\Gamma^2/\pi^2}\,\theta'}^{\Phi_u} \left[\left| \frac{dG}{d\zeta} \right|_{\Psi=0}^{-2} - 1 \right] d\Phi = \frac{1}{2} \int_{\frac{\pi}{2}}^{\theta_s-\theta'} \frac{d\theta}{\sin\theta + \Gamma/4\pi} \,. \tag{C.9a}$$

The integral over θ is most conveniently evaluated by the further change of variable $z = \tan(\theta/2)$. The inverse transformation is multivalued and hence it is convenient to consider the regions $\theta < \pi$ and $\theta > \pi$ separately. With proper attention to the branches we find

$$I_{2,1} = \frac{1}{2\sqrt{1-\Gamma^2/16\pi^2}}\left\{\log\left[\frac{\tan(\pi/4) - \tan(\theta_s/2)}{\tan(\pi/4) - \cot(\theta_s/2)}\right] + \log[\cot(\theta_s/2) - \tan(\theta_s/2) + O(\theta')]\right.$$

$$\left. -\log\left[\frac{\sqrt{1+\Gamma^2/16\pi^2}+1}{\Gamma^2/16\pi^2}\,\theta' + O(\theta'^2)\right]\right\}. \qquad \text{(C.9b)}$$

The integrals of the remaining terms in (C.8b) are elementary. Evaluating these, and taking the limit as $\theta' \to 0$, we find that the $\log\theta'$ arising in the integrals of the first and last terms in (C.8b) cancels, leading to

$$I_2 = \frac{1}{4\sqrt{1-\Gamma^2/16\pi^2}}\left\{-\log|\Psi| + \log 8(1-\Gamma^2/16\pi^2)^{3/2} + \frac{1}{4}\,\frac{\Psi^2}{(\Phi_u - \Phi_s)^2}\right\} - (\Phi_u - \Phi_s)\,. \qquad \text{(C.10)}$$

Next consider the integral arising for streamlines which pass just below the body. We have

$$I_3 = \int_{\Phi_s}^{\Phi_l}\left[\frac{1}{q^2} - 1\right] d\Phi\,. \qquad \text{(C.11a)}$$

The evaluation of I_3 follows that of I_2, except that no multivalued behavior arises from the substitution $z = \tan(\theta/2)$. We obtain

$$I_3 = \frac{1}{4\sqrt{1-\Gamma^2/16\pi^2}}\left\{-\log|\Psi| + \log 8(1-\Gamma^2/16\pi^2)^{3/2} + \frac{1}{4}\frac{\Psi^2}{(\Phi_1 - \Phi_s)^2}\right\} - (\Phi_1 - \Phi_s)\,. \tag{C.11b}$$

Appropriately combining I_1, I_2 and I_3, the total drift (C.1) has the asymptotic expansion

$$D_{u,1}(\Psi) = C_0 \log|\Psi| + C_{u,1} + O(\Psi\log\Psi, \Psi) \tag{C.12a}$$

$$C_0 = -\frac{1}{\sqrt{1-\Gamma^2/16\pi^2}} \tag{C.12b}$$

$$C_{u,1} = 2\,(I_{1,1} + I_{1,3}) + \frac{1}{2\sqrt{1-\Gamma^2/16\pi^2}}[\log 16(1-\Gamma^2/16\pi^2)^{3/2} + \log(\alpha+\Phi_s)] - 2(\Phi_{u,1}-\Phi_s) \tag{C.12c}$$

where $I_{1,1}$ and $I_{1,3}$ are the first and third terms in (C.6b).

Next consider the numerical evaluation of $I_{1,1}$. The path of integration is the streamline $\Psi = 0$. Setting the imaginary part of (5.1b) equal to zero, we find that this streamline is given by

$$\sin\theta = -\frac{\Gamma}{2\pi}\frac{\log r}{r-1/r} \tag{C.13a}$$

Substituting into (C.1b), we obtain

$$q^2\Big|_{\Psi=0} = 1 - \frac{\Gamma^2}{2\pi^2}\frac{\log r}{r^2-1} + \left(\frac{\Gamma^2}{4\pi^2} - 2\right)\frac{1}{r^2} + \frac{\Gamma^2}{2\pi^2}\frac{(\log r)^2}{(r^2-1)^2} - \frac{\Gamma^2}{2\pi^2}\frac{\log r}{r^2}\frac{1}{r^2-1} + \frac{1}{r^4}\,.$$

(C.13b)

To evaluate $I_{1,1}$, $q^2\Big|_{\Psi=0}$ must be expressed in terms of Ψ. The transformation $\Phi = \Phi(r)$ can be found by substituting (C.13a) in the real part of (5.1b). However, since this transformation cannot be inverted in closed form, the inversion was evaluated numerically via the Muller algorithm as described in Section 5.1. The integration domain was also transformed to a finite range through the change of variable $\beta = 1/\Phi$. The integrand then behaves as $1/\beta$ at the "upstream" limit $\beta \rightarrow 0^-$. The resulting $\log|\beta|$ singularity was extracted analytically before applying Romberg integration as described in Section 5.1.

The integral $I_{1,3}$ is also evaluated along the streamline $\Psi = 0$. Here an integrable singularity occurs at $\Phi = \Phi_s$. To extract this singularity analytically, we expand (C.13b) for $r-1 << 1$, and invert the real part of (5.1b) for $\bar{\Phi} = \Phi_s - \Phi << 1$ to obtain

$$\left|\frac{dG}{d\zeta}\right|^{-2}_{\Psi=0} = \frac{A}{\bar{\Phi}} + \frac{B}{\sqrt{\bar{\Phi}}} + C + O(\bar{\Phi}^{1/2}) \qquad \text{(C.14a)}$$

where

$$A = \frac{1}{4(1-\Gamma^2/16\pi^2)^{1/2}} \qquad \text{(C.14b)}$$

$$B = \frac{1}{2(1-\Gamma^2/16\pi^2)^{3/4}} \qquad \text{(C.14c)}$$

$$C = \frac{63-137\Gamma^2/16\pi^2+75\Gamma^4/256\pi^4}{144(1-\Gamma^2/16\pi^2)^3} \quad . \qquad \text{(C.14d)}$$

The first term can be seen to cancel in the integrand of $I_{1,3}$. The second term of (C.10a) is an integrable singularity which is extracted analytically before applying Romberg integration.

Calculations were performed with two different values of α, $1-\Phi_s$ and $1.5-\Phi_s$. In both cases the Romberg scheme converged to a relative error of less than 10^{-5} in fewer than 5 steps, and the results for C_u agreed to this accuracy. Numerical values for C_u for several values of Γ are presented in Table C.1. For $\Gamma = 0$, Darwin obtained the analytical result $C = \log 8 - 2 = 0.0794415$. It can be seen tha: our numerical calculation has produced results which are accurate to 5 digits. Finally it can be shown from (C.12c) that $C_u = C_l - \Gamma$.

θ_s	Γ	C_u
0^0	0.	0.0794362
1^0	0.2193134	-0.0275156
5^0	1.0952314	-0.4006330
30^0	6.2831853	-0.7327045

Table C.1 Coefficient C_u in the asymptotic drift expression C.12a versus θ_s and Γ.

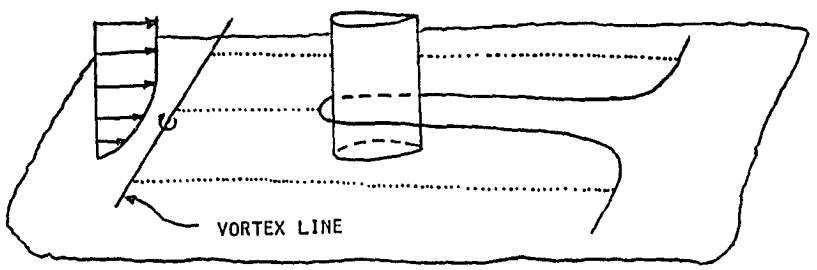

Figure 1.1 Distortion of vortex lines in a strut - boundary layer interaction.

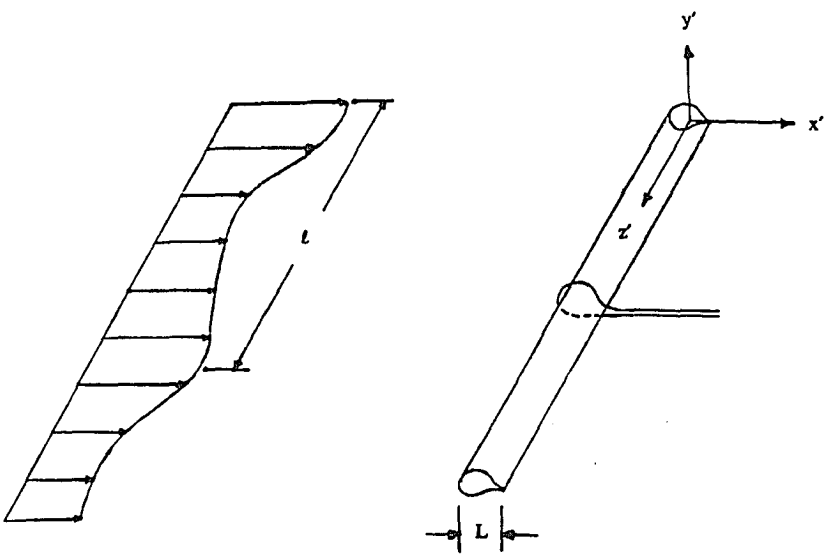

Figure 1.2 Singular perturbation approach.

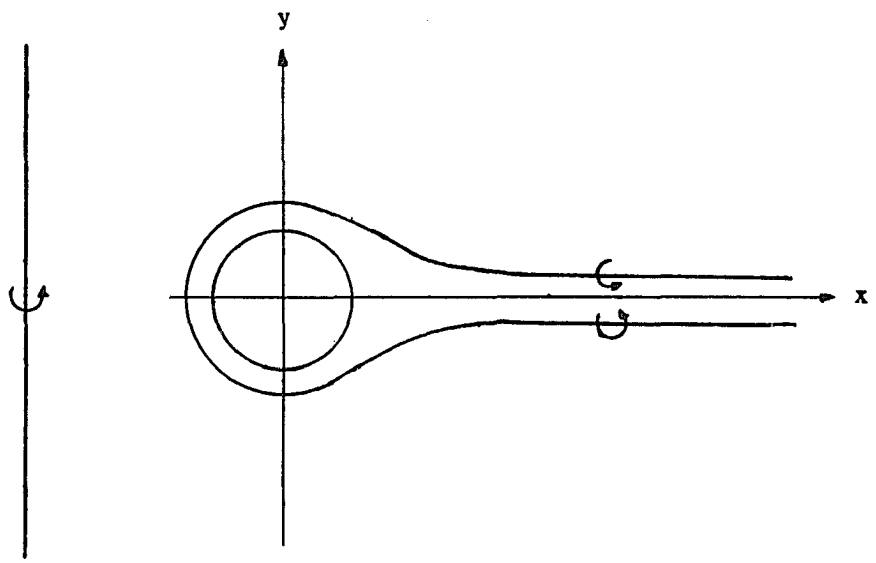

Figure 3.1a Vortex lines wrapping around a body.

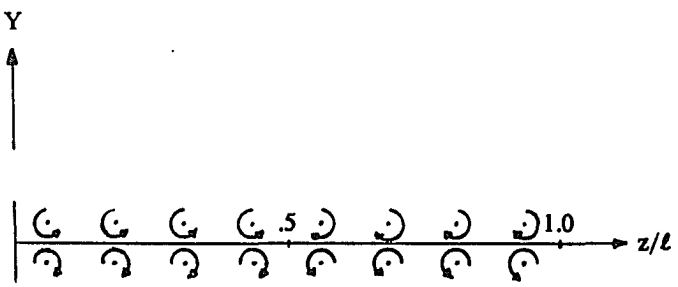

Figure 3.1b Distribution of streamwise vortices in the wake.

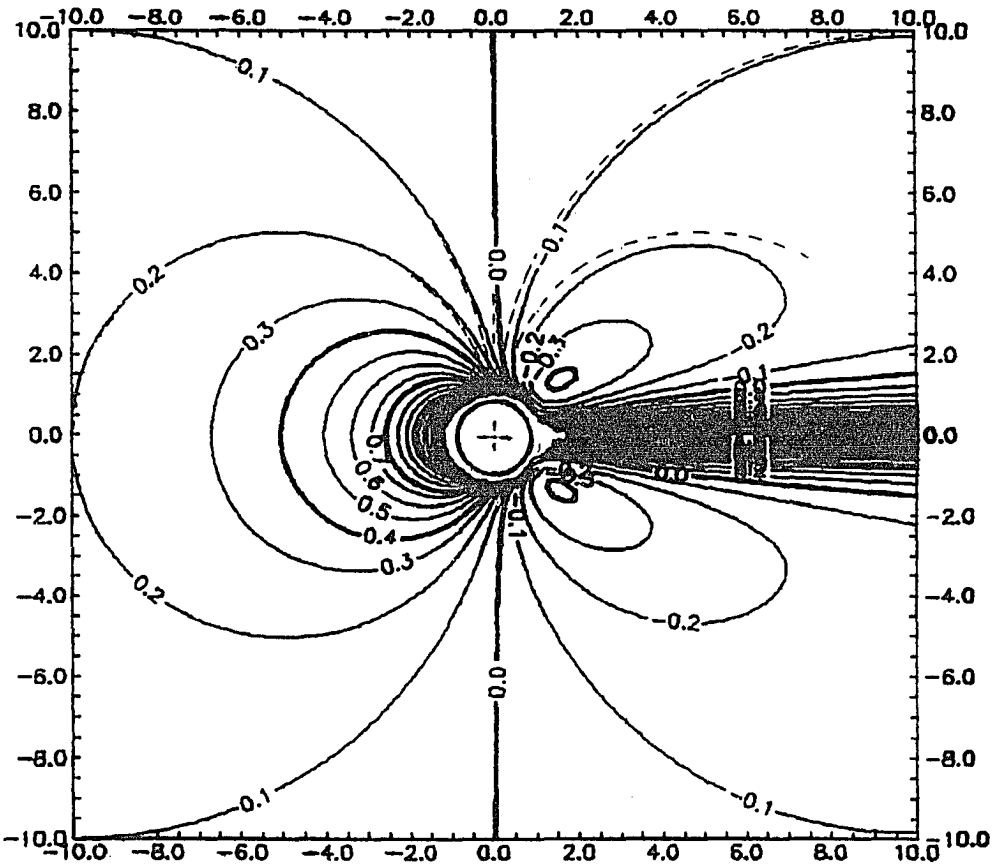

Figure 5.1a Spanwise velocity component for a nonlifting circular cylinder, 10 radii.

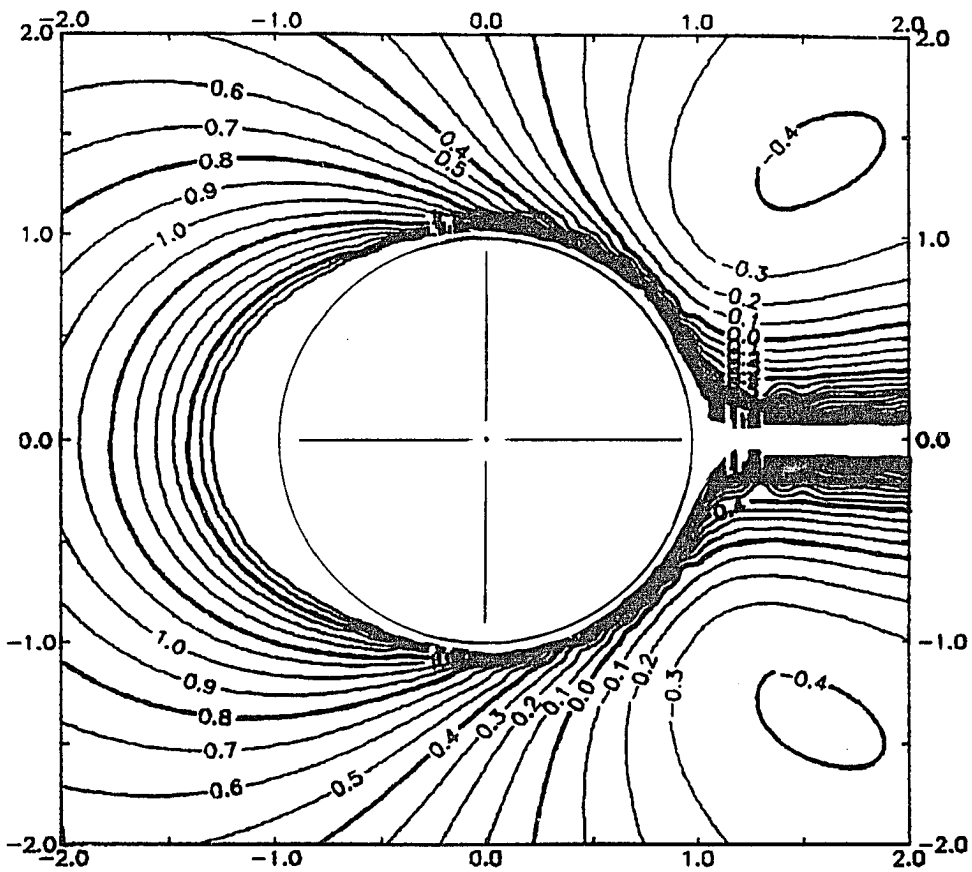

Figure 5.1b Spanwise velocity component for a nonlifting circular cylinder, 2 radii.

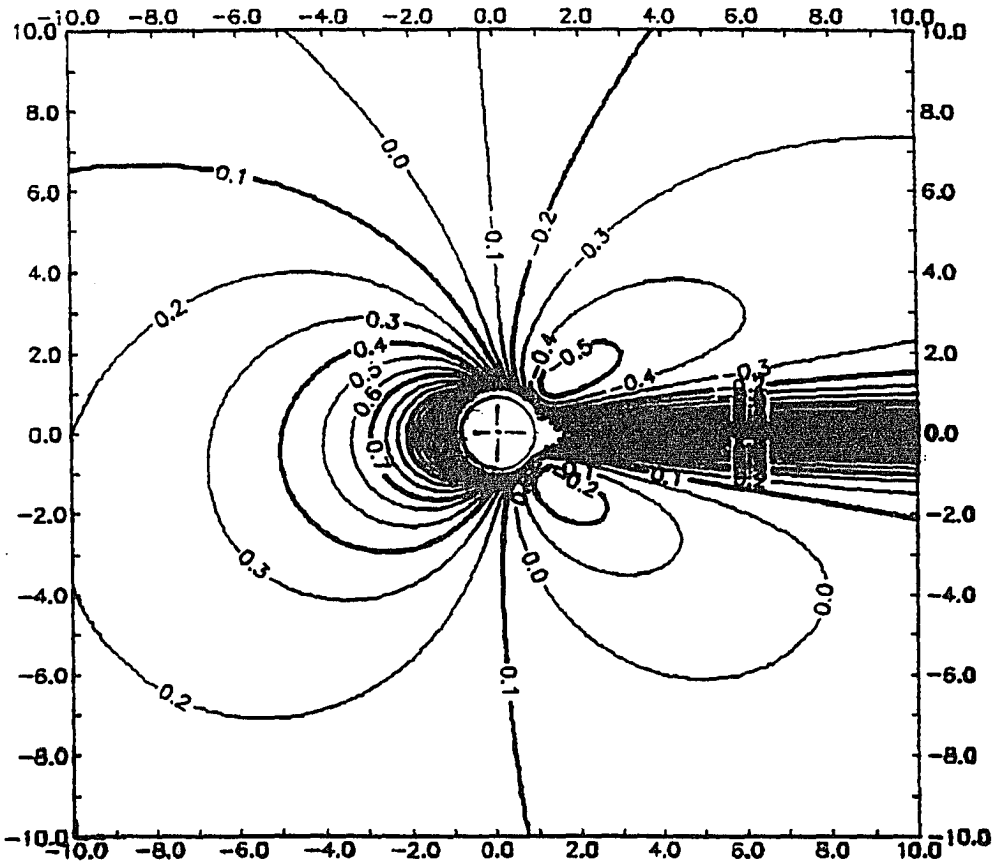

Figure 5.2a Spanwise velocity component for a lifting circular cylinder, $\theta_s = 1^0$, 10 radii.

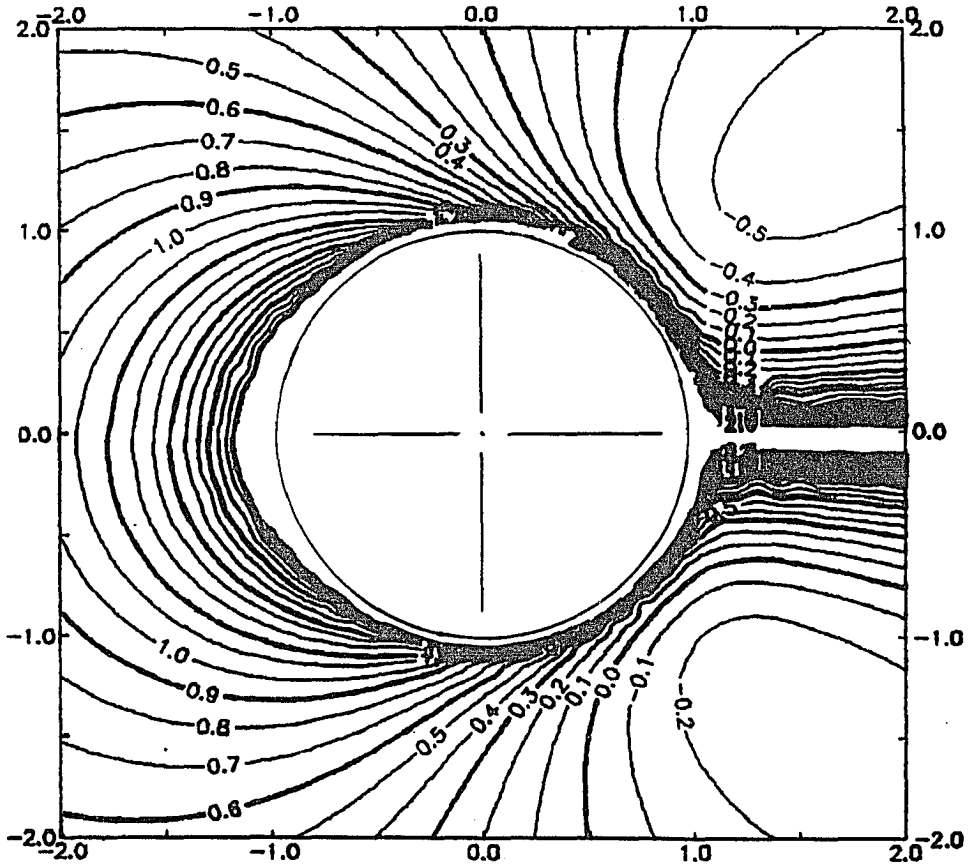

Figure 5.2b Spanwise velocity component for a lifting circular cylinder, $\theta_s = 1^0$, 2 radii.

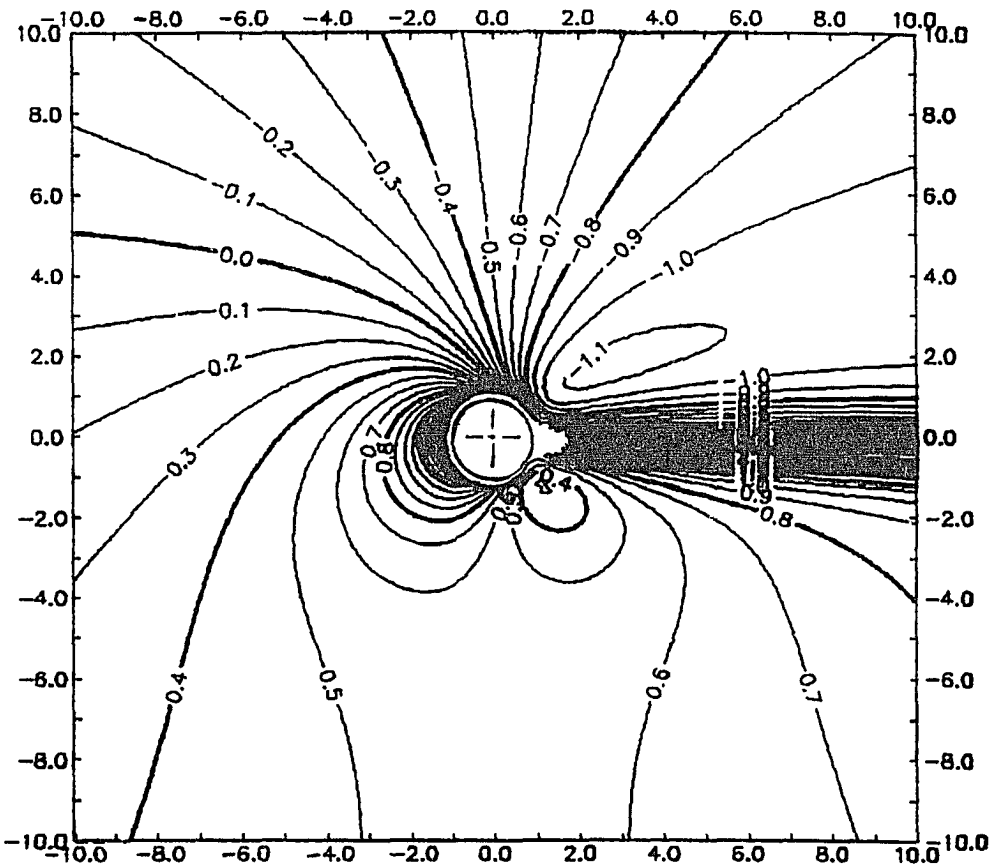

Figure 5.3a Spanwise velocity component for a lifting circular cylinder, $\theta_s = 5^0$, 10 radii.

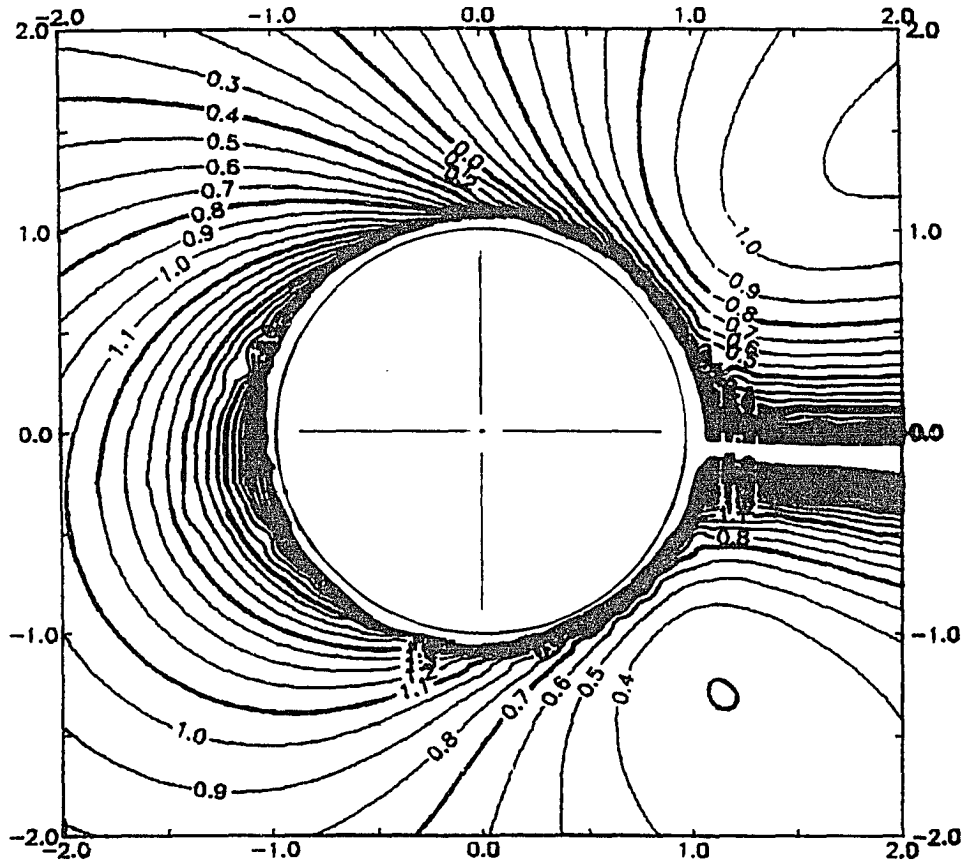

Figure 5.3b Spanwise velocity component for a lifting circular cylinder, $\theta_s = 5^0$, 2 radii.

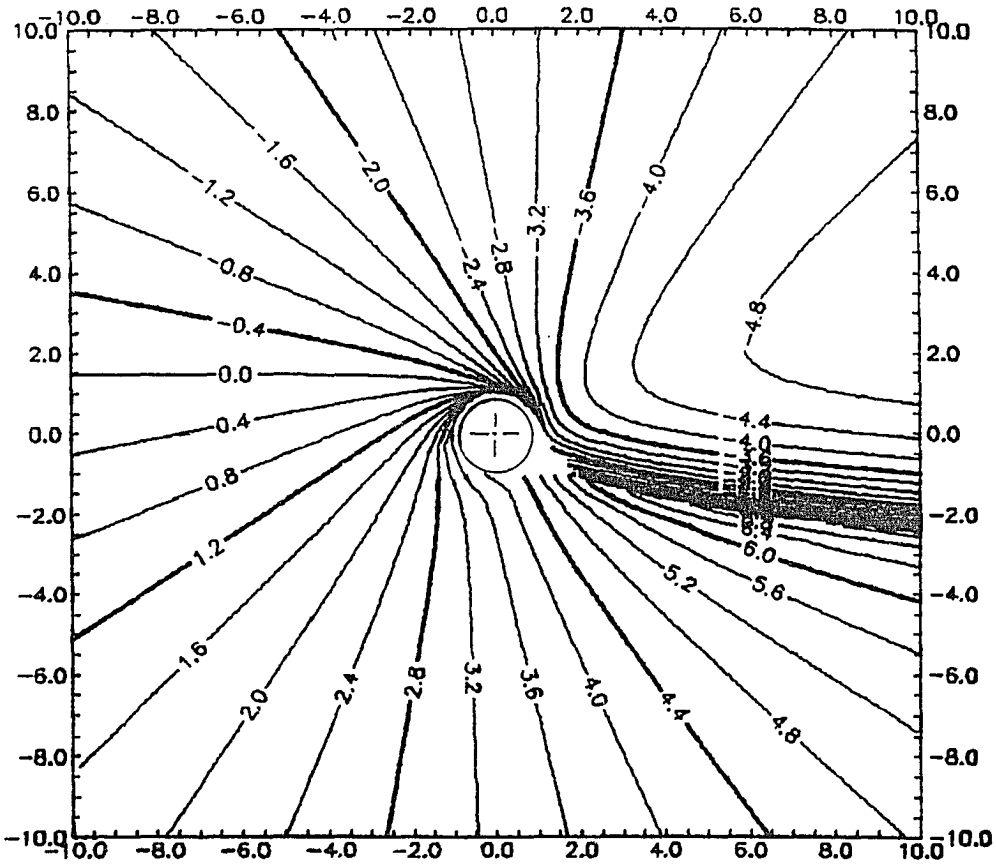

Figure 5.4a Spanwise velocity component for a lifting circular cylinder, $\theta_s = 30^0$, 10 radii.

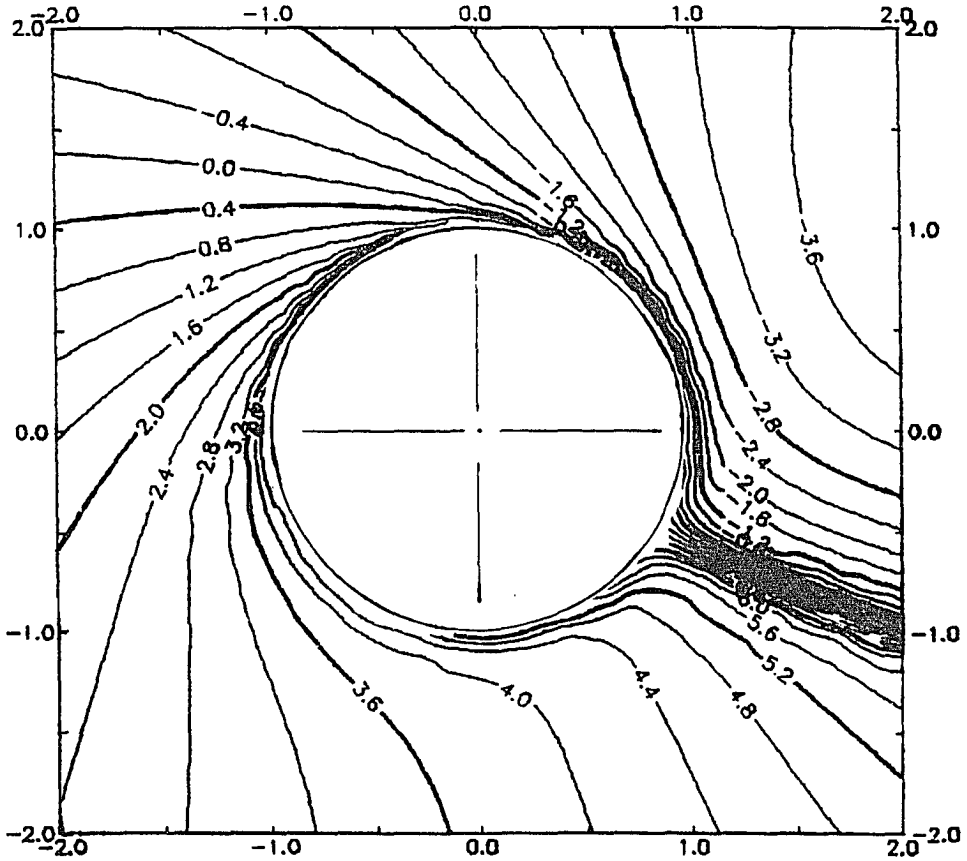

Figure 5.4b Spanwise velocity component for a lifting circular cylinder, $\theta_s = 30^0$, 2 radii.

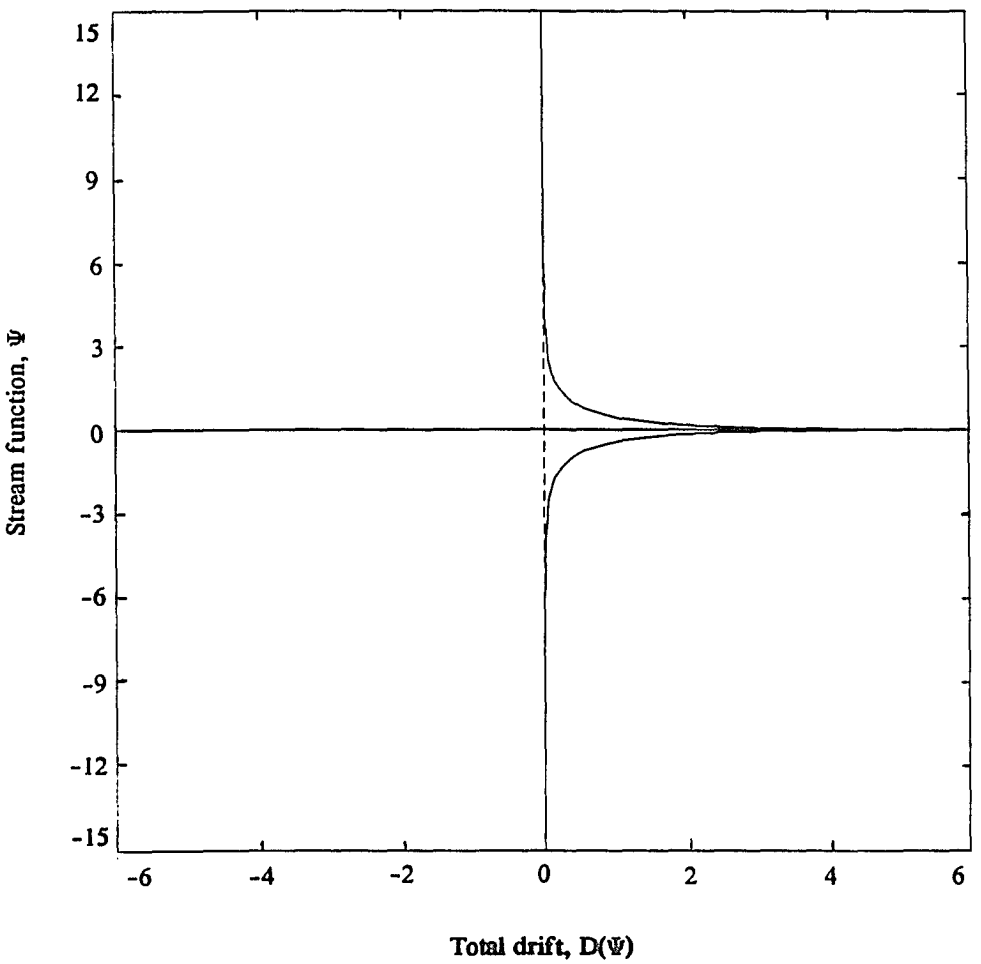

Figure 5.5a Total drift curve for a nonlifting circular cylinder.

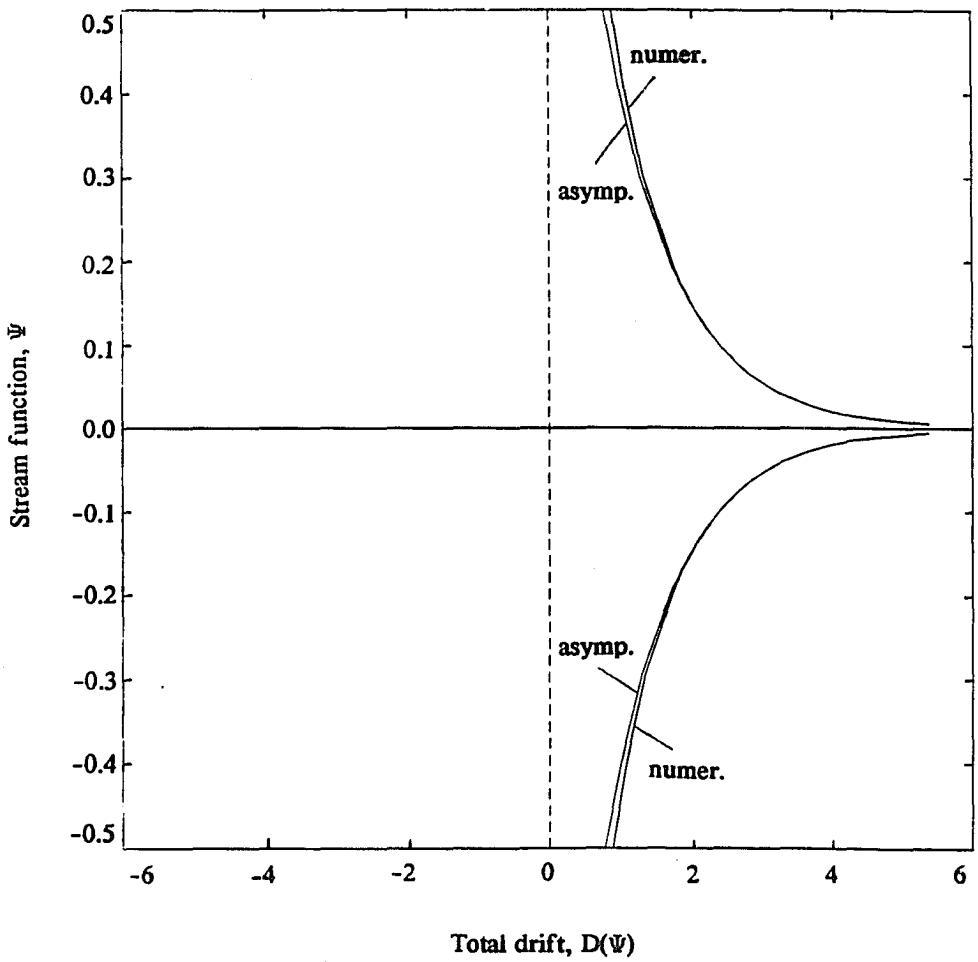

Figure 5.5b Asymptotical expansion vs. numerics comparison for a nonlifting circular cylinder.

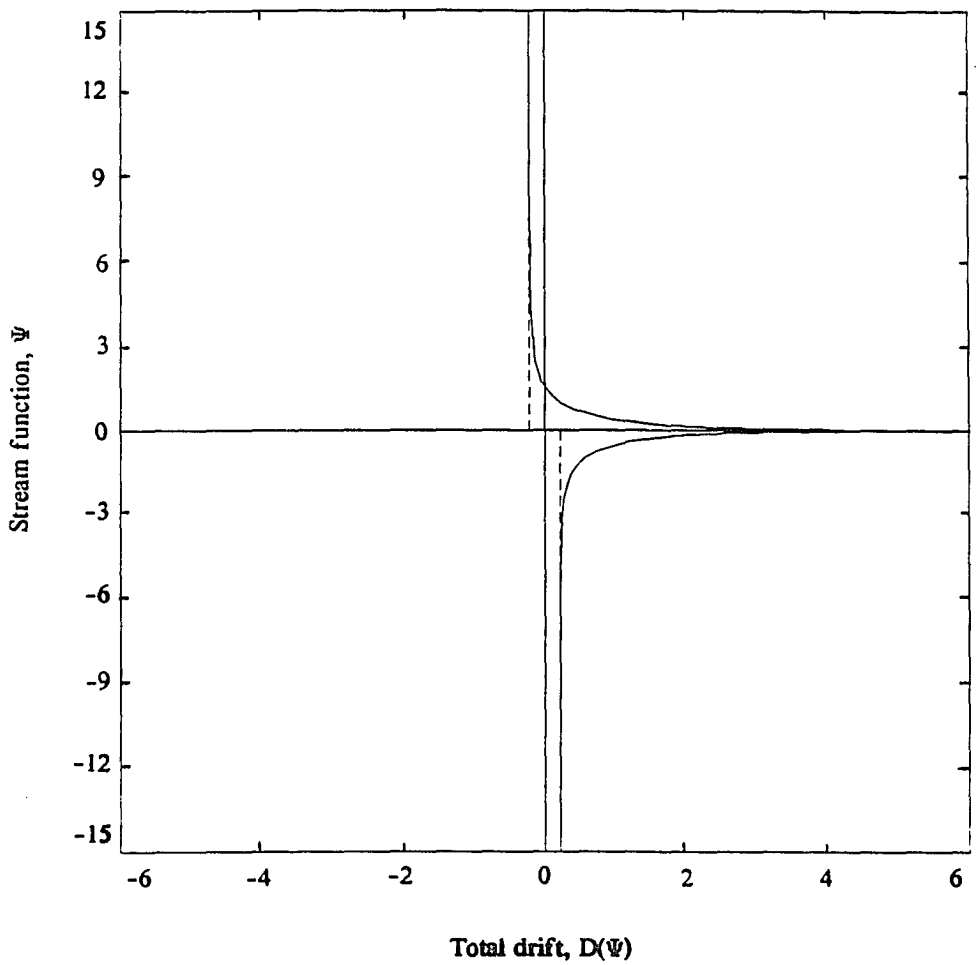

Figure 5.6a Total drift curve for a lifting circular cylinder, $\theta_s = 1^0$.

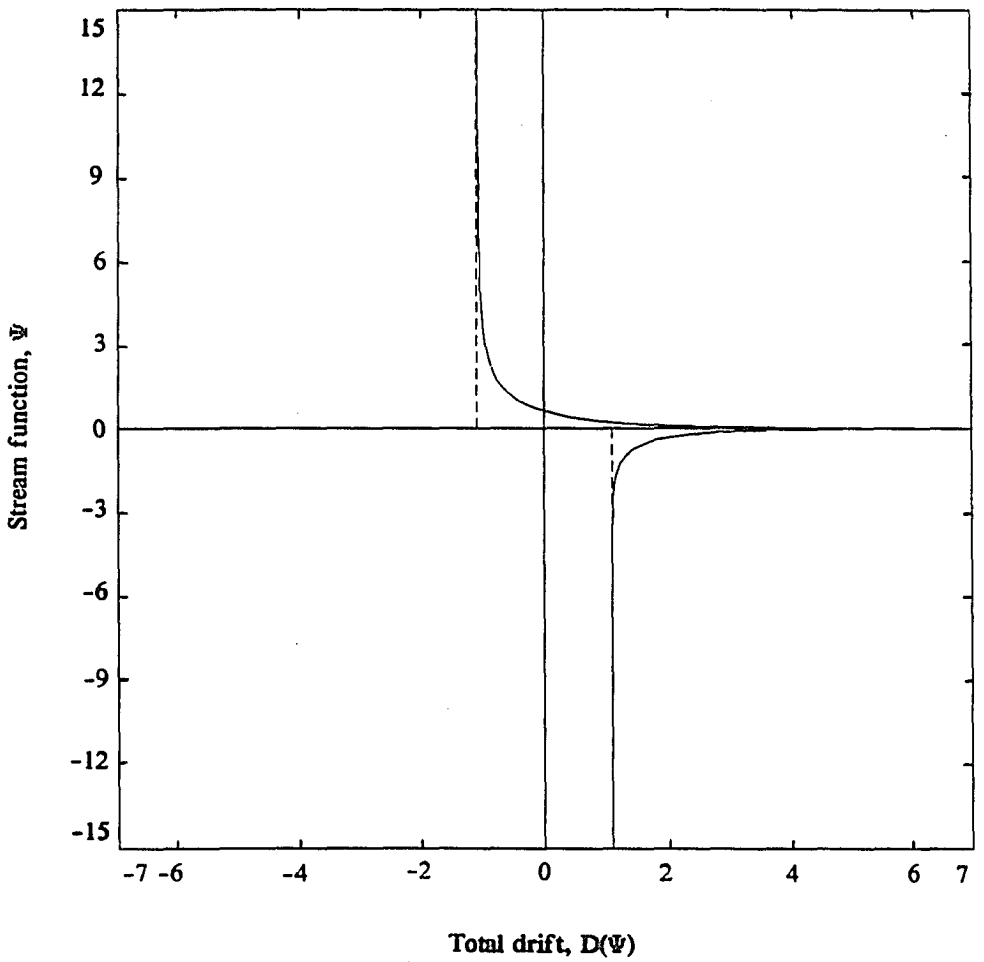

Figure 5.6b Total drift curve for a lifting circular cylinder, $\theta_s = 5^0$.

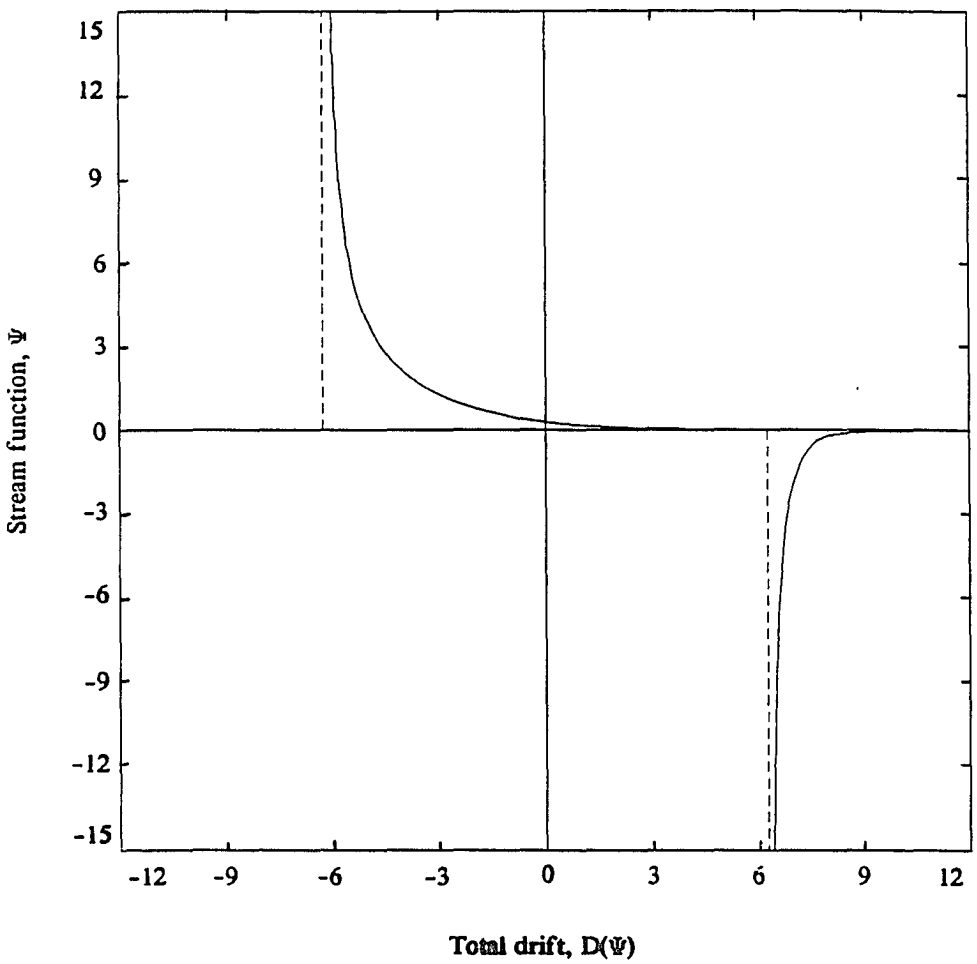

Figure 5.6c Total drift curve for a lifting circular cylinder, $\theta_s = 30^0$.

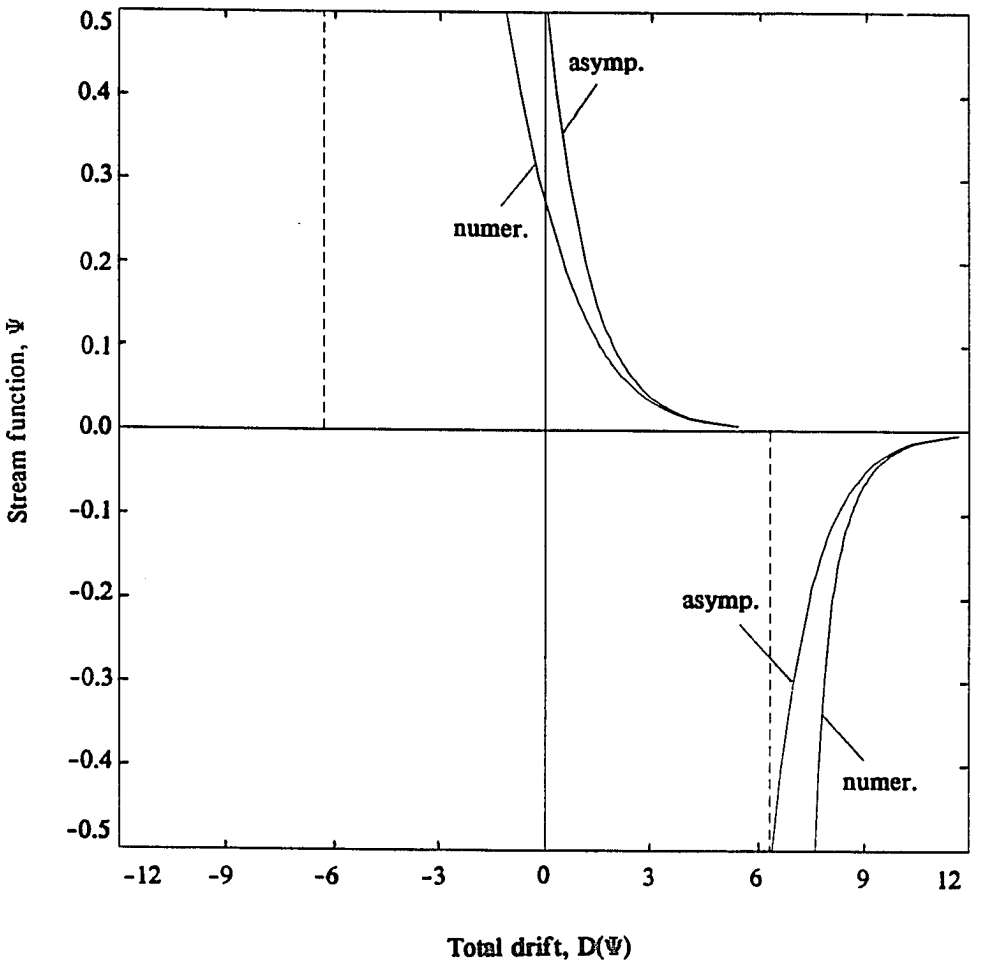

Figure 5.6d Asymptotical expansion vs. numerics comparison for a lifting circular cylinder, $\theta_s = 30^0$.

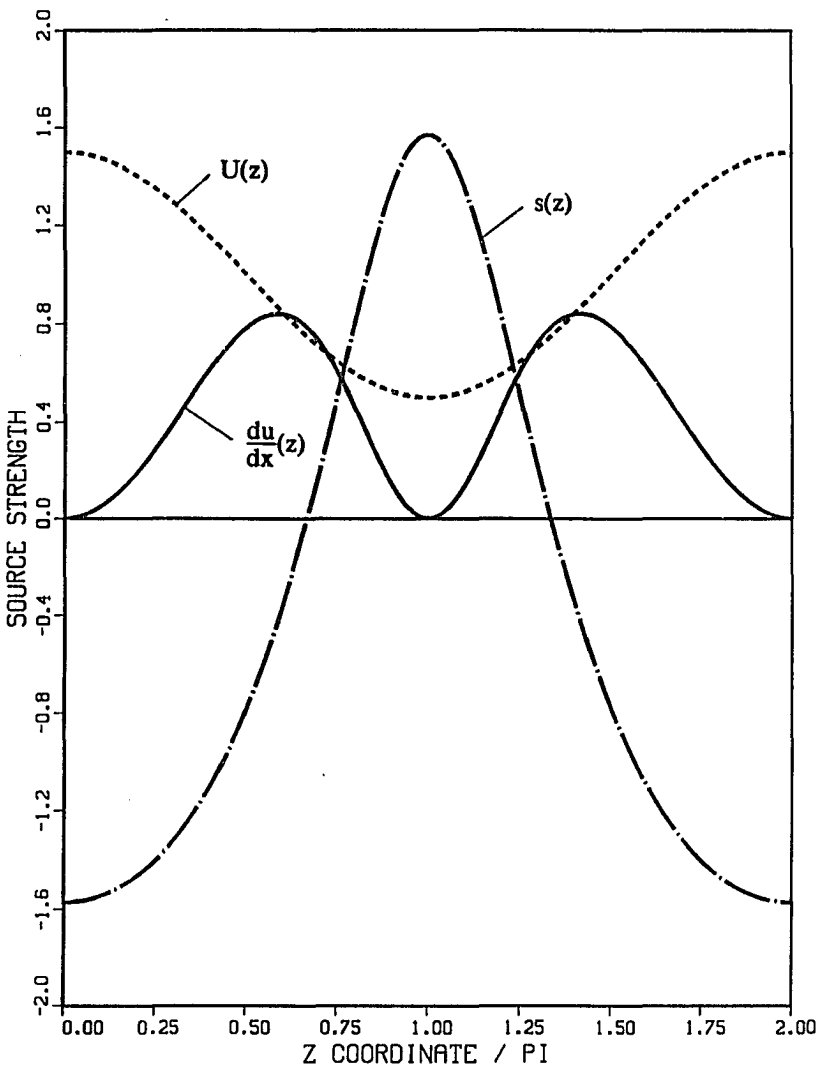

Figure 5.7 Source strength versus du/dx curve for a nonlifting circular cylinder.

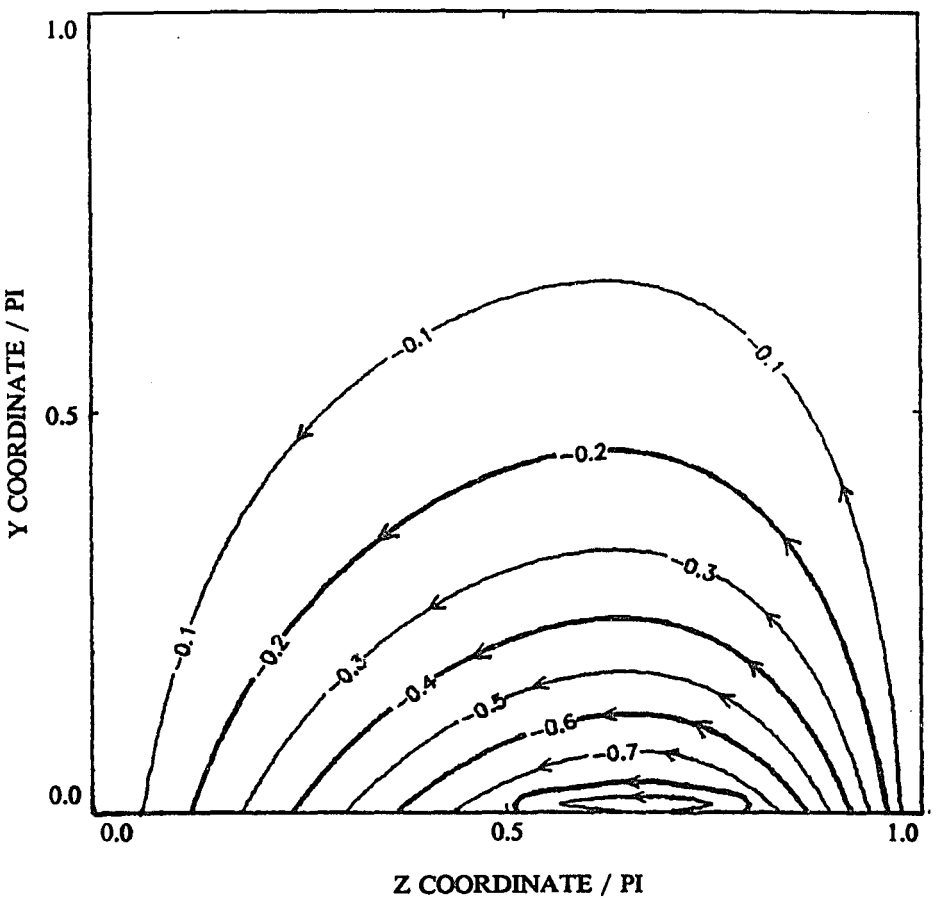

Figure 5.8 Trefftz plane contours for a nonlifting circular cylinder, y > 0.

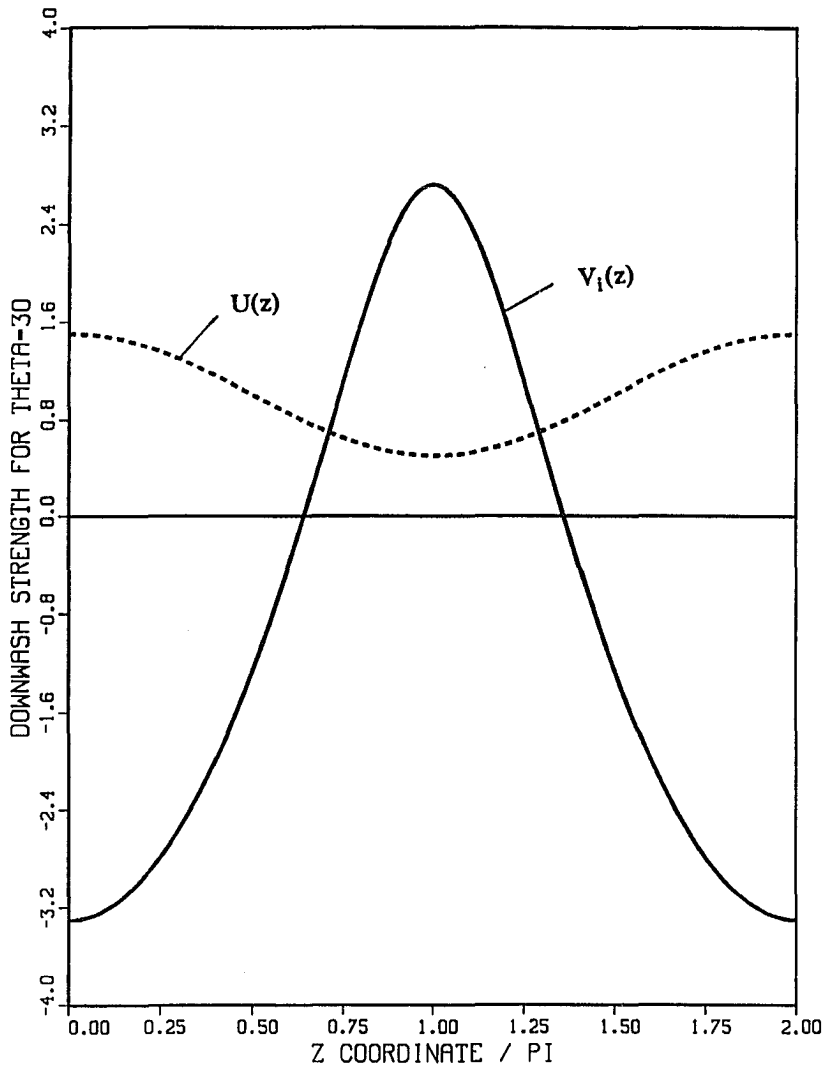

Figure 5.9 Downwash strength for a lifting circular cylinder, $\theta_s = 30^0$.

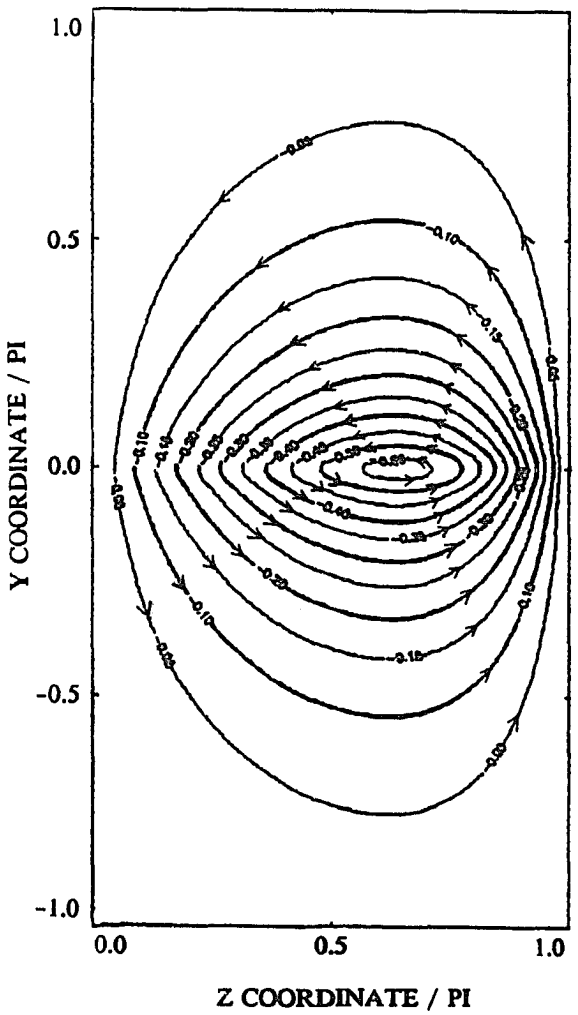

Figure 5.10 Trefftz plane contours for a lifting circular cylinder, $\theta_s = 5^0$.

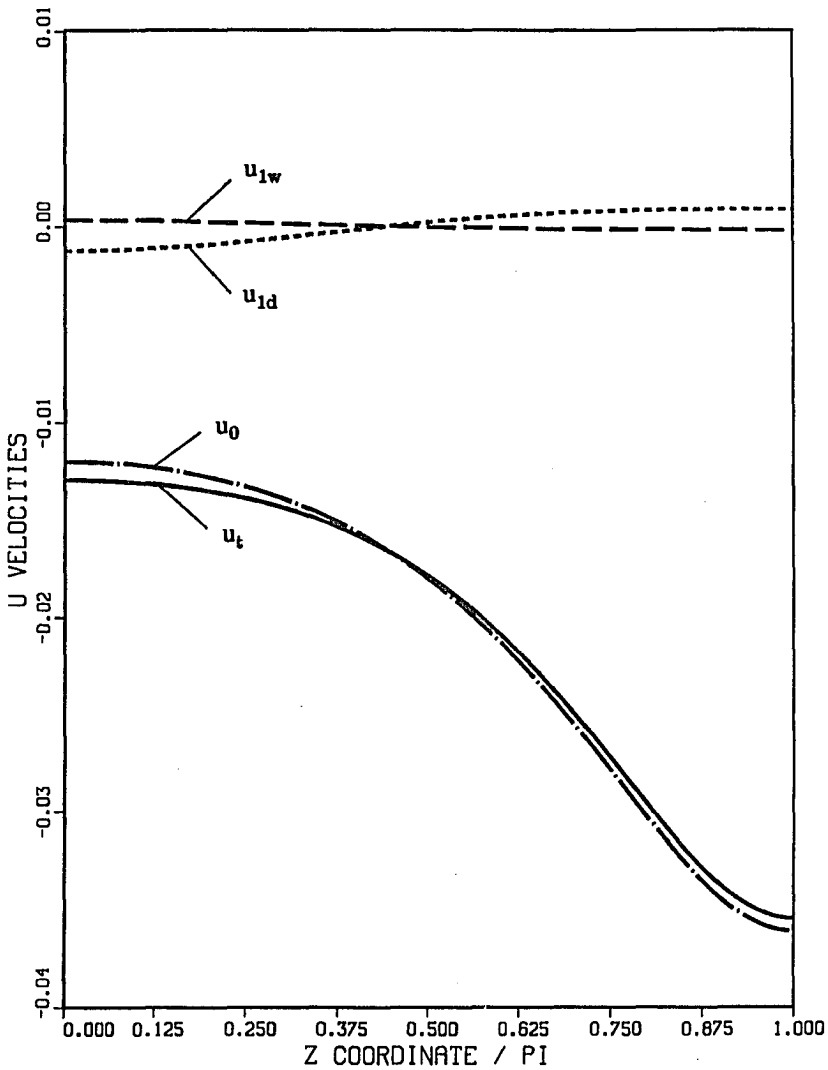

Figure 5.11a Dipole line solution vs. wake solution for a nonlifting body, r = 6, $\theta = 180^0$.

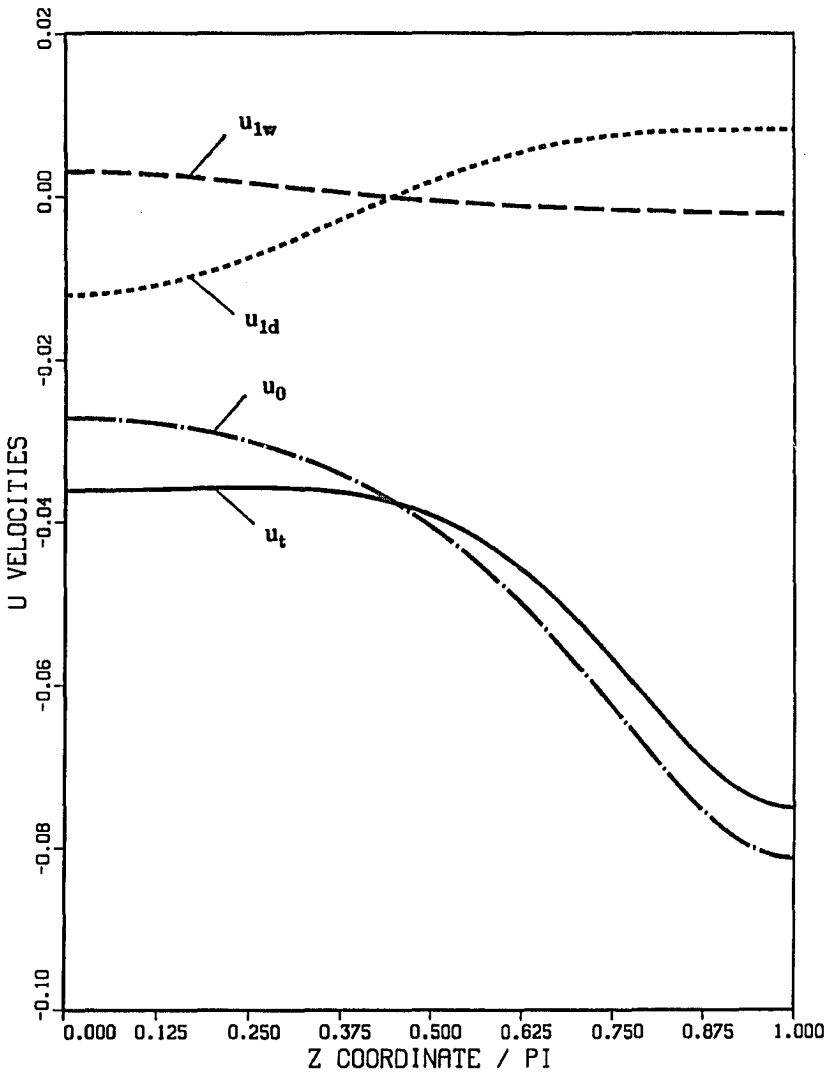

Figure 5.11b Dipole line solution vs. wake solution for a nonlifting body, r = 4, $\theta = 180^0$.

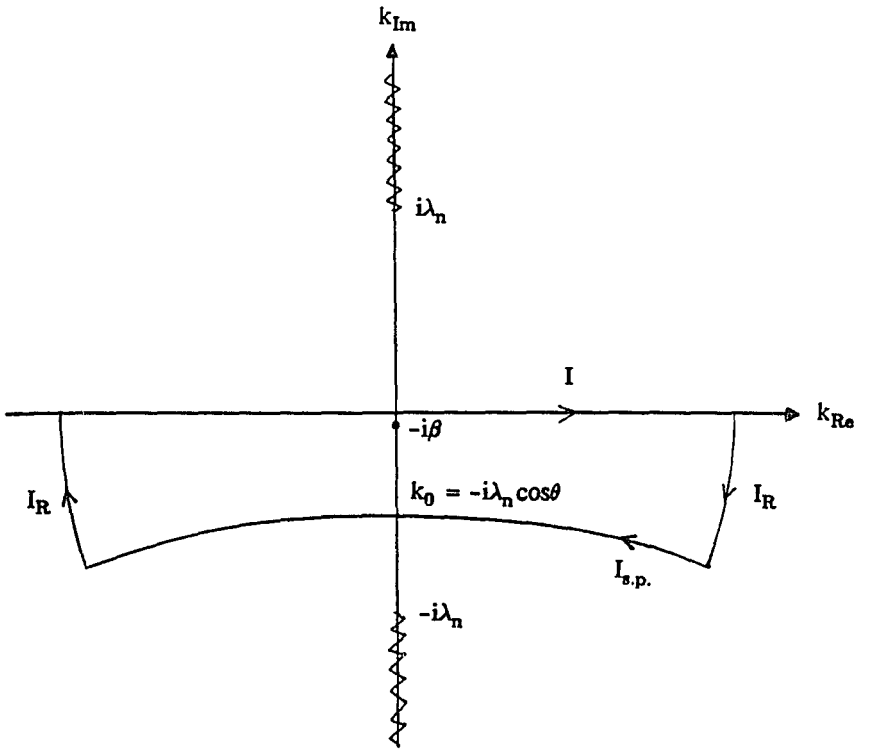

Figure A.1a k plane showing contours for $0 < \theta < \pi/2$.

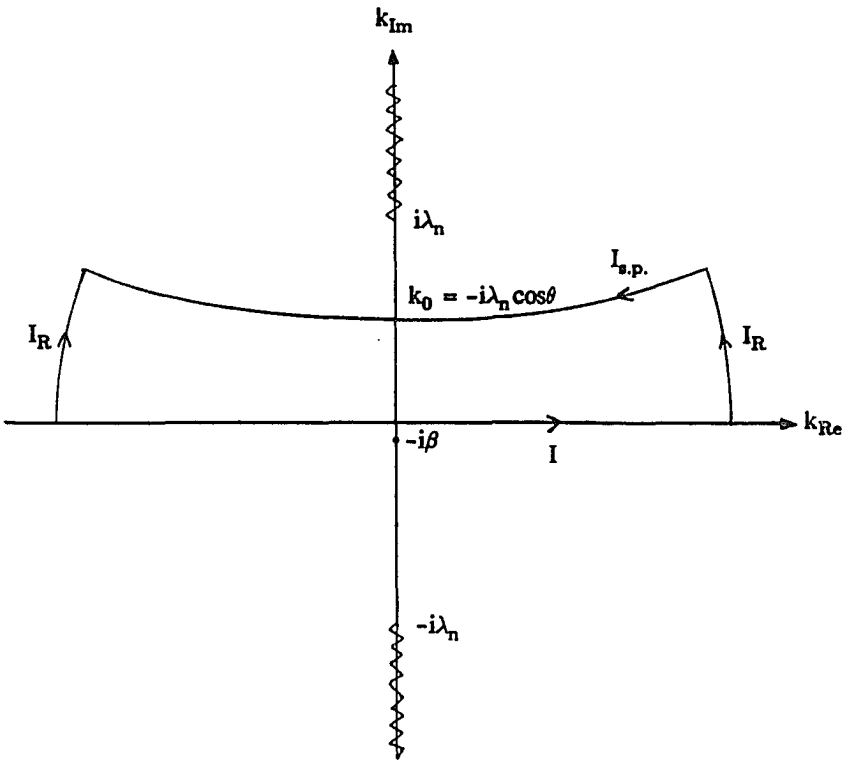

Figure A.1b k plane showing contours for $\pi/2 < \theta < \pi$.

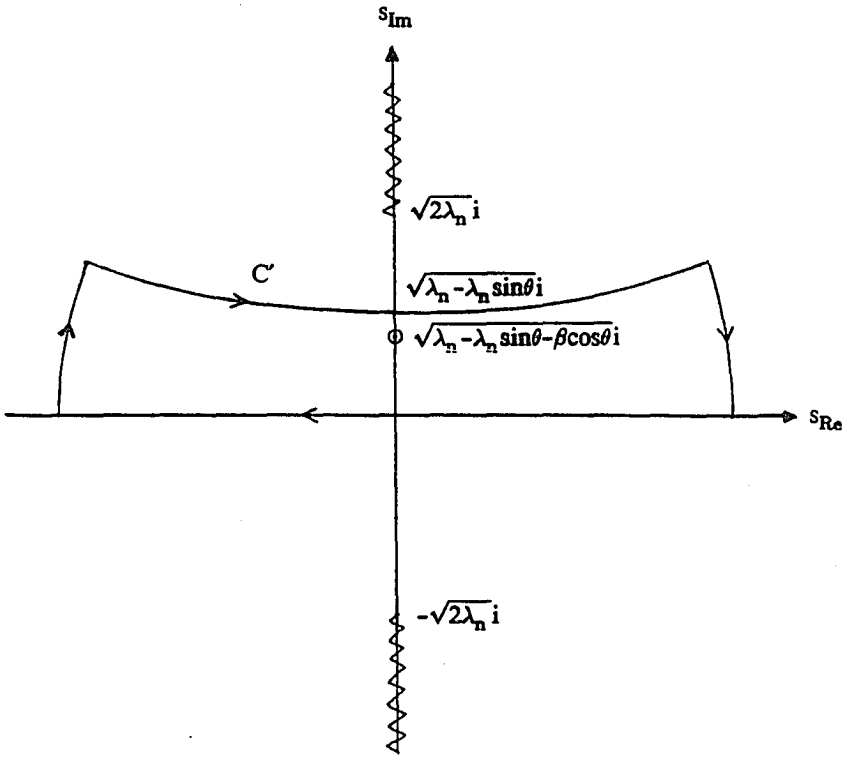

Figure A.2 s plane showing contours for $0 < \theta < \pi/2$.

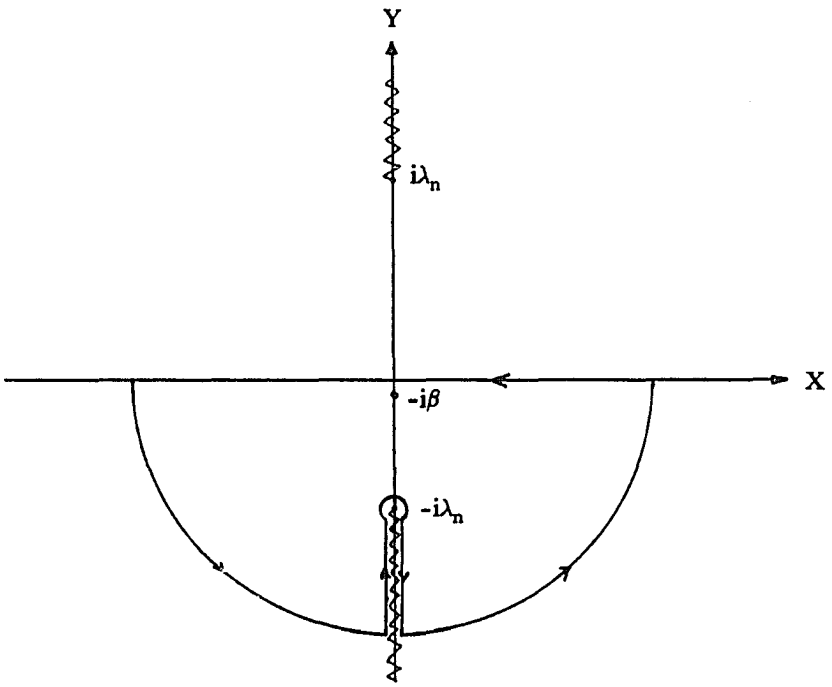

Figure B.1 k plane contour for x > 0, y > 0.

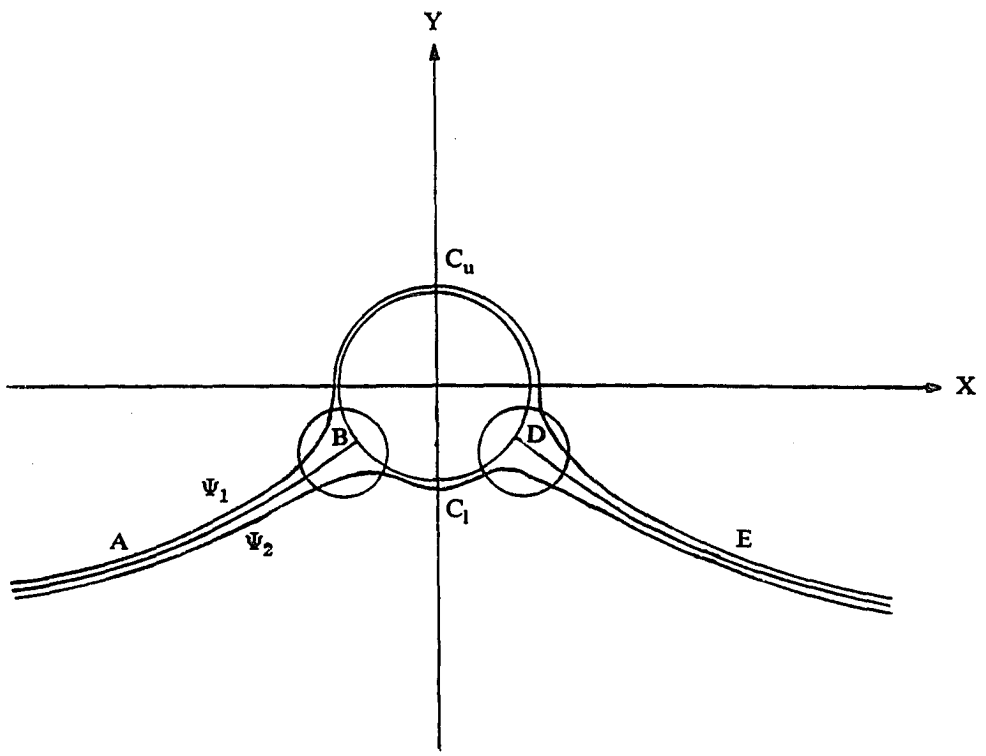

Figure C.1 The regions of small Ψ composite expansion for the drift function for the circular cylinder with circulation.

REFERENCES

Darwin, C. G., "Note on hydrodynamics", Proc. Camb. Phil. Soc. 49, 342 (1953).

Ferziger, J. H., "Numerical Methods for Engineering Application", John Wiley, New York (1981).

Hawtorne, W. R., "Secondary circulation in fluid flow", Proc. Roy. Soc. A, 206, 374-87 (1951).

Hawtorne, W. R., "The secondary flow about struts and airfoils", J. Aero. Sci. 21, 558-608 and 648 (1954).

Hawtorne, W. R., "The Applicability of Secondary Flow Analyses to the Solution of Internal Flow Problems", Fluid Mechanics of Internal Flow, ed. G. Sovran, 263. Amsterdam: Elsevier (1967).

Honda, M., "Theory of a thin wing in a shear flow", Proc. Roy. Soc. A 254, 372 (1960).

Honda, M., "Theory of shear flow through a cascade", Proc. Roy. Soc. A 265, 46 (1961).

Horlock, J. H. and Lakshminarayana, B., "Secondary Flows: Theory, Experiment, and Application in Turbomachinery Aerodynamics", Annual Review of Fluid Mechanics, 247-280 (1973).

Karman, V. T. and Tsien, H.-S., "Lifting line theory for a wing in non-uniform flow", Quart. Appl. Math. 3, 1-11 (1945).

Lighthill, M. J., "Drift", J. Fluid Mech. 1, 31 (1956).

Lighthill, M. J., "Corrigenda to drift", J. Fluid Mech. 2, 311 (1957a).

Lighthill, M. J., "The fundamental solution for small steady three-dimensional disturbances to a two-dimensional parallel shear flow", J. Fluid Mech. 3, 313 (1957b).

Namba, M., "Lifting-surface theory for cascade of blades in subsonic shear flow", J. Fluid

Mech. 36, 735-757 (1969).

Squire, H. B. and Winter, K. G., "The secondary flow in a cascade of airfoils in a nonuniform stream", J. Aero. Sci. 18, 4 (1951).

Tsien H.-S., "Symmetrical Joukowsky airfoils in shear flow", Q. Appl. Math. I, 130 (1943).

Van Der Waerden, B. L., "On the method of saddle points", App. Sci. Res., B2, 33 (1950).

Van Dyke, M., "Lifting-line theory as a singular perturbation problem", Arch. Mech. Stos. 16, No. 3 (1964).

Van Dyke, M., "Perturbation Methods in Fluid Mechanics", The Parabolic Press, Stanford (1975).